ISSN 1028-8546

Azərbaycan Milli Elmlər Akademiyası
Fizika-Riyaziyyat və Texnika Elmləri Bölməsi
Fizika İnstitutu

2

Fizika

Cild
VIII
2002

Bakı ✵ Elm

HIGH-EFFECTIVE AND DURABLE SOLAR ELEMENTS ON THE BASIS OF a-Si:H

Sh.S. ASLANOV, I.R. NURIYEV, V.A. ALIYEV, A.M. NAZAROV
Institute of Photoelectronics National Academy of Sciences
F.Agayev str., quarter 555, Baku, 370141, Azerbaijan

In the paper authors have developed the technology for preparation of the thin films *a*-Si:H by means of the method of magnetron sputtering. Solar elements were made on glass and dielectric substrates on the basis of the obtained films. At the present moment the elements were made with the parameters on the level of the world analogues (within the intensity of illumination in 100 mW/cm^2, AM1), open-circuit voltage U_{oc}=0.88 mV, short-circuit current I_{sc}=15.3 mA/cm^2, the efficiency about 23%.

For recent years photogalvanic transformers of solar energy on the basis of hydrogenated amorphous silicon *a*-Si:H have been investigated widely and are of great scientific and practical interest. As a result of investigation, photoelectric properties of films are improved at the process of silane decomposition in plasma at superimposition of magnetic field.

Therefore thin films *a*–Si:H obtained by the method of magnetron sputtering at constant current have several advantages:

- good control for keeping of hydrogen in camera and in films;
- control of wide range of substrate temperature;
- allows to use for magnetron sputtering of compound composition;
- have high speed of precipitation;
- precipitation is obtained at the voltage less than 400 V that limits the negative influence of ion energy on heterostructure and hydrogen links in the films;
- easily applicated in mass production.

Silicon target of 99.99 purity was used for creation of films *a*–Si:H. Precipitation parameters of films were controlled: pressure of hydrogen P_H, pressure of P_{Ar}, temperature of substrate T_s, entrance power P and displacement on substrate V_B. Best films are created within the parameters shown in table 1.

Table 1

Technological conditions creation films α–Si:H

T(°C)	P_H(%)	P_{Ar}(%)	P_{total}(mtorr)	V_B(V)
250	50	50	10	-100

The results of complex investigation of film characteristics are given in table 2, where 1 is the hydrogen content in silicon, 2 is the oxygen content in silicon, 3 is the optical width of band gap, 4 is the density of states, 5 is the dielectric constant, 6 is the ratio of conductivity to dark conductivity on glass substrate.

Table 2

Characteristics of the investigated solar cells

Hydrogen content H in Si (%)	Oxygen content O in Si (%)	Optical band gap (eV)	Density of states ($cm^{-3}\cdot eV^{-1}$)	Dielectr. Constant	Light to dark conductivity ratio
1	2	3	4	5	6
19	1	1.92	$8\cdot10^{16}$	8.5	10^5

Mono-, trio- and multicascade solar elements were created on the basis of p-n junction, heterojunction and structures with Shottky-barrier. Area of the created elements is 2×2 cm^2. Amorphous layers Al+Ni and Ti+Cu were used as metal electrodes, monocrystalline films of PtSi were used for creation of the Shottky-barrier. Thermo treatment of creation of monocrystalline PtSi and stabilization of α-Si:H parameters are combined and conducted in the vacuum and in the medium of forming-gas (N_2+H_2).

The structure of metal films are determined by X-ray diffractometry and electronography. The results are given in fig.1.*a* is the X-ray diffractometry figure of PtSi and *b* is the electronographic figure of amorphous films Al+Ni and Ti+Cu.

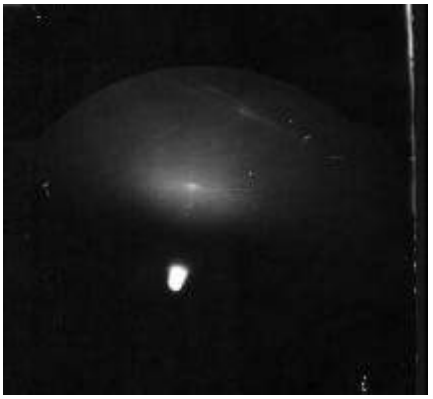

(a)

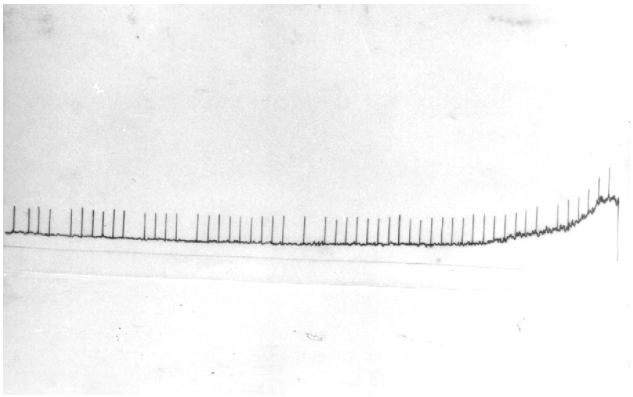

(b)

Fig.1. The structure of metal films determined by the X-ray (a) and electron diffraction (b) methods.

Application of amorphous and monocrystalline films provides durability and reliability of the elements.

Construction of created solar elements on the basis of monocascade *p-n* junction is represented in fig.2, where: 1 is the glass substrate, 1/ is the SiO_x thin film, 2 and 5 are electrodes, 3 is the *p*-type α-Si:H, 4 is the *n*-type α-Si:H, 6 is the enlightening covering.

Diboran ($Â_2Í_4$) and phosphine PH_3 were used in the sputtering process with the purpose of obtaining the films conductivity of p - and *n*-types.

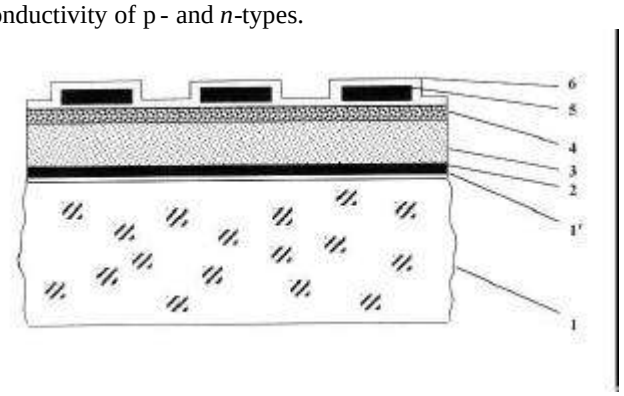

Fig.2. Construction of created solar elements.

The thin layer of SiO_x with the thickness of 0.01 mkm is plated on the glass substrate for improving the adhesion of metal electrodes.

Parameters of produced elements were determined on the special test-bench with the regulated illumination. The current voltage characteristic of the α-Si:H monocascade solar elements are given in fig.3.

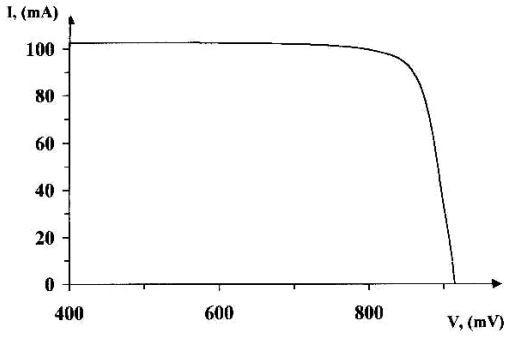

Fig.3. Current voltage characteristic of the α-Si:H monocascade solar elements.

Maximization of effectiveness is important for solar elements i.e. obtaining the highest coefficient of photogalvanic transformers of energy is the basic factor. It is determined as:

$$\eta = \frac{P_m}{P_i},$$

where P_m is the maximal entrance power of the instrument, P_i is the power of incident optical radiation. Maximum importance can be determined from the following: $P_m = I_m \cdot V_m$

$$V_m = V_{O_c} - \frac{nkT}{q} ln\left(1 - \frac{qV_m}{nkT}\right),$$

$$V_{O_c} = \frac{nkT}{q} ln\left(\frac{I_L}{I_S} + 1\right),$$

$$I_m = \frac{qI_s V_m}{nkT} exp\left(-\frac{qV_m}{nkT}\right).$$

Measuring of the tension value of idling and short-circuit current,

$$I_{SC} = I_S\left[exp\left(\frac{qV}{nkT}\right) - 1\right]$$

at the constant illumination are considered from the equation given above. Here I_s is the saturation current of diode, I_L is the current formed by the superfluous carriers within the optical excitation. If consecutive resistance can be neglected then I_L can be presented as a short-circuit current I_{SC}, that is $I_L = I_{SC}$.

The higher coefficient of effectiveness of the solar elements, the closer the coefficient of ideality (n) of the junction to the unit. In this case n=1.02. After application of hydrogenated amorphous nitric of silicon as enlightening covering the effectiveness reached up to 23% (within the intensity of illumination in 100 mW/cm^2, AM1, open circuits voltage U_{oc}=0.88 mV, short-circuit current I_{sc}=15.3 mA/cm^2) due to decrease of rate of the surface recombination.

The repeated measurement of the element parameters after five years showed that their parameters didn't significantly change. So, it can be concluded that high effective elements can be created on the basis of hydrogenated amorphous silicon with the application of amorphous and monocrystalline films as the metal electrodes.

[1] Koladzie, S. Nowak. Characteristics of hydrogenated amorphous silicon thin film transistors fabricated by D.C. Magnetron sputtering.- *Thin Solid Films*, 1989, v. 175, N8, pp.37-42.

Received:18.03.02

THE REFLECTION OF THE CROSS -POLARIZED ELECTROMAGNETIC WAVE AT ITS INCIDENCE UNDER THE ANGLE ON THE TWO-LAYER DIELECTRIC-METAL SYSTEM

E. R. KASIMOV
Institute of Photoelectronics, Azerbaijan NAS
370141, F.Agayev str., 555 quarter, Baku

The conditions of the full reflectionless absorption origin of the cross-polarized electromagnetic wave at its incidence under the angle on the absorbing dielectric layer, applied on the metal substrate, were found. Its dependence on the cover thickness on the angle of the wave incidence, and on the dielectric properties of the cover material is under investigation.

The effect of the full or reflectionless radiation absorption occurs at the normal incidence of the plane-polarized electromagnetic wave on the absorbing cover, applied on the metal substrate [1]. The absorption has a spectral nature and manifests in the region of the cover substance dispersion at strictly fixed selective values of the incident radiation frequency and the cover layer thickness [2].

It is necessary to carry out the research of characteristics of the substance wave reflection in the wide interval of frequencies and thicknesses for the direct proof of this effect existence, what is hard to be realized. One of methods of this effect experimental detection at the fixed frequency of the incident radiation is realized by results of characteristics of the microwave radiation reflection by binary solutions of polar liquids in non-polar solvents, obtained in works [3,4].

It was established, that at the given frequency of the incident radiation the full wave absorption in polar molecule solutions occurs at strictly fixed, belonged to the given solution, layer thickness and concentrations of the polar solution component. Obviously, similar experimental proofs of this effect existence in pure substances at the given radiation frequency may be realized by research of their wave reflection characteristics with the change of the cover substance temperature or the angle of the wave incidence on it.

For the basis of the last proof, let's examine theoretical conditions of the full radiation absorption origin at its incidence under the angle á$_0$ to the surface of the plane layer of the absorbing dielectric, applied on the ideal metal substrate.

The thickness l of the layer cover is regulated, and the cover substance has the complex value of the dielectric constant $\varepsilon=\varepsilon'-i\varepsilon''$, where ε' is the dielectric constant and ε'' is dielectric losses. With regard of the vector position of the electric polarization E of the wave with respect to the plane of its incidence, we will distinguish reflection cases of the parallel-polarized (TH type wave) and cross-polarized (TE type wave) wave, respectively when the vector E is parallel and perpendicular to the plane of the wave incidence. As the initial step let's confine by the case of the reflection from such two-layer system of the cross-polarized wave.

For the given type of the incident wave polarization, the complex expression of the wave reflection coefficient ρ from the examined plane two-layer system is equal to:

$$\dot{r} = \frac{Z_{âõ}\cos\alpha_0 - Z_0\cos\alpha}{Z_{âõ}\cos\alpha_0 + Z_0\cos\alpha} \qquad (1)$$

where $Z_{bx}=Zthgl$ the input resistance of the two-layer system, Z_0, Z are the wave resistances of the vacuum and the cover substance, respectively, $\cos\alpha = \sqrt{1-\sin^2\alpha_0/\varepsilon}$; α is the angle of the wave refraction in the cover layer and is simultaneously the angle of the wave incidence on the dielectric-metal interface, l is the thickness of the cover layer [5-7].

The constant of the wave distribution γ in the cover substance included in the expression for the input resistance, is equal to:

$$\gamma = \gamma_0\frac{\cos\alpha}{\cos\alpha_0} \quad ; \qquad (2)$$

where $\gamma_0=i2\pi/\lambda$, λ is the constant of the wave distribution and the wave length in the vacuum, respectively.

The reflectionless wave absorption in the examined two-layer system may occur in the minimum point of the dependence of the modulus of the wave reflection coefficient ρ on the thickness l of the cover layer and at the fulfillment of the condition ρ=0 in this point. Let's introduce notations $\varrho=\sin 2\alpha_0$ and $l_b = l/\sqrt{1-p}$, λ_b is the wave length in the free space in the direction of the wave spreading respectively to the normal to the layer surface. As $Z = Z_0/\sqrt{\varepsilon}$, then with regard of expressions (1) – (2) and accepted symbols, the condition of the full radiation absorption may be represented in the form:

$$th\frac{2\pi l}{\lambda_b}\sqrt{\varepsilon^\bullet} = \frac{Z_0\cos\alpha}{Z\cos\alpha_0} = \sqrt{\varepsilon^\bullet} \quad ; \qquad (3)$$

where

$$\varepsilon^\bullet = \varepsilon_1 - i\varepsilon_2\,; \quad \varepsilon_1 = \frac{\varepsilon' - p}{1-p}\ ;\ \varepsilon_2 = \frac{\varepsilon''}{1-p}\ .$$

The dielectric constant ε' and dielectric losses ε'' of the cover substance are connected with the refraction coefficient n and the factor of dielectric losses of this substance by known equations:

$$\varepsilon' = n^2\left(1-y^2\right);\ \varepsilon'' = 2n^2y \quad ; \qquad (4)$$

where $n = \lambda/\lambda_g$; $y = tg\delta/2$; $\delta = arctg\,\varepsilon''/\varepsilon'$; λ_g is the wave length in the cover material.

For the convenience of the further examination let's assume, that ε_1 and ε_2 by the analogy to the expression (4) are represented in the form:

$$\varepsilon_1 = \hat{n}^2(1-\hat{y}^2)\ ;\ \varepsilon_2 = 2\hat{n}^2\hat{y}\ ; \qquad (5)$$

where $\hat{n} = \lambda_b / \lambda_g^{\bullet}$; $\hat{y} = tg\delta^{\bullet}/2$; $\delta^{\bullet} = arctg\,\varepsilon_2/\varepsilon_1$; $\lambda_g^{\bullet}$ is the wave length in the cover substance at the wave spreading under the given angle to its limiting plane surfaces.

Using this notations in equations (3), after transformations we receive:

$$th(2\pi x\hat{y} + i2\pi x) = \hat{n}(1-i\hat{y})\ ; \qquad (6)$$

where $x = l / \lambda_g^{\bullet}$.

Let‘s divide the equation (6) on imaginary and real parts. After corresponding transformations we receive two equations, which describe the condition of the reflectionless wave absorption in the examined system:

$$\hat{y}sh4\pi x\hat{y} + \sin 4\pi x = 0\ ; \qquad (7)$$

$$\hat{n}(1+\hat{y}^2) = th2\pi x\hat{y} - \hat{y}tg2\pi x\ . \qquad (8)$$

From their joint solution, we have:

$$th4\pi x\hat{y} = \frac{2\hat{n}}{\hat{n}^2(1+\hat{y}^2)+1}; \qquad (9)$$

$$tg4\pi x = \frac{2\hat{n}\hat{y}}{\hat{n}^2(1+\hat{y}^2)-1}. \qquad (10)$$

As conditions of the reflectionless wave absorption in the system are fulfilled in the minimum point of the dependence ρ on l and at cover thicknesses, close to the values multiple to $\lambda_g^{\bullet}/4$, let‘s take, that:

$$x = \frac{2N-1}{4} + \Delta; \qquad (11)$$

where *N* is a number of the zero minimum of the dependence ρ on *l*, Δ is in common case is low, but not the zero value, determined from the joint solution of equations (10) and (11):

$$\Delta = \frac{1}{4\pi} arctg \frac{2\hat{n}\hat{y}}{\hat{n}^2(1+\hat{y}^2)-1}\ . \qquad (12)$$

By substituting expression (12) in equations (9) and (10) and excluding the value Δ as the intermediate parameter, we receive:

$$\pi(2N-1) + arctg\frac{2\hat{n}\hat{y}}{\hat{n}^2(1+\hat{y}^2)-1} = \frac{1}{2\hat{y}} ln\frac{(1+\hat{n})^2+(\hat{n}\hat{y})^2}{(1-\hat{n})^2+(\hat{n}\hat{y})^2}\ . \qquad (13)$$

The equation (13) determines the connection between values $\hat{n}$ and $\hat{y}$, and consequently, between ε' and ε of the cover substance of the two-layer system, at which the full absorption of the incident radiation occurs in the system. The required thickness of the cover layer is determined, as it follows from equations (11) and (12) from the expression

$$\frac{l_0}{\lambda} = \frac{1}{\hat{n}\sqrt{1-p}}\left[\frac{(2N-1)}{4} + arctg\frac{2\hat{n}\hat{y}}{\hat{n}^2(1+\hat{y}^2)-1}\right] \qquad (14).$$

Obtained equations (12)-(14) were used for the dependence determination between selective values ε', ε'', l_0 of the cover substance, the length of the radiation wave ë and the angle of the wave incidence á$_0$, at which conditions of the full absorption of the electromagnetic radiation in the examined two-layer system is fulfilled. These dependences at N=1,2 and 3 are given on the fig.1. Dependences ε''on ε' shift to the X axis with the value á$_0$ growthand at á$_0$=90 coincide with it. At the given number of the zero minimum N of the function ρ(l) all curves of the family are placed below the limiting dependence for á$_0$=0, which corresponds to the case of the normal wave incidence. The similar family type of curves $\varepsilon''(\varepsilon')$ exists also at the growth of N, but with closer its position to the X axis (see fig. 1b,c).

Selective values of the cover layer thickness l_0 increase with $\varepsilon'$and á$_0$ growth and reduce with growth of N, but numerically they are always higher than the multiple value $\lambda_g^{\bullet}/4$. The value of these deflections Ä on the multiplicity reduces with å$^{/}$ and N growth (see fig.2).

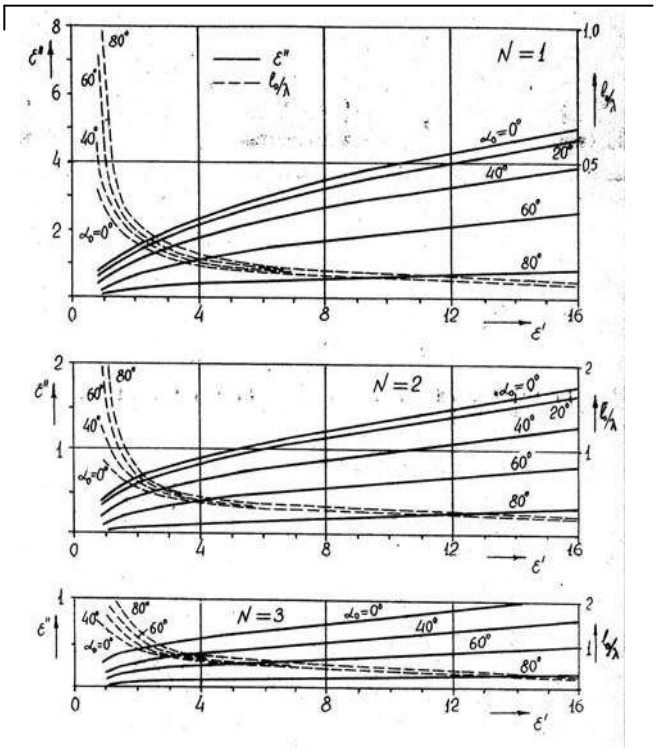

Fig.1. The dependence between the dielectric constant ε' and dielectric losses ε'' at the reflectionless absorption of the cross-polarized wave, incident under the angle á$_0$ on the two-layer dielectric metal system at *N*=1,2,3. *N* is the number of the zero minimum of the dependence of the modulus of the wave reflection coefficient on the thickness of the cover layer.

Selective values of the wave incidence angles and corresponding to them the cover layer thickness, at which the wave reflection is absent, may be determined by equations (12)-(14) or graphically; if values ε'_0 and ε''_0 of the cover substance are known for the given frequency of the incident radiation.

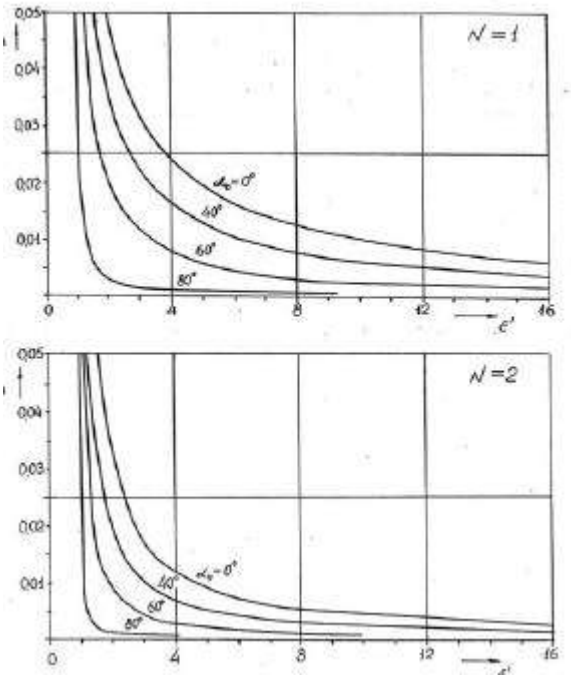

Fig.2. The deflection value *D* of the cover layer thickness on multiple values of wave length quarter in the cover substance versus its dielectric constant and the incidence angle á$_0$ at *N*=1,2; N is the number of the zero minimum of the dependence of the modulus of the wave reflection coefficient on the thickness of the cover layer.

It follows from the fig.1, that if the working point with such values ε'_0 and ε''_0 is placed in the coordinate plane [ε', ε''] at N=1, which is higher than the limiting dependence for á$_0$=0, then the manifestation of the reflectionless radiation absorption is impossible in the two-layer system with such cover. If the working point with such values ε'_0, ε''_0 is placed between two limiting dependences with N=1 and N=k, then in such cover substance k-1 of strictly fixed angles of the wave incidence and corresponding to them the thickness of the cover layer, at which the full absorption of the incident radiation occurs, are observed. The lesser selected thickness of the cover layer will correspond to the greater angle of the reflectionless wave incidence.

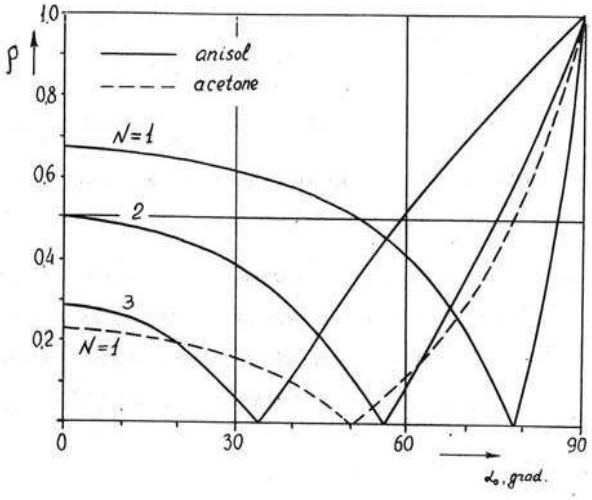

Fig.3. The dependence of the modulus of the cross-polarized wave reflection coefficient ρ on its incidence angle α_0 on the two-layer dielectric-metal system.

Dependences of the modulus of the wave reflection coefficient of the two layer system on the angle of the radiation incidence on the cover layer at the calculated selective values of its thicknesses at the wave length of the incident radiation ë=3.2 cm are presented on fig.3. The polar liquids with known values ε' and ε'' were used as the cover substance at this wave length and the temperature 20° C [8]. At ë=3.2 cm for acetone ε' =20.5, ε''=3.55 and its working point in the coordinate plane [ε', ε''] is placed between limiting curves 1 and 2 for the case á$_0$=0. Therefore, for acetone the reflectionless absorption of the incident radiation is expected only at á$_0$=51.1° (N=1) and at the relative cover thickness *l*/ë=0.056. Unlike the acetone, for anizole ε' =3.04, ε'' =0.38, and its working point is placed between limiting curves 1 and 4. In accordance with conducted calculations, the reflectionless radiation absorption should exist for the anizole at incidence angles 78.0°(N=1), 55.7°(N=2); 33.8°(N=3), respectively, and at the corresponding relative thickness *l*/ë of the cover layer: 0.174, 0.49 and 0.76.

Obtained results allow to express the supposition on possibilities of the experimental observation of the reflectionless absorption of the electromagnetic radiation, incident under the angle on the absorbing cover, applied on the metal substrate.

[1] R.M. Kasimov. Engineer-physical journal, 1994,v .67, ¹ 5-6, p.489-492.
[2] M.A. Sadikhov, E.R. Kasimov, R.M. Kasimov, Ch.O. Qajar. Physics 1998, v.4, ¹4, p.63-66.
[3] E.R. Kasimov, M.A. Kalaphi, Ch.O. Qajar. Physics, 1995, v. 1, ¹ 2, p.37-44.
[4] R.M. Kasimov, M.A. Kalaphi, E.R. Kasimov, Ch.O. Qajar, E.Y. Salayev. Journal of the technical physics, 1996, v.66, ¹ 5, p.167-171.
[5] A.F. Kharvei: " The technique of superhigh frequencies" M: Issue Sov. Radio, 1965, part 1, p.724.
[6] L.M. Brekhovskikh. "Waves in layered mediums" M: Issue AN SSSR, 1967, p.502.
[7] J. Preiâner. NTZ Arch, 1989, v.11, ¹ 4, p.175 -182.
[8] Y.Y. Akhadov. "Dielectric parameters of pure liquids" M: Issue MAI, 1999, p.856.

Received: 10.04.02

INFLUENCE OF ELECTRON-ELECTRON COLOUMB REPULSION ON PHOTOTHRESHOLD OF THE GROUP III-VI LAYERED SEMICONDUCTORS

F.M. HASHIMZADE, N.B. MUSTAFAEV
Institute of Physics Azerbaijan National Academy of Sciences
H. Javid av, 33, Baku, 370143

The photothreshold correction related to electronic relaxation has been calculated for the group III-VI layered semiconductors. The band structure and anisotropy of dielectric permeability of the semiconductors have been taken into account. Results of the calculation are compared with experimental data. The best agreement is obtained for GaSe.

1.Introduction

The group III-VI layered semiconductors are useful for various electronic devices. The semiconductors consist of a pile of packets with atoms bound by covalent and ionic-covalent bonds inside the packet, whereas between the packets there are only weak Van der Waals forces. As a consequence, the semiconductors are easily cleaved parallel to the layers, and the resultant surfaces are very smooth. The surfaces are inert against adsorption, and they have a low density of surface states. These features of the layered semiconductors facilitate greatly the fabrication of homojunctions, heterojunctions, metal-semiconductor Schottky barriers and metal-insulator-semiconductor structures (see e.g. Ref.1). They can be used as photodiodes, high-speed switches, spectral and/or electric memory devices, light modulators and solar energy converters.

The molecular-beam epitaxial growth of InSe and GaSe crystals reported in Refs.2 and 3 makes it also possible to build InSe/GaSe quantum-well structures and superlattices. For such structures, theoretical studies of energy spectrum were made in Refs.4 and 5. It follows from the considerations that a determination of the band parameters has paramount importance for the group III-VI layered crystals.

2. Photothreshold Problem

By definition, a photothreshold *Ö* is the energy required for an electron transition from the top of valence band to the vacuum level. For diamond-like crystals, it has been stated that experimental values of Ö are by 3 to 4 eV smaller than the energy value at the top of valence band calculated using the tight-binding method (see Ref.6). Similar disagreement between experimental and calculated values of work of exit occurs also in metals. In paper [7], a shift of the photoemission threshold of metals was interpreted in terms of the electron-electron Coloumb repulsion. In principle, the same interpretation had been suggested earlier by authors of paper [8] in order to explain the Coloumb shift of photothreshold in diamond-like semiconductors. According to Ref.8, the photothresholds are considerably lowered due to the relaxation of valence electrons around positive hole. A certain amount of negative polarization charge is attracted from the hole during the relaxation. It repels the photoelectron and increases its kinetic energy by the same amount that the remaining electron system of total Coloumb energy loses in the final state as compared with the initial state. If the hole relaxation self-energies are subtracted from the distances between valence-band maxima and vacuum level, then the large discrepancies between one-electron LCAO predictions and experimental observations of photothreshold are essentially removed. However, some difference (less than 1 *eV*) remains by reason of surface charge and other effects discussed in Ref.9.

In the present paper, the energy correction related to electron-electron correlation has been calculated for the group III-VI layered semiconductors. The approach developed in Ref.8 has been used. We have modified the calculation procedure in order to take into account the anisotropy of dielectric permeability in the layered semiconductors. The valence-band wavefunctions needed for our calculation have been taken from Ref.10. According to Ref.10, the valence-band top in the group III-VI layered semiconductors is formed only by valence-electron states of cation. For these semiconductors, the top energy values were obtained by using conventional one-electron tight-binding theory [11, 12] and empirical pseudopotential method [13]. In Refs.12 and 13, the absolute position of energy bands was not given. Nevertheless, one can determine energies of valence-band maxima starting from the given position of *s*-level of the anion. In order to evaluate photothreshold, the energy correction calculated by us has to be subtracted from the values of valence-band top energy given in Refs.11-13. The photothreshold values calculated in this manner have been compared with their experimental values given in Refs.14-17.

3. Basic Formulae

The correlation part of self-energy due to electron relaxation is defined as [8]

$$\Sigma_v^{rel}(\vec{k}) = \frac{1}{2}\int \frac{d\vec{q}}{(2\pi)^3}[V_0(\vec{q}) - V(\vec{q})] \ , \qquad (1)$$

where

$$V_0(\vec{q}) = \frac{4\pi}{q^2} e^2 \mid \rho_v(\vec{q}) \mid^2 \quad , \qquad (2)$$

$$\rho_v(\vec{q}) = \int d\vec{r} \exp(i\vec{q}\vec{r}) \psi^*_{v\vec{k}}(\vec{r}) \psi_{v\vec{k}}(\vec{r}) \ , \qquad (3)$$

Here ψ_{vk} is the Bloch wavefunction of a valence electron, $V_0(\vec{q})$ is the Fourier transformation of the electrostatic interaction potential, and $V(\vec{q})$ is the Fourier transformation of the screened Coulomb potential.

Within the bond-orbital approximation, the Bloch factor for electrons (at the top of valence band) has the following form [10]:

$$f_v(\vec{r}) = \left(1 + b_c^2\right)^{-1/2}\left[b_c f_s^c(\vec{r}) \mp f_{p_z}^c(\vec{r})\right] \quad (4)$$

Here

$$f_s^c(\vec{r}) = \frac{1}{\sqrt{3\pi}} b_c^{5/2} r \exp(-b_c r) \quad (5)$$

and

$$f_{p_z}^c(\vec{r}) = \sqrt{\frac{2b_c^7}{15\pi}} zr \exp(-b_c r) \quad (6)$$

are the Slater wavefunctions of a cation atom (these functions are often used for LCAO calculations), b_c is a parameter which characterizes the hybridization of electronic *s*- and p_z - states of the cation.

The signs $\mp$ refer to two different cations taking part in the cation-cation covalent bond. As for b_c, in Ref.8 this parameter is given for cubic crystals in the units of $2\pi/a$ (a is the lattice constant). For our calculations, it is more convenient to give b_c in units of the reciprocal length of cation-anion bond *l*. In layered GaSe, InSe and GaS crystals, the values of *l* are close to those of GaAs, InAs and ZnS, respectively.

The Coulomb potential screening has been taken into account by analogy with Ref.8, but a distinction has been made between the components of static dielectric permeability parallel $\varepsilon_0^{||}$ and perpendicular $\varepsilon_0^{\perp}$ to the crystal axis *C*, i.e. we have used the following expression:

$$\varepsilon^j(\vec{q}) = 1 + \left[\left(\varepsilon_o^j - 1\right) - 1 + \frac{q^2}{q_{TF}^2} + \frac{4}{3}\cdot\frac{1}{(\pi_{aB})^2}\cdot\frac{q^4}{q_{TF}^6}\right]^{-1}, \quad (7)$$

where the superscript $j = ||, \perp$ corresponds to the directions parallel and perpendicular to *C*, a_B is the Bohr radius, and q_{TF} is the Thomas-Fermi wavevector of valence electrons.

4. Comparison with Experiment

Values of the parameters needed for numerical calculation are given in table 1.

Table 1.
Parameters of the group III-VI layered semiconductors.

	GaSe	GaS	InSe
b_c[10]	1.02	1.02	1.10
L (nm) [12,13]	0.246	0.234	0.263
$b_c l$	4.35	5.17	4.38
$\varepsilon_0^{\perp}$	7.44 [18]	7 [19]	6.2 [19]
$\varepsilon_0^{||}$	5.76 [18]	5.9 [19]	4.9 [19]
q_{TF}(nm^{-1})	19.438	19.833	18.765

In Table 2, we give values of the relaxation self-energy correction Σ_v^{rel} calculated on the basis of formulae (1) to (7). The difference between the value Σ_v^{rel} calculated by us and the valence-band top energy $|E_v|$ taken from [11] is given in the same table. A comparison of the difference $|E_v| - \Sigma_v^{rel}$ with the experimental values of photothreshold Φ_{exp}, given in table 2, shows the best agreement for GaSe.

Table 2.
The relaxation self-energy correction Σ_v^{rel}, the valence-band top energy $|E_v|$ and experimental values of photothreshold Φ_{exp}. All values are given in units of *eV*.`

	GaSe	GaS	InSe
Σ_v^{rel}	2.4	3	2.3
$\|E_v\|$ [11] - Σ_v^{rel}	5.5	4.9	5.4
$\Phi_{exp.}$ [14]	5.4±0.1	6.5±0.15	
$\Phi_{exp.}$ [15]	5.3 – 5.4	5.5 -5.8	5.8
$\Phi_{exp.}$ [16]			5.8
$\Phi_{exp.}$ [17]			5.0

We could not obtain a good agreement for GaS and InSe. Nevertheless, the agreement is not generally worse than for of the diamond-like semiconductors (see table 2 in [8]), and it is within an accuracy of the used calculation method. Some difference remains by reason of surface charge and other effects discussed in [9].

[1] *V.N.Katerinchuk, M.E.Kovalyuk, A.D.Ogorodnik.* Neorganicheskie Materialy (Inorganic Materials), 1996, v.32, p.937.

[2] *J.Y.Emery, L.Brahime-Ostmane, C.Hirlimann, A.Chevy.* J.Appl.Phys., 1992, v.71, p.3256.

[3] *A.Koma.* Surf.Sci., 1992, v.267, p.29.

[4] *[a].Erkoç, K.Allahverdi, Z.Ibrahim.* Solid State Commun., 1994, v.90, p.553.

[5] *F.M.Gashimzade, N.B.Mustafaev.* Z.Phys. B, 1996, v.99, p.219.

[6] *W.A.Harrison.* Electronic Structure and Properties of Solids. San Francisco, 1980.

[7] *B.A.Volkov, S.V.Sharov*. Zh.Eksp.Teor.Fiz. Pisma v Red., 1995, v.62, p.634.

[8] *F. Bechstedt, R. Enderlein, O. Heinrich.* Phys. Status Solidi (b), 1984, v.126, p.575.

[9] *F.Bechstedt, R.Enderlein.* Semiconductor Surfaces and Interfaces. Acad. Verlag, Berlin, 1988.

[10] *A.Nakanishi, T.Matsubara.* J. Phys. Soc. Japan, 1982, v.51, p.3219.

[11] *E.Doni, R.Girlanda, V.Grasso, A.Balzarotti, M.Piacentini.* Nuovo Cimento B, 1979, v.51, p.154.

[12] *J.Robertson.* J.Phys. C, 1979, v.12, p.4777.

[13] *Y.Depeursinge.* Nuovo Cimento B, 1981, v.64, p.111.

[14] *R.H.Williams, A.J.McEvoy.* Phys. Status Solidi (a), 1972, v.12, p.277.

[15] *G.Margaritondo, J.O.Rowe, S.B.Christman.* Phys.Rev. B, 1977, v.15, p.3844.

[16] *V.L.Bakumenko, Z.D.Kovalyuk, L.N.Kurbatov, V.G.Tagaev, V.F.Chishko.* Fiz.Tekh.Poluprovod., 1980, v.14, p.1115; Sov. Phys. Semicond., 1980, v.14, p.661.

[17] *S.G.Guseinov, G.D.Guseinov, G.G.Bannaev, P.G.Ismailova, G.A.Mamedova, E.G.Abdullaev.* Neorganicheskie Materialy [Inorganic Materials], 1993, v.29, p.781.

[18] *R.Toullec, N.Piccioli, M.Mejatty, M.Balkanski.* Nuovo Cimento, 1977, v.38 B, p.159.

[19] *K.R.Allakhverdiev, S.S.Babaev, E.Yu.Salaev, .M.Tagiev.* Phys. Status Solidi (b), 1979, v.96, p.177.

Received: 28.03.02

VAPOR PRESSURE AND OSMOTIC COEFFICIENTS USING BROMLEY EQUATION FOR 1:1 ELECTROLYTES IN METHANOL AT 298.15K

KARAMAT NASIRZADEH

Department of Chemistry, Faculty of Science, Azerbaijan University of Tarbiat Moallem, P.O.Box 51745-406, Tabriz, IRAN

In this study the Bromley model was developed for the non-aqueous electrolyte solutions. This model contains four adjustable parameters (ρ, B, B° and a) and has been used to estimate osmotic coefficients and vapor pressures of LiCl, LiBr, $LiCH_3COO$, KCH_3COO, $NaCH_3COO$, KI, NH_4SCN, NaSCN and NaBr in methanol at 298.15 K. In addition, comparisons were made to the model of Pitzer and Mayorga for the osmotic coefficients and vapor pressures of these electrolytes.

Keywords: Osmotic coefficient; Vapor pressure; Bromley Model; Mixtures; Methanol; Inorganic salts

INTRODUCTION

Simple methods for representing deviations from ideality in electrolyte solution are needed to design industrial processes, especially for transformation of raw materials and pollution control. In the past few decades, considerable progress has been made in measuring and modeling of thermodynamic properties of electrolyte systems. However, most of studies have been restricted by aqueous systems. Much less attention has been given to non-aqueous electrolyte solutions. In this article, the Bromley equations [1] is proposed for prediction of osmotic coefficients and vapor pressures of LiCl, LiBr, $LiCH_3COO$, $NaCH_3COO$, KCH_3COO, KI, NH_4SCN, NaSCN and NaBr in methanol based on the experimental isopiestic data of these electrolytes at 298.15 K. In our previous works [2,3] the Pitzer and Mayorga model [4,5] was used for the prediction of activity and osmotic coefficients of methanol + LiCl, LiBr and $+LiCH_3COO$ and self-consistent local composition [6] model (SCLC) was used for the prediction of osmotic coefficients and vapor pressures of $CaCl_2$ and $Ca(NO_3)_2$ in methanol at 298.15 K.

The Bromley model [1] contains four adjustable parameters (r, B, B°and a). In some aqueous and nonaqueous electrolyte solutions the parameter r=1 were used and three remaining parameters were calculated [1, 7]. In this study, the four parameters of the Bromley equations were calculated for methanol solutions of LiCl, LiBr, $LiCH_3COO$, $NaCH_3COO$, KCH_3COO, KI, NH_4SCN, NaSCN and NaBr. Furthermore, comparisons were made for osmotic coefficients and vapor pressures of investigated systems obtained with Bromley model to the model of Pitzer and Mayorga and experimental isopiestic measurements of our previous works.

BASIC DEFINITION AND THEORETICAL TREATMENTS

The isopiestic method is the most accurate, simple experimental technique available for measuring of the solvent activity of solutions that contain nonvolatile solutes. It is the base of phenomenon when different solutions, connected through the vapor space, approach to equilibrium by transfer of solvent mass by distillation. The accuracy of the method depends on the standard solutions that are used, sample mixing during the equilibration period, temperature stability, and the time allowed for the equilibration process. Equilibrium has been established one, the temperature and pressure are uniform through out the system, provided that no concentration gradients exist in the liquid phases. At the equilibrium the chemical potentials of the solvent in each of the solutions in the closed system are identical:

$$m_S^a = m_S^b = \ldots m_S^w \qquad (1)$$

where μ_s is the chemical potentials of the solvent in each of the solutions α through ω. The solvent activity is related to the solvent chemical potential by

$$\ln a_s = \frac{\left(m_s - m_s^o\right)}{RT} \qquad (2)$$

where a_s is the solvent activity, R is the gas constant, $\mu_s°$ is the standard state chemical potential of the solvent, and T is the absolute temperature. After the equilibrium, the solvent activity equals between the investigated solutions. Since the solvent activity is known for one or more standard solutions, it will be known for each solution within the isopiestic system.

Several models are available in the literature for the correlation of osmotic coefficients as a function of molalities. The model of Pitzer and Mayorga [4,5] has been successfully used for aqueous, in a few cases, for non-aqueous electrolyte solutions [2,3]. The experimental osmotic coefficients data were correlated with the model of Pitzer and Mayorga [6] for solutions of LiCl, LiBr, $LiCH_3COO$, KCH_3COO, $NaCH_3COO$, KI, NH_4SCN, NaSCN and NaBr in methanol. For 1:1 electrolytes, this model has the following form

$$\phi - 1 = f^f + mB^f + m^2C^f, \qquad (3)$$

where

$$f^f = -A_f I^{1/2}/(1+bI^{1/2}), \qquad (4)$$

$$A_f = (1/3)(2\pi N_A d_s)^{1/2}(e^2/4\pi\varepsilon_0 DkT)^{3/2}, \qquad (5)$$

and

$$B^f = \beta^{(0)} + \beta^{(1)} exp[-\alpha_{(1)} I^{1/2}]. \qquad (6)$$

For some aqueous and non-aqueous electrolyte solutions, it was found that by adding a $\beta^{(2)}$ term to equation (6) better

agreement with the experimental results could be obtained with the Pitzer model [2].

$$B^f = b^{(0)} + b^{(1)} exp[-a_{(1)} I^{1/2}] + b^{(2)} exp[-a_{(2)} I^{1/2}] \quad (7)$$

In these equations $b^{(0)}$, $b^{(1)}$, $b^{(2)}$ and C^f are Pitzers ion-interaction parameters, $a_{(1)}$, $a_{(2)}$ and b are adjustable parameters, and A_f is Debye-Hückel (DH) constant for the osmotic coefficient on the molal basis. The remaining symbols have their usual meaning. For methanol solutions A_f=1.294 $Kg^{1/2} \cdot mol^{-1/2}$ was calculated using equation (5). From the analysis of the experimental osmotic coefficient data, Zafarani-Moattar and Nasirzadeh [2] found that the values of b=3.2 $Kg^{1/2} \cdot mol^{-1/2}$, $a_{(1)}$=2.0 $Kg^{1/2} \cdot mol^{-1/2}$ and $a_{(2)}$=1.4 $Kg^{1/2} \cdot mol^{-1/2}$ were satisfactory at 298.15 K. Ion-interaction parameters were obtained from the fitting experimental osmotic coefficient data for the investigated systems and are shown in Table 1. In this table $b^{(0)}$, $b^{(1)}$, $b^{(2)}$ and C^f are the Pitzer parameters, $s(f)$ and $s(p)$ are the standard deviation for the osmotic coefficients and vapor pressures, respectively.

Table 1.

Pitzer parameters for methanol solutions of LiCl, LiBr, $LiCH_3COO$, KCH_3COO, $NaCH_3COO$, KI, NH_4SCN, NaSCN and NaBr calculated from osmotic coefficients at 25°C.

No.of data	molality range	β°	β1	β2	Cϕ	σ(ϕ)	σ(p) /kPa
	LiCl						
32	0.22-4.18	-0.11458 0.02167	-3.95303 0.09548	3.421 0	0.06478 0.01431	0.006 0.015	0.008 0.021
	LiBr						
27	0.19-3.90	0.00275 0.24842	-2.6665 0.06083	2.238 0	0.05542 0.01649	0.005 0.009	0.003 0.005
	$LiCH_3COO$						
20	0.24-3.01	0.19224 0.05542	1.39440 0.06113	-1.202 0	-0.01017 0.014365	0.004 0.005	0.005 0.008
	KCH_3COO						
23	0.18– 2.51	0.008128 0.114109	-0.687219 0.200517	0.838449 0	0.004572 -0.016451	0.0001 0.001	0.0002 0.0005
	$NaCH_3COO$						
26	0.26 -1.76	-0.128391 0.174060	-2.118794 -0.165151	1.9988 0	0.026218 -0.047509	0.002 0.003	0.005 0.008
	KI						
19	0.13 -0.98	-0.983997 0.215944	-5.000851 0.109784	6.0448 0	0.322375 -0.079194	0.001 0.002	0.0002 0.0004
	NH_4SCN						
24	0.36 –4.35	0.056495 0.141341	-1.085211 0.079836	0.9453 0	-0.00583 -0.018001	0.008 0.009	0.009 0.002
	NaSCN						
24	0.16-3.36	0.184719 0.283717	-0.904255 0.020163	0.8182 0	-0.007136 -0.022223	0.005 0.006	0.007 0.009
	NaBr						
18	0.18 –1.57	0.757993 -0.027613	5.607655 0.838263	-4.98352 0	-0.098082 0.102425	0.002 0.004	0.002 0.005

[a] A_ϕ=1.294 $kg^{1/2} \cdot mol^{-1/2}$; b=3.2 $kg^{1/2} \cdot mol^{-1/2}$; α(1)=2 $kg^{1/2} \cdot mol^{-1/2}$; α(2)=1.4 $kg^{1/2} \cdot mol^{-1/2}$.

The Bromley equations [1] are:

$$f - 1 = A f |Z_+ Z_-| \sqrt{I}.s\left(r\sqrt{I}\right) + 2.303(B^o - B)\left(\frac{I}{2}\right) j(aI) + 2.303\left(\frac{I}{2}\right), \quad (8)$$

where

$$s(r\sqrt{I}) = \left(\frac{3}{r^3\sqrt{I}}\right)\left[1 + r\sqrt{I} - \frac{1}{1 + r\sqrt{I}} - 2\ln(1 + r\sqrt{I})\right] \quad (9)$$

$$Y(aI) = \left(\frac{2}{aI}\right)\left[\frac{1 + 2aI}{(1 + aI)} - \ln\frac{1 + aI}{aI}\right] \quad (10)$$

In these equations F is the osmotic coefficient and other parameters have the usual meaning.

The Bromley model contains four adjustable parameters (r, B, B°and a). These parameters for the LiCl, LiBr, $LiCH_3COO$, KCH_3COO, $NaCH_3COO$, KI, NH_4SCN, NaSCN and NaBr in methanol solutions were calculated and are shown in table 2. In this table ρ, B, B°and a are the Bromley parameters, σ(ϕ) and σ(p) are the standard deviation for the osmotic coefficients and vapor pressures of this solutions, respectively.

Table 2.

Bromley parameters of LiCl, LiBr, $LiCH_3COO$, KCH_3COO, $NaCH_3COO$, KI, NH_4SCN, NaSCN and NaBr in methanol solutions at 25°C

salts	no. of points	r	$B°$	B	A	$s(f)$	$s(p)$
LiCl	32	1.4345	-7.488×10^{7}	0.22	83.836	0.0234	0.006
LiBr	27	1.4676	-2.245×10^{5}	0.2463	3.7026×10^{8}	0.0020	0.004
$LiCH_3COO$	20	1.5517	-7.3676×10^{6}	0.0634	5.1877×10^{9}	0.0103	0.015
KCH_3COO	23	2.1762	588.7344	0.0197	6.2388×10^{4}	0.0027	0.006
$NaCH_3COO$	27	1.9307	469.3899	0.0249	2.6746×10^{4}	0.0045	0.012
KI	19	2.167	0.0545	0.0548	-0.8615	0.0021	0.005
NH_4SCN	24	2.3069	5.1258×10^{4}	0.0213	1.7539×10^{7}	0.0146	0.021
NaSCN	24	2.1806	5.5277×10^{5}	0.1347	1.0294×10^{8}	0.0115	0.017
NaBr	18	1.9985	-1.9702×10^{8}	0.1072	39.616	0.0125	0.019

Bromley also has presented a one-parameter version of his model for aqueous systems by setting

$$(B°-B)=(0.06-0.6B)|Z_+Z_-| \qquad (11)$$

and

$$a=\frac{1.5}{Z_+Z_-}.$$

Use of equations (11) and (12) with the Bromley model for the methanol systems gave, as expected, very poor results [7] and didn't present in this paper.

CONCLUSION

Tables 1 and 2 shows the Pitzer and Bromley parameters for the electrolytes of LiCl, LiBr, $LiCH_3COO$, KCH_3COO, $NaCH_3COO$, KI, NH_4SCN, NaSCN and NaBr in methanol solutions at 25°C respectively.

The Bromley model was found to correlate the experimental data with good accuracy.

The application of both forms of the Pitzer model has been shown to correlate the experimental osmotic coefficient data with very good accuracy, especially using the Pitzer model with the $B^{(2)}$ term. Data analysis shows that the values of b=3.2$Kg^{1/2}\cdot mol^{-1/2}$, $\alpha_{(1)}$=2.0$Kg^{1/2}\cdot mol^{-1/2}$ and $\alpha_{(2)}$=1.4$Kg^{1/2}\cdot mol^{-1/2}$, based on the optimum representation of the Lithium salts+methanol systems, also give the better overall results for other salts in methanol systems. For some of the electrolytes studied in this work, relatively large negative numbers were found for $B^{(2)}$, which may indicate significant ion-pairing of these electrolytes in methanol.

[1] *L.A. Bromley*; AIChE J; 19, 1973, 313-320

[2] *M. T. Zafarani-Moattar and K. Nasirzadeh*, J. Chem. Eng. Data, 43, 1998, 215-219.

[3] *M. T. Zafarani-Moattar, J. Jahanbin, K.Nasirzadeh*; Fluid Phase Equilibria; 2002, (In press)

[4] *K.S.Pitzer;G.Mayorga;* J. Phys. Chem.; 77(19), 1973, 2300-2308.

[5] *K.S. Pitzer, , "Activity coefficient in Electrolyte solutions"*, 2nd ed., CRC Press, 1991.

[6] *M.S. Ananth and S. Ramachandran*, AIChE J., 36, 1990, 370-386.

[7] *Tamasula,P.;Czerwienski,J.Gregory;P.Tassions;*Fluid Phase Equilibria, 38, 1987, 129-153.

Received: 29.04.02

ABOUT THE THEORY OF THE NON-HEISENBERG MAGNETS

A.M. SULEIMANOV, M.B. HUSEINOV
The Institute of Physics, National Azerbaijan Academy of Sciences,
H.Javid ave. 33, Baku

The non-Heisenberg crystal has been investigated when the atom states multiplicity is taken into account. The additional branches in the spectrum of spin excitations have been obtained. The curves of the frequency dependence on the wave vector and the external magnetic field have been constructed.

In non-Heisenberg magnetics the terms of the higher order have been taken into consideration side in addition to the bilinear exchange [1,2].

In these works it is usually assumed, that the exchange parameters of the higher order are much smaller than parameters of the bilinear exchange.

In the present work the case, when parameters of bilinear and biquadratic exchange are equal has been investigated.

It is known, that the atom with the spin S has $2S+1$ energy states (the atom states multiplicity). The method of standard basic operators (SBO) [3], which allows to consider the atom states multiplicity has been chosen for the mathematical apparatus.

For the spin $S=1$ case, which we have considered, the spin operators are expressed through SBO by the following way:

$$\begin{aligned} S_i^+ &= \sqrt{2}(L_{12}^i + L_{23}^i) \\ S_i^- &= \sqrt{2}(L_{21}^i + L_{32}^i) \\ S_i^z &= L_{11}^i + L_{33}^i) \end{aligned} \tag{1}$$

L_{ab}^i are SBO, characterizing the spin transition between a and b states in the site i.

The Hamiltonian for the case under consideration has a form:

$$H = -J\sum_{i,j} S_i S_j - B\sum_{i,j}(S_i S_j)^2 - V\sum_i (S_i^z)^2 - h\sum_i S_i^z \tag{2}$$

where J and B are parameters of bilinear and biquadratic exchange, respectively, V is the single-ion anisotropy; $h=g\mu_B H$; H is an external magnetic field, g is the *Lande* factor; μ_B is the Bohr magneton . If we assume that $J=B$, then

$$H = -J\left[\sum_{i,j} S_i S_j + \sum_{i,j}(S_i S_j)^2\right] - V\sum_i (S_i^z)^2 - h\sum_i S_i^z \tag{3}$$

From (1), (3) and the equation of motion:

$$i\frac{dL_{ab}^j}{dt} = \left[L_{ab}^j, H\right] \tag{4}$$

we will calculate for spin excitation frequencies :

$$\begin{aligned} \omega_1(\vec{k}) &= 2J(0)(D_{13} - D_{23}) - 2J(\vec{k})D_{12} + V + h \\ \omega_2(\vec{k}) &= 2J(0)(D_{13} - D_{23}) - 2J(\vec{k})D_{23} - V + h \end{aligned} \tag{5}$$

$$\omega_3(\vec{k}) = 2\left[J(0) - J(\vec{k})\right]D_{13} + 2h \tag{6}$$

$D_{ab}=D_a-D_b$, D_a is the occupation probability of the level a.

Frequencies ω_1 and ω_2 correspond to the excitations with the change of S_z by $1(|\Delta S_z| = 1)$ and frequency ω_3 corresponds to the excitation with the change of S_z by $2(|\Delta S_z| = 2)$.

The energy gap ($k=0,h=0$) looks as :

$$\begin{aligned} \omega_1(0) &= V \\ \omega_2(0) &= -V \\ \omega_3(0) &= 0 \end{aligned} \tag{7}$$

For the simple cubic crystal the frequency dependence on the wave vector $\vec{k}$ reads:

$$\begin{aligned} \omega_1(k) &= V + h + \frac{1}{3}J(0)\hat{e}^2 \quad \text{(does not depend on k)} \\ \omega_2(\hat{e}) &= V + h \\ \omega_3(\hat{e}) &= zh + \frac{1}{3}J(0)k^2 \end{aligned} \tag{8}$$

Schemes of frequencies dependence on $\vec{k}$ in the isotropic case ($V=0$) are presented on fig.1.

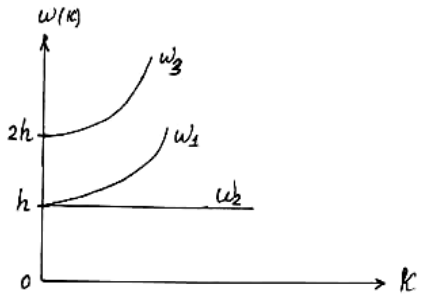

Fig.1. Dependence *w(k)* on the wave vector *k* for the isotropic crystal.

In the case of $k=0$ the frequencies dependence on the external field is presented on fig.2.

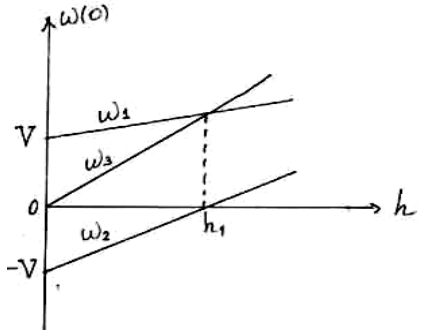

Fig.2. Field dependence of frequencies for the case $k=0$ $(h1=V)$.

As it is seen from the figure when $h=V$, $w_1=w_3, w_2=0$. It means that levels with $S_z=0$ and $S_z=-1$ coincide when $h=V$, and therefore $w_2=0$, $w_1=w_3$.

Let us note that w_1 corresponds to the transition between states $S_z=0$ and $S_z=1$, w_2 – between $S_z=0$ and $S_z=-1$, and w_3- between $S_z=1$ and $S_z=-1$.

We have for the probability of levels filling:

$$D_1 = \frac{1}{F}(1+f_1)(1+f_2)$$
$$D_2 = \frac{1}{F} f_1(1+f_2) \qquad (9)$$
$$D_3 = \frac{1}{F} f_1 f_2$$

$F = 1 + 2f_1 + f_2 + 3f_1 f_2$; $\quad f_1 = \left(e^{\frac{w_i}{kT}} - 1 \right)$ the function of Bose-Einstein distribution.

In the region of low temperatures parameters of dipole and quadrupole ordering

$$t = 1 - \frac{1}{N}\sum_n f(w_1) \qquad (10)$$

$$Z = 1 - \frac{3}{N}\sum_k f(w_2) \qquad (11)$$

In this temperature area t and Z depend on the temperature according to the law $T^{3/2}$. At high temperatures:

$$s = \frac{4}{J(0)}(q_c - q)^{1/2} \qquad (12)$$

$$Z = \frac{3}{J(0)}(q_c - q) \qquad (13)$$

where $q_c = \frac{4J(0)}{3}$ is the Curie temperature, $q = \frac{T}{J(0)}$.

[1] *E.L.Nagayev*. UFN; 1982; 136; issue 1; p. 61-103.
[2] *Y.M.Seyidov, M.B.Huseynov, N.G.Huseynov.* FMM, 1985,59, issue 2, p. 253-260.
[3] *S.B.Haley and Erdos P.* Phys.Rev.B.1972, v. 5, p.1106-1119.k

Received: 08.11.01

INFLUENCE OF TEMPERATURE-TEMPORARY CONDITION OF CRYSTALLIZATION AND DISCHARGE PROCESSING ON SPECTRA OF PHOTOLUMINESCENCE OF COMPOSITIONS ON THE BASIS OF POLYMER – SEMICONDUCTOR

A.A. ISMAYILOV, M.A. RAMAZANOV
Institute of Physics of National Academy of Sciences of Azerbaijan
370143, H. Javid Av. 33 a, Baku, Azerbaijan

The influence of temperature-temporary condition of crystallization of polymer matrix and discharge processing on the spectra of photoluminescence of compositions on the basis of 70% PVDF + 30% CdS and 70% PEHD + 30% CdS at the range of wavelengths l=350÷650 nm is investigated. The assumption is stated that the technology of reception and discharge processing of composition influences on interaction between phases, on structure of interphase layer and on charging condition of the composition.

The change photoelectric and electrophysical properties of polymer compositions on the basis of polymer – semiconductor can occur not only at the expense of variation of these properties of separate components, and also at the expense of change of interaction between phases of a polymer matrix and particles of semiconductor [1-3]. The interaction between phases besides their nature also depends on other factors, for example, on technology of composition preparation, on influence of external factors on them. One of the ways of change of interphase interactions in polymer compositions is their preparation at various temperature-temporary conditions of crystallization and discharge processing.

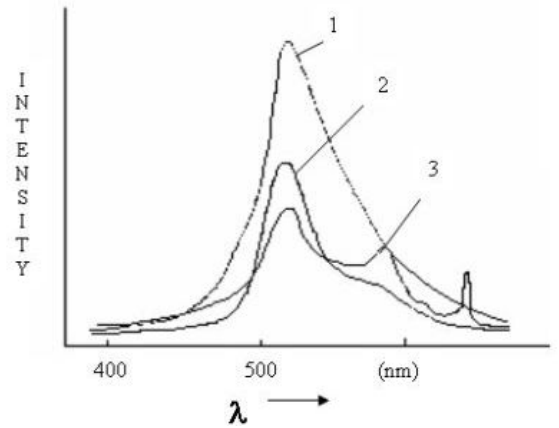

Fig.1. Spectra of photoluminescence of compositions 70% PVDF+ +30% CdS at T=293K 1. pure CdS; 2. 70% PVDF+30% CdS by FC; 3. 70% PVDF + 30% CdS by SC

In the given work the results of research of influence of temperature-temporary conditions of crystallization of polymer matrixes and discharge processing on photoluminescence of compositions on the basis of Polyvinylidenfluoride (PVDF), Polyethylene of high density (PEHD) and photosensitive semiconductor as filler of the cadmium sulphide (CdS) at the range of wavelengths l=350÷650 nm are presented.

The photoluminescent polymer compositions were prepared by the method of hot pressing at the melting temperature of polymer matrix under pressure 15 ÌPà during 15 min., at the condition of "fast cooling" (FC) with rate 1000°C/min, and at the condition of "slow cooling" (SC) with the rate 15°C/min. Semiconductors with sizes of particles 50<d<63 microns were used. Mechanical and electrical durability, and also dielectric characteristics of investigated compositions were determined at the temperature 293 K, and last were measured at the frequency 1 êHz. The compositions were processed in a gas inclusion under action of an electrical field at intensity of spark-over of the gas inclusion In the fig. 1 the spectra of photoluminescence are given of compositions on the basis of 0% PVDF+30% CdS prepared at the condition of FC and SC and pure CdS. It is seen that unlike CdS, for the composition PVDF+CdS, prepared by the FC, besides of the basic maximum, two additional maxima are observed. Intensity of these maxima changes depending on the condition of preparation of compositions.

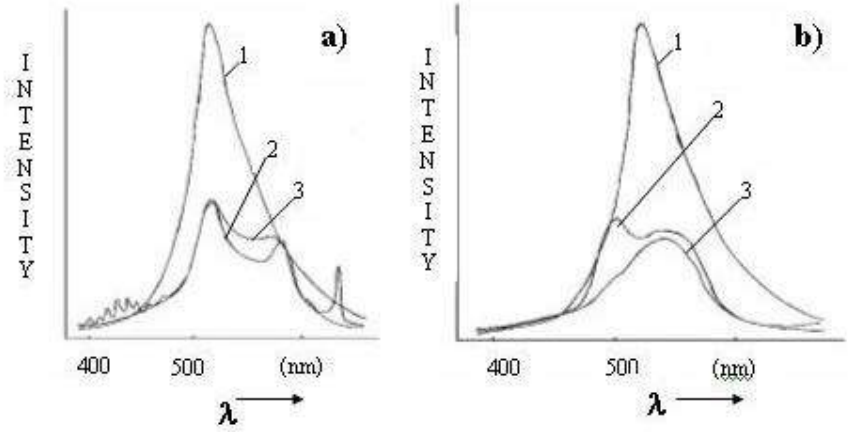

Fig.2. Spectra of photoluminescence of composites at T=293K a) 70% PVDF+30% CdS; 1. pure CdS; 2. before discharge processing; 3. after discharge processing; b) 70% PEHD + 30% CdS 1. pure CdS; 2. before discharge processing; 3. after discharge processing

In the fig. 2 the spectra of photoluminescence are given for compositions on the basis of 70% PVDF+30% CdS and 70% PEHD+30% CdS before discharge processing. It is experimentally established, that the discharge processing of compositions with various polymer matrix of strongly changes the spectra of photoluminescence, and the change of spectra for a composition 70% PVDF+30% CdS is more, than for 70% PEHD+30% CdS. Besides of the above-mentioned maxima, also a few additional small fine maxima appear.

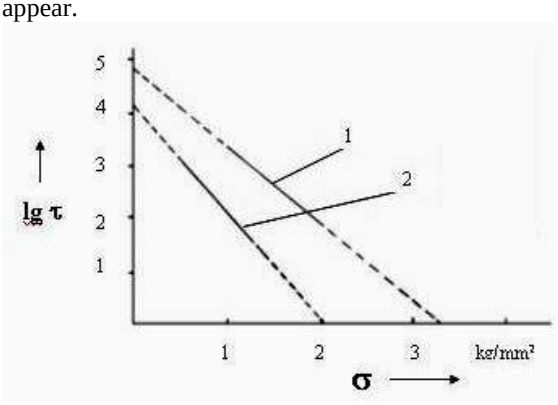

Fig.3. Temporary dependence (*lg t)* of mechanical durability for the composition 70% PVDF+30% CdS received by FC and SC at T=293K. 1. mechanical durability by FC; 2. mechanical durability by SC

Fig. 3 presents changes of temporary dependence $lg\tau$ of mechanical durability of the composition 70% PVDF+30% CdS prepared by method of FC and SC. It is seen, from fig. 3, that such dependence is more for composition prepared by FC, than by SC. The greater value of $lg\ \tau$ of samples of FC compositions in comparison with a sample preparing by SC is explained by formation of more ordered super molecular structure of the polymer layer between particles of sulphide cadmium and by improvement of polymer œver of particles CdS in case of composition FC. In fig. 4 the dependence of dielectric constant ε, dielectrical loss-angle $tg\ \delta$ and specific volumetric resistance ρ_v for composition of 70%PVDF+30 %CdS are shown at Ò=293 Ê depending on volume contents received by method of FC and SC. It is seen, from fig.4, that with increase of the CdS concentration, the values ε, $tg\ \delta$, $lg\ \tau$, and ρ_v vary depending on a temperature-temporary condition of crystallization.

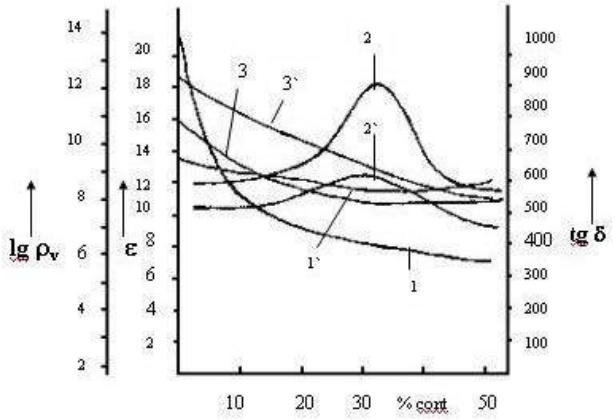

Fig.4. Dependence of dielectric constant *e*, dielectrical loss-angle *tg d* and specific volumetric resistance ρ_n compositions of 70% PVDF+30% CdS, at Ò=293Ê. 1. *e* received by FC; 2. *tg d* received by FC; 3. ρ_v received by FC; 1. *e* received by SC; 2. *tg d* received by SC; 3. ρ_v received by SC.

Thus according to above-mentioned experimental data the technology of preparation and discharge processing of composition (polymer–semiconductor) strongly influence upon the spectra of photoluminescence of compositions. Observable features in spectra of photoluminescence and values ε, $tg\ \delta$, $lg\ \tau$, and ρ_v also are connected with change of supermolecular structure of polymers and the charging condition. It is caused by change of the degree of interaction of polymer with cadmium sulphide i.e. the process of combination of polymer with filler and excitation of new luminescent centres in single crystal CdS which strongly depend on interface interaction between components of composition.

[1] *A.A. Ismayilov, M.A. Ramazanov*. J. Power Engineering Problems, Baku, Azerbaijan, ¹3-4, 2000, p. 114-117.

[2] *A.A. Ismayilov, M.A. Ramazanov.* Photoelectric properties of composition on the basis of polymer-semiconductor *6th* International Symposium on Polymers for Advanced Technologies PAT-2001, Eilat, Israel, 2001, p. 119.

[3] A.A. Ismayilov, Ramazanov M. A. Feauteres the formation of photoluminescence spectra in composition system on the basis of polymer-semiconductor.17-th Inernational technological conference on photoelectronics and night vision devices, Moscow, Russia, May 27-31, 2002.

Received: 30.04.02

PHOTOVOLTAIC EFFECT IN MONOCRYSTALS $CuGaSe_2$

I. KITAY OGLU, A.G. BAGIROV
Institute of Physics Azerbaijan NationalAcademy of Sciences
H.Javid av, 33, Baku, 370143

At the temperature 77 K the photovoltaic current of the short-circuit is observed in monocrystals $CuGaSe_2$ in the region of wavelengths (400-1200). At the increase of the light intensity from1 to 6.7 lux the negative peak reduces in the dependence $J_{s.c} \sim f(\lambda)$ and changes the sign. At further rise of the light intensity the spectrum form has the initial view. Depths of the impurity levels disposition (0.4 eV and 0.6 eV) were valued.

Triple semiconductors of $A^I B^{III} C_2^{VI}$ type are perspective materials for the creation on their base of high-effective transformers of the solar energy, photoreceivers of the high efficiency. The interest to the compound $CuGaSe_2$ is caused by the perspective of its use as the nonlinear transformers. The stimulated radiation is observed in $CuGaSe_2$ [1].

Results of the research of the short-circuit current dependence on the wave length in monocrystals $CuGaSe_2$ with the purpose of the opportunities clarification of its use as photocells of the high efficiency are shown in the present paper. Monocrystals $CuGaSe_2$ are crystallized in the chalcopyrite structure (the spatial group D_{2d}^{12}).

The compound $CuGaSe_2$ was obtained by the melting of initial components, taken in the stechiometric ratio.

The synthesis of the semicrystalline product was carried out in evacuated quartz ampoules up to 10^{-4} mm. m.c.

Monocrystals were grown by the method of the chemical transport reactions. The crystalline iodine was used as a conveyer. Lattice parameters (a=5.607, c=10.99, c/a=1.960) were determined in the consequence of the roentgenography research. Obtained monocrystals had the specific resistance $\rho=10^2 \div 10^7$ Ohm·cm and p-type conductivity.

Contacts from In and In-Ga eutectics were applied on samples for the measurement of the short-circuit current from the wavelength. Samples were illuminated by the monochromator SPM-2.

Samples were connected to the device B7-30 at measurements of the short-circuit current. Measurements were carried out at the temperature of the liquid nitrogen on samples with the specific resistance from $\rho=10^2$ Ohm cm. to 10^7 Ohm cm.Samples may be divided into 2 groups. In the first group of samples (low-resistance), the sign inversion of the short-circuit current is observed in the dependence of the short-circuit current on the wavelength $J_{s.c} \sim f(\lambda)$. In the second group of samples (high-resistance), the sign inversion of the short-circuit current is not observed.

The typical spectral dependence of the short-circuit current on the wavelength for low-resistance samples is presented on fig.1. It is seen on figure, that the dependence of the short-circuit current on the wave lenght has a complicated nature. In the range of wavelengths λ=625-825 nm the short-circuit current changes the polarity. In the range of wavelengths 500÷900 nm the diffusion photo e.m.f. exceeds the surface-barrier photo e.m.f. [2].

At first, at illumination the photodiffusion flow is directed from the illuminated side to back rear side and the positive peak $J_{s.c}>0$ is observed.

At the increase of the ligth intensity the reduction of the positive peak rise and inversion $J_{s.c}<0$ are observed. The latter fact is in agreement with results [2,3]. At the increase of the light intensity from 1 to 6.7 lux the growth of the negative peak reduces and changes the sign. At further increase of the ligth intensity the value of the short-circuit current $J_{s.c}$ does not depend on the wavelenght (fig.2).

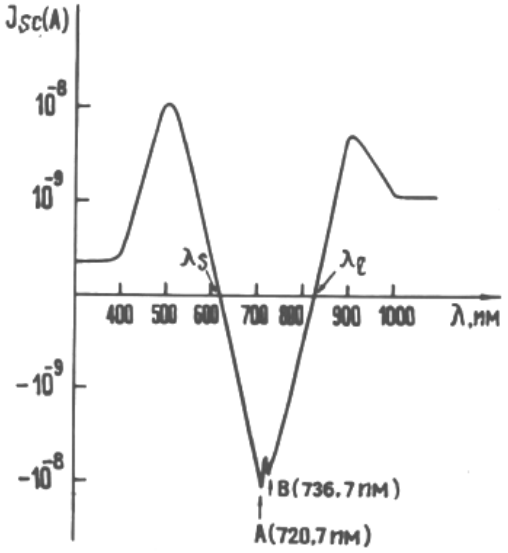

Fig 1. The inversion of the short-circuit current spectrum of monocrystals $CuGaSe_2$ after the irradiation by the light.

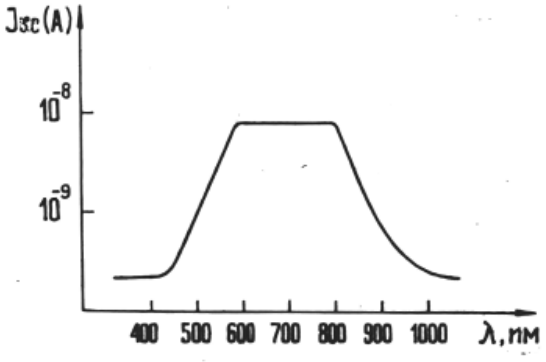

*Fig.2.*The dependence of the short-circuit current at the light intensity from 0,1 to 6,7 lux in the region of the fundamental absorption edge.

The negative peak is observed in the region of the fundamental absorption edge and has the fine structure A (720.7 nm) and B (736.7 nm)-fig.1. The mechanism of the PVE creation may be described by two methods:

I – By the charges division because of electrons and holes diffusion at the presence of the concentration gradient,

II – By the charges division because of spatial heterogeneities in samples [4].

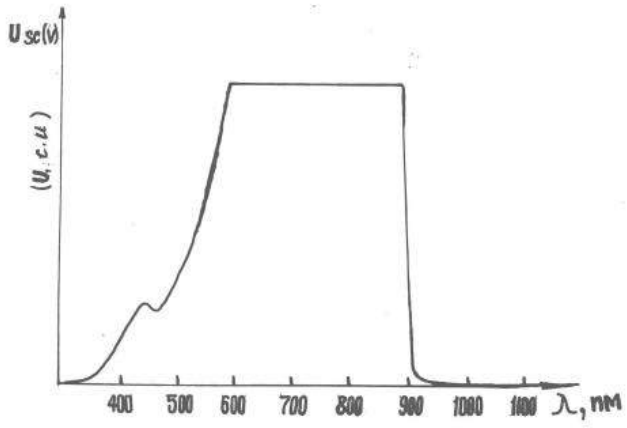

Fig.3. The spectral dependence of the short-circuit current photovoltage in monocrystals $CuGaSe_2$ after the preliminary irradiation by the laser (l=0,63 mkm)

In low-resistance samples $CuGaSe_2$ (partially compensated crystals) Fermi level is placed between the valent band and acceptor level, the semiconductor reveals the p-type conductivity with the acceptor concentration N_A-N_D. At the increase of the light intensity in consequence of the free holes capture the compensation of the initial conductivity occurs on levels of radiation donors. Fermi level shifts in the direction of the forbidden band middle, the sample resistance increases (the conductivity reduces). This process is profitable in the energy respect, especially for wide-band semiconductors, as, for example, monocrystals $CuGaSe_2$.

The peak A (720.7 nm), observed in spectra, has the exciton nature [4,5]-fig.1. Obviously, the independence of the short-circuit current on the wavelength in the range 600-900 nm is connected with the compensation of acceptor levels by donor levels and the appearance of impurity bands. At further increase of the impurity centers concentration (at the expense of the compensation) the impurity band expands and mixes with the valent band, that is why the short-circuit current reduces (fig.2).

The PVE saturation is observed at the irradiation by the laser light (fig.3). The influence of the preliminary exposure time by the laser light on the PVE spectrum was investigated. Depths of the two levels disposition (0.4 eV and 0.6 eV) were valued from the part of the PVE spectrum saturation.

[1] *J.L.Shay, B.Tell and H.M.Kasper*, Visible Stimulated Emission in Ternary Chalcopyrite Sulphides and Selenides, Appl. Phys. Letters, 19,1971, p. 366-368

[2] Academician *Adirovich*. On anormal Dember effect, Academy reports RF- v.150, ¹6 p.1252-1256.

[3] *G.G. Babichev, I.P.Jadko, B.K. Seredecha.* On spectral characteristics of cross Dember and photo-magnetic effects in heterogeneities semiconductors-UFJ. 1977. v.22. ¹9, p.1523-1529.

[4] *M.P.Vecchi, J.Ramos and W.Girat.* Photoluminescence in $CuGaSe_2$ Solid State Electronics 1978, Vol. 21, p 1609-1612

[5] *A.V. Mudryi, I.V. Bodnar, I.A. Victorov, V.F. Gremenok, A.I. Patuk and I.A.Shakin*. Excitonic photo-luminescence properties of $CuJnSe_2$ and $CuGaSe_2$ se-miconductor compounds- Paper, presented at the 11th Int. Conf. on Ternary and Multinary Compounds, ICTMC-11, Salford, 8-12 September1997, p.413-417.

Received: 11.02.02

ENERGY SPECTRUM OF SUPERLATTICE IN MAGNETIC FIELD

N.M. HUSEYNOV
Institute of Physics Azerbaijan National Academy of Sciences
H.Javid av, 33, Baku, 370143

An expression defining energy of electron in superlattice with thin conducting layers in magnetic field is solved. The magnetic field is in layers plane. A potential of the superlattice is defined as δ-functions. Influence of weak magnetic field on minizone spectrum is investigated. It was shown that the influence of magnetic field leads to slight shift of minizones.

Many theoretical and experimental investigations of electron spectrum of heterostructures, in which a magnetic field was directed along semiconductor layers containing two-dimensional electron gas, have been fulfilled. For example, a spectrum of quantum wells systems in magnetic field was investigated theoretically in works [1,2]. An electron mass, connected with movement along the axes of GaAs-$Al_xGa_{1-x}As$ superlattice, was experimentally investigated in work [3] using the cyclotron resonance method.

The modern technology allows to make superlattices with thickness of layers of a few or even of one inter-atomic distance. In this case one can use the model of potential of superlattice being chosen as δ-functions.

The aim of the present paper is to investigate influence of magnetic field directed along the layers of superlattice, on the electron minizone spectrum within the framework of the δ-potential model.

The axes of the superlattice is chosen along x-axes. The magnetic field in layers plane is chosen along y-axes. The vector potential is chosen as follows A=(0, 0,-Bx). In the approximation of effective mass the Schrodinger equation is the following:

$$-\frac{h^2}{2m}\left(\frac{\partial^2}{\partial x^2}+\frac{\partial^2}{\partial y^2}\right)\psi+\frac{1}{2m}\left(ih\frac{\partial}{\partial z}+\frac{|e|Bx}{c}\right)^2\psi+u(x)=E\psi, \tag{1}$$

where $u(x)=(h^2W/m)\sum\delta(x-nd)$, d is the period of the superlattice, W is potential power, n= 0, ±1, ±2,… is the number of a dielectric layer.

The wave function may be written in the following form:

$$\psi=e^{ik_z z+ik_y y}\,\varphi(x)\ . \tag{2}$$

Substituting (2) into equation (1) we obtain the following equation:

$$-\frac{h^2}{2m}\frac{\partial^2\varphi}{\partial x^2}+\frac{h^2}{2ml^4}(x-x)^2\varphi+\left[u(x)-\left(\varepsilon-\frac{h^2k_y^2}{2m}\right)\right]\varphi=0, \tag{3}$$

where $l=\{ch/|e|B\}^{1/2}$ is the magnetic length, $x=l^2k_z$ is the center of electron orbit in the magnetic field.

We shall make the following replacement of variable:

$$x=\frac{1}{2^{1/2}}\left(\xi+\bar{x}\right),\quad \bar{x}=2^{1/2}x/l \tag{4}$$

As a result the equation (2) will obtain the following form:

$$\left[\frac{\partial^2}{\partial\xi^2}-\frac{\xi^2}{4}+\varepsilon-U(\xi)\right]\Phi(\xi)=0, \tag{5}$$

where $\varepsilon=\left(E-\frac{h^2k_y^2}{2m}\right)\frac{ml^2}{h^2}$,

$$U(\xi)=2^{1/2}W\delta\left(\xi+\bar{x}-\frac{2^{1/2}dn}{l}\right).$$

By $\xi\neq-\bar{x}+\frac{2^{1/2}dn}{l}$ the equation (5) has the following form:

$$\frac{\partial^2}{\partial\xi^2}\Phi+\left(p+\frac{1}{2}-\frac{\xi^2}{4}\right)\Phi=0 \tag{6}$$

where $p=\varepsilon-½$.

It is well known equation for the parabolic cylinder function and it has the following common solution:

$$\Phi_n=A_nD_p(\xi)+B_nD(-\xi), \tag{7}$$

where D_p is the parabolic cylinder function, n is the number of conducting layer which is defined by the following inequalities:

$$-\bar{x}+\frac{2^{1/2}dn}{l}\le\xi\le-\bar{x}+\frac{2^{1/2}d(n+1)}{l} \tag{8}$$

The border conditions for the functions Φ_n are defined by the system of the following equations:

$$\Phi_n(\xi_n+0)=\Phi_{n-1}(\xi_n-0) \tag{9}$$

$$\Phi'_n(\xi_n+0)=\Phi'_{n-1}(\xi_n-0)+l\Phi_{n-1}(\xi_n)$$

where $\xi_n=-\bar{x}+nh$, $l=2^{1/2}W$, $h=2^{1/2}d/l$.

In x-axes ξ_n corresponds to coordinates of the dielectric layers $x=nd$.

Subscript n at the function $\Phi_n(\xi)$ is defined by the inequalities (8), and corresponds to the conducting layer $nd\le x\le(n+1)d$.

We have from the Bloch theorem:

$$\Phi_0(\xi)=A_0D_p(\xi)+B_0D_p(-\xi) \tag{10}$$

$$\Phi_1(\xi)=e^{ik_xd}\,[A_0D_p(\xi-h)+B_0D_p(-\xi+h)$$

Substituting (10) into the border conditions (9) one can obtain an equation for the electron spectrum taking into account that

$D_p(x)\,D_p'(-x) - D_p(-x)\,D_p'(x) = 2p/G$, where G is gamma function

$$\cos k_x d = \frac{1}{2}\left[D_p(x_1)D_p'(-x_1+h) - D_p(-x_1)D_p'(x_1-h)\right] + \frac{1}{2}\left[D_p(x_1-h)D_p'(-x_1) - D_p(-x_1+h)D_p'(x_1)\right] + \frac{l}{2D}\left[D_p(x_1-h)D_p'(-x_1) - D_p(-x_1+h)D_p'(x_1)\right] \quad (11)$$

where $D=(2p)^{1/2}/G(-p)$.

Let us consider a weak magnetic field so that $d<<1$.

Having chosen the center of the electron's orbit $\bar{x}$ inside the area $(0,d)$ we shall obtain:

$$x_1, x << 1. \quad (12)$$

The parabolic cylinder function we can represent in the form of the following combination of degenerated hypergeometric functions:

$$D_p(z) = 2^{p/2}\exp(-z^2/4)\left[\frac{p^{1/2}}{G((1-p)/2)}F(-p/2,1/2,z^2/2) - \frac{(2p)^{1/2}z}{G(-p/2)}F((1-p)/2,3/2,z^2/2)\right], \quad (13)$$

where the hypergeometric function is represented by the following row:

$$F(a,b;z) = 1 + \frac{a}{g}\frac{z}{1!} + \frac{a(a+1)z^2}{g(g+1)}\frac{z^2}{2!} + \ldots$$

Taking into account (12), representing $p=e-1/2$ and assuming that $x_1 e^{1/2}$, $\bar{x}\varepsilon^{1/2}$ @ 1 while calculating the expression for the spectrum we shall keep all members proportional to the quantities $(x_1 e^{1/2})^k$, $(x e^{1/2})^k$, where k=1, 2, 3,…

After a long calculation we shall obtain:

$$\cos k_x d = \cos e^{1/2}h + \left(l/2e^{1/2}\right)\sin e^{1/2}h + K\left(e^{1/2}\bar{x}, e^{1/2}\bar{x}_1\right)\bar{x}^4 + L\left(e^{1/2}x, e^{1/2}x_1\right)c + \left(l/2e^{1/2}\right)M\left(e^{1/2}x_1, e^{1/2}\bar{x}\right)x_1^4 + \left(l/2e^{1/2}\right)M\left(e^{1/2}x, e^{1/2}x_1\right)\bar{x}^4 \quad (14)$$

where K, L and M unwieldy expressions of the order of unity.

We shall define $c=(2m)^{1/2}(E-h^2k_y^2/2m)^{1/2}/h$ and take into account that $e^{1/2}h=cd$, $l/2e^{1/2}=W/c$. By neglect of the members x_1^4 and $\bar{x}^4$ in the expression (14) at the limit $B\to 0$, we obtain the standard expression of the electron spectrum in the Dirac comb:

$$\cos k_x d = \cos cd + (W/c)\sin cd \quad (15)$$

Assuming that the electron spectrum doesn't depend on the position of the center of electron's orbit within the layer $(0, d)$, in order to estimate influence of the weak magnetic field on the spectrum, we can assume that $\bar{x}=0$.

The equation (14) will be reduced to the form:

$$\cos k_x d = \cos cd + (W/c)\sin cd + [K(cd) + (W/c)M(cd)]\,h^4, \quad (16)$$

where $K(cd) = K(e^{1/2}x, e^{1/2}x_1)$, $M(cd)] = M(e^{1/2}x_1, e^{1/2}x)$ by $\bar{x}=0$.

We shall search a solution of the equation (16) in the following form $c = c_0 + \bar{c}$, where $\bar{c} << c_0$. c_0 is the solution of (15) by k_x=0

$$tgx = Wd/2x, \quad x = c_0 d/2. \quad (17)$$

Keeping the member $\bar{a}\,\bar{c}$, it is easy to obtain:

$$E = \frac{h^2 k_y^2}{2m} + \frac{h^2 c_0^2}{2m} + D(1-\cos k_x d) + 4D\left[K(c_0 d) + (W/c_0)M(c_0 d)\right](d/l)^4 \quad (18)$$

where the width of minizone is

$$D = \frac{h^2 c_0}{md\sin c_0 d\left[1 + W/dc_0^2 - (W/c_0)ctgc_0 d\right]}.$$

So, the influence of weak magnetic field leadscomes to the slight shift of minizones of the order of $4D(W/c_0)(d/l)^4$.

Let us make estimation of the following quantities: $c_0 d$, D, $h^2 c_0^2/2m$.

We shall consider the superlattice GaAs – $Al_x Ga_{1-x}$ As with x=0.3, d= 200Å and the width of barrier a = 50Å. For such parameters the distance between conduction zones of GaAs and $Al_x Ga_{1-x}$ As is DE_c=100meV [4]. One can

estimate the power of potential from the following expression: $h^2 W/m = DE_c a_0$

So, one can define the quantity $c_0 d$=2.5 from the equation (17) for the first minizone. According to this value we shall obtain position of the lowest minizone $h^2 c_0^2 / 2m$ =13.8meV. The width of the minizone is D=3meV.

Using these quantities one can estimate that the lowest minizone's shift is

$$36(d/l)^4 meV \quad . \qquad (19)$$

Though, the expression (19) has been obtained at $d \ll l$, one can suppose that at $d \leq l$ the minizone's shift may be of the order of minizone's width.

[1] G. Gumbs. Phys.Rev. B 54, 16, 11354, 1996.
[2] V.I. Belyavski, Yu.V. Kopaev, S.V. Shevtsov. FTT, 40, 9, 1719, 1998.
[3] T. Duffield, R. Bhat, H. Koza, M.C. Tamargo, J.R. Harbison, F. DeRoza, D.H. Hwang, P. Grabl, K.M. Rush, S.J. Allen. In: Proc. 18th Int. Conf. On the Physics of Semiconductors, Stockholm, Sweden, 1, 239, 1986.
[4] A.P. Silin. UFN , 143, 3, 485, 1985.

Received: 29.04.02

THE CAPACITIVE CHARACTERISTICS OF THIN FILM PHOTOELECTRIC CELLS ON THE BASE OF THE MAGNESIUM PHTHALOCYANINE

M.M. PANAHOV, S.A. SADRADDINOV, J.H. JABBAROV, B.SH. BARKHALOV
Baku State University
acad. Z. Khalilov str., 23, Baku, 370145

The magnesium phthalocyanine MgPc, as well as other phthalocyanine compounds, has rather valuable physical-mechanical properties and thin film structures on its base can make a severe competition to well-known inorganic materials at application in the microtransducers. The conducted examination has demonstrated, that on the electronic processes in MgPc at alternating electric field the considerable effect can be rendered by the conditions on the contacts. In the present paper we show, that depending on a degree of doping by oxygen and the concentration of the traps in MgPc it is possible to obtain the essentially distinguished characteristics for metal - MgPc - metal structures.

The layer structures on the basis of the organic semiconductor MgPc have been obtained by a thermal evaporation in a vacuum $\approx 10^{-6}$ Torr of the MgPc layer and second Al electrode onto the quartz substrate with the previously applied transparent SnO_2 electrode. The thickness of the amorphous MgPc layer was 0,2-2,0 μm, an operating area of the structures was equal to 0,1-1,0 sm^2. Doping by oxygen was conducted by the exposure of the MgPc film in the oxygen atmosphere at the temperature 390-420 K. All measurements were conducted in a vacuum $\approx 10^{-5}$ Torr.

The examination of the dependence of the SnO_2/MgPc/Al structures capacity on the temperature and bias voltage evidenced for the presence of the depleted by holes high-resistive layer on the Al/Mg Pcinterface [1]. At low temperatures capacity of the structure is constant. With increasing of the temperature it grows and reaches the upper limiting value $\tilde{N}_n$, depending on a degree of the processing MgPc in the oxygen atmosphere (Fig.1). The values of the $\tilde{N}_n$ for the samples with different oxygen exposure differ strongly. It must be noted, that the effect of such processing on the photoelectric properties of the Al/MgPc/Ag structure was described earlier in [2]. It is easy to explain apparent growth of capacity, if one supposes, that the Al-MgPc interface is characterized by the capacity C_{sch} of the depleted by the charge carrier's layer, shunted by the resistance R_{sch}. If one accepts, that for the considered alternating-current range ($\omega=2\pi f$) a relation $R_{sch} >> (\omega C_{sch})^{-1}$ is valid, so the capacity of the Al/MgPc/Ag "sandwich" can be calculated by the equation [3, 4]:

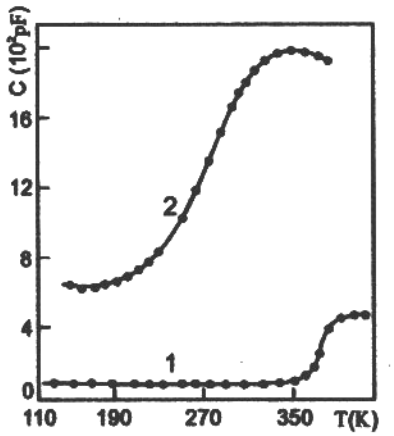

Fig.1. The capacitance versus temperature curves for SnO_2/MgPc/Al structures, proceeded in high vacuum (1) and oxygen atmosphere (2).

$$\tilde{N} = \tilde{N}_{sch}\left(1+\omega^2\tilde{N}^2_{MgPc}R^2_{MgPc}\right)\cdot\left[1+\omega^2\tilde{N}^2_{MgPc}\left(\tilde{N}_{sch}+\tilde{N}_{MgPc}\right)R^2_{MgPc}\right]^{-1} \quad (1)$$

where C_{MgPc} and R_{MgPc} are the capacity and the shunting resistance of the MgPc layer, respectively.

At low temperatures $RMgPc \gg R_0 exp(Et/KT)$ (where E_t is a depth of the oxygen levels equal to 0,62 eV [5, 6]) is big enough, and the capacity of the Al/MgPc/Ag "sandwich" is determined by the capacity of series-connected capacitors (Fig.1, T<240K),

$$C \approx \left(C^{-1}_{sch} + C^{-1}_{MgPc}\right)^{-1} \quad (2)$$

and for not too thin MgPc layers, that is for a case when $C_{MgPc} << C_{sch}$, it is determined by the capacity of the MgPc layer, i.e. $C=CMgPc$ (see fig. 1, T<240K). At high temperatures, when R_{MgPc} becomes small, $\left[\omega^2\tilde{N}^2_{MgPc}\left(\tilde{N}_{sch}+\tilde{N}_{MgPc}\right)R^2_{MgPc} << 1\right]$, the formula (1) is reduced to:

$$\tilde{N} = \tilde{N}_{sch}\left(1+\omega^2\tilde{N}^2_{MgPc}R^2_{MgPc}\right) \quad (3)$$

At sufficiently high temperatures $\left(\omega^2\tilde{N}_{MgPc}R^2_{MgPc} << 1\right)$,

$$C = C_{sch}\,. \quad (4)$$

Using this limiting value of the capacity for a known thickness of the MgPc layer, it is possible to find the width of a depletion layer l_s from the expression:

$$l_s = \varepsilon\varepsilon_0 S C^{-1}_{sch} \quad (5)$$

Calculated by this manner a Schottky barrier width (for MgPc $\varepsilon=3$) has appeared to be equal 115Å for a sample, proceeded in the oxygen atmosphere, and 900Å for one, proceeded in the high vacuum.

Knowing l it is possible to determine the density of the trap centers Nt from the equation:

$$N_t = 10^6 \left(j_{sch} - j_i \right) \varepsilon \varepsilon_0 / l_s , \quad (6)$$

where j_{sch} and j_I are the work function, for a contact material and MgPc layer accordingly. Determined by such manner the trap centers density has appeared to be equal $3.8 \cdot 10^{16}$ and $2.5 \cdot 10^{18} cm^{-3}$, accordingly, for the samples, proceeded in the high vacuum and in the oxygen atmosphere.

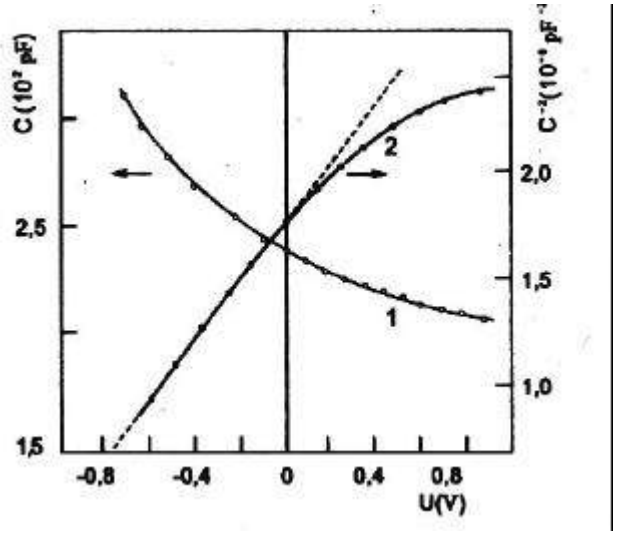

Fig.2. The capacitance versus bias voltage curves for SnO_2/MgPc/Al structures, proceeded in high vacuum.

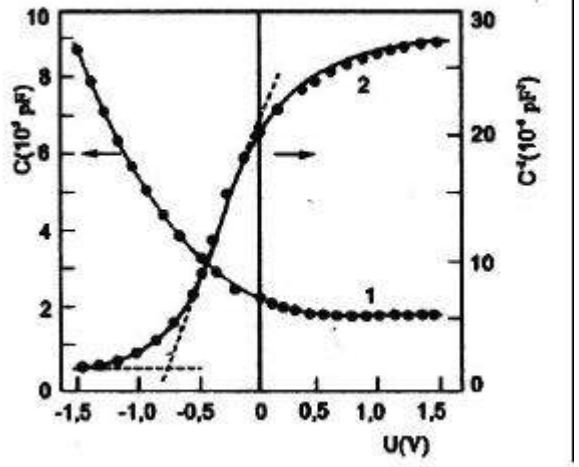

Fig.3. The capacitance versus bias voltage curves for SnO_2/MgPc/Al structures, proceeded in oxygen atmosphere.

The experimentally observed strong dependence of the capacity of the asymmetrical Al/MgPc/Ag " sandwich " on the bias voltage (Fig.2 and 3) testifies, that only up to some small value of an dectric field, applied to the "sandwich", the basic mechanism of an electrical conductivity is the tunneling of the equilibrium charge carriers through a Richardson-Schottky barrier. Last circumstance determines a strong dependence of this field value on temperature (Fig.2). Beginning from this value of an electric field, at further increase of the bias voltage in the "locking" direction (negative potential is applied on Al electrode) of the Al/MgPc/Ag "sandwich", starts to prevail the charge carrier transfer through the MgPc bulk, which initially is determined by a linear growth of the transport rate of the equilibrium charge carriers through the MgPc layer (Fig. 2), and then by the velocity of the thermal-field generation of the non-equilibrium charge carriers (Poole-Frenkel effect section). The growth of the thickness of the depleted by the charge carriers layer under growth of the bias voltage (U_b>1V) is accompanied by decrease of the equilibrium capacitance of the *Al-MgPc* junction at the "locked" state of the Al/MgPc/Ag "sandwich". It is described by the relation:

$$C_{sch}^{-2} = U_{bias} \quad (7)$$

and the slope of this linear sketch (see Fig.2 and 3) is determined, in particular, by the density of the ionized trap centers of the non-equilibrium charge carriers [5]:

$$\frac{\partial}{\partial U}\left(C_{sch}^{-2} \right) = 2\left(q \varepsilon_0 \varepsilon s^2 N_t \right)^{-1} \quad (8)$$

Determined by this manner the trap centers density $N_t = 3.7 \cdot 10^{16} sm^{-3}$ for a sample, proceeded in a high vacuum and $N_t = 2 \cdot 10^{18} sm^{-3}$ for a sample, proceeded in the oxygen, atmosphere are in a good agreement with the values, determined in [3].

The properties of a Schottky barrier manifest themselves self also in the photocurrent-versus-light intensity characteristics of the structure. In the Fig.4 the voltage-capacitance characteristics of the SnO_2/MgPc/Al structure has been shown. Under illumination, a separation of the non-equilibrium charge carriers on a surface barrier between Al and MgPc takes place in the MgPc, doped by the oxygen. A resistance of the barrier layer at high *L*, even at room temperature, decreases so that capacity of the barrier layer at small bias voltages decreases sharply (Fig. 4, curve 1).

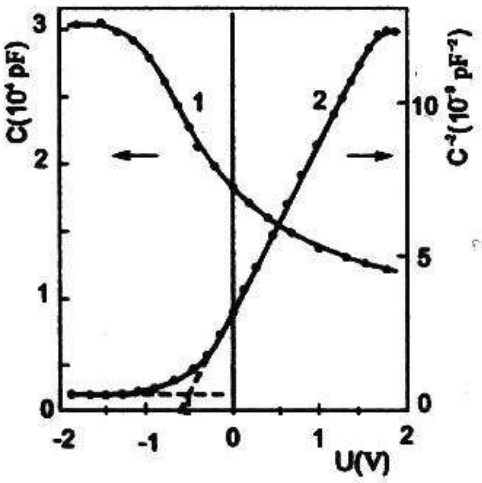

Fig.4. The barrier capacitance versus bias voltage curves for SnO_2/MgPc/Al structures, proceeded in oxygen Atmosphere, at T=298K and $L = 3 \cdot 10^4$Lx light intensity ($f = 10^4$Hz).

The intersection point of an extrapolated linear section of the $\tilde{N}^{-2} \propto U_{bias}$ dependence, under the constant illumination $L = 3 \cdot 10^4$Lx with the voltage (Fig. 4, curve 2) gives the value of the diffusion potential U_d=0.4V. Using this value of U_d and taking into consideration a Schottky decreasing of the barrier [7], equal to 0.12 eV on the Al/MgPc interface, we obtain the width of the Schottky barrier $\hat{O}$=0.52 eV, that is in

a good agreement with the results, observed on a direct current.

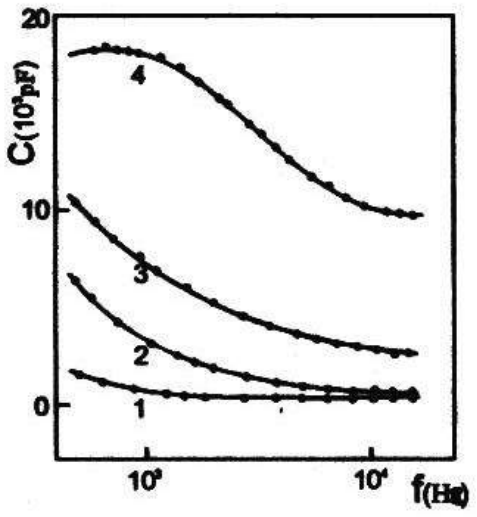

Fig.5. The barrier capacitance versus alternating current frequency curves in dark (1.3) and under steady-state illumination $L=3\cdot10^4$Lx for SnO_2/MgPc/Al structures, proceeded in high vacuum (1,2) and oxygen atmosphere(3,4).

A frequency dependences of the capacity of the SnO_2/MgPc/Al "sandwich" at room temperature are given in a fig. 5. The dark capacity for undoped by the oxygen "sandwich" is high enough and does not depend on the frequency. At the same time, under illumination capacity of the structure considerably increases (Fig. 5, curve 2) at low frequency region, because of the effect of the surface electron defects on depleted by the charge carriers layer. With growth of the frequency the light increment of capacity decreases sharply. After the doping of the MgPc layer in the oxygen atmosphere, capacity of the structure sharply grows and has irreversible character (Fig. 5, curve 3). Under illumination the capacity of the *MgPc* layer, doped by the oxygen, exhibits a strong changes, promptly decreasing with the frequency growth. The apparent behavior of the capacity is completely correlated with the results of the analysis of the equation (1), from which it follows, that at high light intensities in the low frequency region the capacity of the sample should be equal $C\approx C_s$. It is seen from the Fig. 5 (the curve 4), that this limiting value of the capacity is reached at the light intensity $L=10^4$Lx.

The obtained results allow to conclude, that on the basis of the magnesium phthalocyanine films it is possible to produce thin-film photoelectric cells with high enough light sensitivity. In contrast to earlier what described earlier, the photoelectric cells offered by us have more stable characteristics.

[1] *Yu. Vidadi, S.F. Sadraddinov, S.Sh. Khalilov*. Properties of film structures with a Schottky barrier on the basis of the MgPc doped by the oxygen, in: "Electronics of organic materials", Moscow, "Nauka" Publishing House, 1985, p. 179 (in Russian).

[2] Organic semiconductors (Review of the literature for 1968). The Ukrainian Academy of Sciences, Institute of Physics, Kiev, 1969 (in Russian).

[3] *B.Sh. Barkhalov, Yu.A. Vidadi*. Properties of Al /Copper Phthalocyanine/ Ag Diode Structure with the Sehottky Barriers.Thin Solid Films, 1970, V. 40, ¹. 2, L5.

[4] *F.G. Simmons, G.S. Nadkarni, M.C. Lancaster*. Alterenating Current Electrical Properties of Highly Doped Insulating Films. J. Appl. Phys., 1970, v. 41, p. 538.

[5] Organic semiconductors (Review of the literature for 1969). The Ukrainian Academy of Sciences, Institute of Physics, Kiev, 1970 (in Russian).

[6] *D.D. Eley, G.D. Parfitt*. Semiconductor Character of the Electrical Conductivity of Organic Matters. Trans. Faraday Soc., 1955, v. 51, p. 1529.

[7] *S.M. Zee*. Physics of the Semiconductor Devices. Ì oscow, «Energia» Publishing House, 1973.

Received: 07.05.02

THERMODYNAMICS OF SEMICONDUCTIVE FILM WITH A PARABOLIC POTENTIAL IN A STRONG MAGNETIC FIELD

F.M. GASHIMZADE, A.M. BABAEV, KH. A.GASANOV
Institute of Physics Azerbaijan National Academy of Sciences
H.Javid av, 33, Baku, 370143

The expressions for the density of states, magnetic susceptibility, entropy, heat capacity and also for the transverse magnetothermopower of electron gas in a quantum well have been obtained for the cases of nondegenerate statistics and strong degeneracy. It is demonstrated that in the case of strong degeneracy, quantum levels lying below the Fermi level intersect the Fermi level with an increase of the magnetic field, which leads to jumpwise oscillations of theirs magnitude.

INTRODUCTION

In the past decade, numerous experimental and theoretical investigations have been focused on the variety of thermodynamic and galvanomagnetic properties of semiconductor dots, films and the wires [1-5]. In [1] a linear-response theory was developed for the thermopower of a quantum dot of small capacitance and in the quantum regime of resonant tunneling and at a constant number of electrons on the quantum dot and the oscillations were predicted.

Thermoelectric properties of nanowires in the magnetic field were investigated in [2], where the magnetic splitting of thermopower peaks was predicted and a scheme for measuring of thermopower in a circuit containing a nanowire and leads made from the same material was described. Thermopower peaks are due to the magnetic field on-and-off switching of the energy levels.

The thermoelectric power and longitudinal magneto-Seebeck coefficient of 200 nm diameter single-crystal bismuth nanowire were measured in [3]. It was theoretically calculated that bismuth nanowires should have a high thermoelectric figure of merit over bulk Bi, when the diameter become less than 10 nm. The thermopower and conductance of atomic-size metallic contacts have been studied in [4]. For contacts of atomic dimensions, abrupt steps in the thermopower which coincide with jumps in the conductance were observed.

The electronic conductance in nanowires modeled by soft- and hard-wall confining potentials under the influence of a magnetic field and in the linear and nonlinear rate was investigated in [5]. The behavior of the conductance demonstrates a ``magnetic switch" (on and off) effect of the quantum electronic transport in nanowires.

It is assumed that a similar behavior should also be observed for thermodynamical parameters of electrons in the quantum well under the conditions of strong degeneracy. This assumption stems from the fact that under these conditions, the dependence of thermodynamical parameters simply reproduces the behavior of the density states at the Fermi level [6].

In the present work the density of states, magnetic susceptibility, entropy, electron heat capacity and magnetothermopower of electrons in a parabolic quantum well are calculated.

At first, the expression for the electron spectrum and the density of states will be given, and then the thermodynamical parameters for the case of nondegenerate statistics and for strong degenerate one will be calculated.

ELECTRON SPECTRUM IN A PARABOLIC QUANTUM WELL IN A LONGITUDINAL MAGNETIC FIELD

For standard electron dispersion law, the sought spectrum can be represented in the following form [7-10].

$$\varepsilon_{N,k_y,k_z,\sigma} = (N+1/2)\hbar\omega + \frac{\hbar^2 k_z^2}{2m} + \frac{\omega_0^2}{\omega^2}\frac{\hbar^2 k_y^2}{2m} + \sigma g m_B H \qquad (1)$$

Here, the Landau gauge is chosen for the vector-potential $\vec{A}(0,x\cdot H,0)$; ω_0-characterizes the parabolic potential of the well

$$U = \frac{m\omega_0^2 x^2}{2} \qquad (2)$$

$\omega = \sqrt{\omega_0^2 + \omega_C^2}$, $\omega_c = \frac{eH}{mc}$ is the cyclotron frequency, m_B is the Bohr magneton, g is the factor of spin splitting, $\sigma=\pm 1/2$, and N is the number of the quantum level.

The coordinate wave function which corresponds to the energy eigenvalue (1), has the form [8,10]

$$\psi_{N,K_y,K_z}(r) = \varphi_N(x-x_O)e^{ik_y\cdot y+ik_z\cdot z} \qquad (3)$$

where

$$\varphi_N(x-x_o) = \frac{1}{\pi^{1/4}a^{1/2}\sqrt{2^N N!}} e^{-\frac{(x-x_0)^2}{2a^2}} H_N\left(\frac{x-x_O}{a}\right) \qquad (4)$$

$$a = \sqrt{\frac{\hbar}{m\omega}} \qquad (5)$$

$$x_O = -\frac{\omega_c}{\omega}\cdot\frac{\hbar k_y}{m\omega} = -\frac{\omega_c}{\omega}a^2 k_y \qquad (6)$$

$H_N(x)$- is the Hermite polynomial [11].

The density of states is defined by the expression:

$$\nu(\varepsilon) = \sum_{N,k_y,k_z,\sigma}\delta(\varepsilon_{N,k_y,k_z,s} - \varepsilon) \qquad (7)$$

Then, by moving from the summation over k_z and k_y to the integration and using the expression (6), we obtain

$$r(e)=\frac{L_{ó}L_Z}{(2p)^2}\frac{\sqrt{2m}}{\hbar}\cdot 2\frac{mw}{\hbar}\cdot\frac{w}{w_c}\cdot\sum_{N,s}\int_0^{x_0^m}\frac{dx_0}{\sqrt{e-e_{Ns}-bx_0^{\,2}}} \tag{8}$$

Here,

$$e_{Ns}=(N+{}^1\!/_2)\hbar w+sgm_BH \tag{9}$$

$$b=\frac{mw_0^2}{2w_c^2}\cdot w^2 \tag{10}$$

Therefore, we have

$$r(e)=\frac{L_yL_z}{2p\hbar^2}\cdot\frac{mw}{w_0}\cdot\begin{cases}\sum_{N,s}\hat{O}(-e+e_{N,s}+b\,{}^{L_x^2}\!/_4)\cdot\hat{O}(e-e_{N,s})\\ \frac{2}{p}\sum_{N,s}arcsin\sqrt{\frac{b\,{}^{L_x^2}\!/_4}{e-e_{N,s}}}\cdot\hat{O}\left(e-e_{N,s}-b\,{}^{L_x^2}\!/_4\right)\end{cases} \tag{11}$$

where L_x is the well width and $\hat{O}(x)$ is the Heaviside function.

NONDEGENERATE STATISTICS

It is known that the thermodynamical Gibbs potential is determined by the formula

$$W=-k_0T\sum_{N,k_y,k_z,s}ln\left(1+exp\left(\frac{x-e_{N,k_y,k_z,s}}{k_0T}\right)\right) \tag{12}$$

Entropy

$$S=-\left(\frac{\partial\Omega}{\partial T}\right)_{x,\mathrm{H}} \tag{13}$$

magnetic susceptibility

$$c(H,T)=-\frac{1}{VH}\left(\frac{\partial W}{\partial H}\right)_{x,T} \tag{14}$$

heat capacity

$$C_V=S\left(\frac{\partial S}{\partial T}\right)_{V,H} \tag{15}$$

For the nondegenerate statistics,

$$W=-n\cdot k_0\cdot T \tag{16}$$

where

$$n=\frac{mk_0T}{2p\hbar^2}\cdot\frac{w}{w_0}\cdot\frac{ch\left(\frac{gm_BH}{2k_0T}\right)}{sh\left(\frac{\hbar w}{2k_0T}\right)}\cdot exp(h)\cdot erf(t)$$

n is the electron concentration (in our case it is two dimensional concentration), and

$$c=\frac{1}{L_xH^2}nk_0T\frac{w_c^2}{w^2}\left(1+n_s\frac{w^2}{w_c^2}thn_s-nthn-\frac{2t\,exp(-t^2)}{\sqrt{p}erf(t)\frac{w_c^2}{w_0^2}}\right) \tag{17}$$

$$S=nk_0\left(2-h+nthn-n_sthn_s-\frac{t\,exp(-t^2)}{\sqrt{p}erf(t)}\right) \tag{18}$$

$$C_V=nk_0\left(1+n^2\frac{1}{sh^2n}+n_s\frac{1}{ch^2n_s}-\frac{t\,exp(-t^2)}{\sqrt{p}erf(t)}\left(\frac{1}{2}-t-\frac{t\,exp(-t^2)}{\sqrt{p}erf(t)}\right)\right) \tag{19}$$

Here, $$t=\sqrt{\frac{b\cdot L_x^2}{4\cdot k_0\cdot T}} \tag{20}$$

erf(t) is the probability integral [11], k_0 is the Boltzmann constant.

$$n=\frac{\hbar w}{2k_0T},\quad n_s=\frac{gm_BH}{2k_0T},\quad h=\frac{x}{k_0T} \tag{21}$$

From the Obraztsov's formula for the transverse thermopower [13] follows that,

$$\alpha(H) = -\frac{S}{en} \tag{22}$$

we obtain

$$\alpha = -\frac{k_0}{e}\left(2 - \eta + n\,\mathrm{cth}\,n - n_s\,\mathrm{th}\,n_s - \frac{t\exp(-t^2)}{\sqrt{\pi}\,erf(t)}\right) \tag{23}$$

In our calculations for GaAs, we used the data from [10] given for the parabolic well with width $L_x=4000Å$, and the height $\varepsilon_1=150meV$, and electron mass $m=0{,}067m_0$ in order to obtain the estimate $\omega_0=4{,}437\cdot10^{12}s^{-1}$. Note that according to Fig.1 in [10], $\varepsilon_1 \approx (m\omega_0^2/2)\cdot(L_x/2)^2$ in a zero magnetic field.

For InSb semiconductors we assumed that $m=0{,}016m_0$, and $\hbar\omega_0=7{,}5meV$ in accordance with [12]. In addition, we put $n=2\cdot10^{10}cm^{-2}$, and $5\cdot10^{10}cm^{-2}$ for InSb and GaAs, respectively. The calculated dependences $\eta(H)$ and $C_V(H)$ for InSb, ($g=-51{,}2$, curve 1) and GaAs ($g=-0{,}44$, curve 2) at $T=300\,K$ are shown in Fig.1 and Fig.2, respectively.

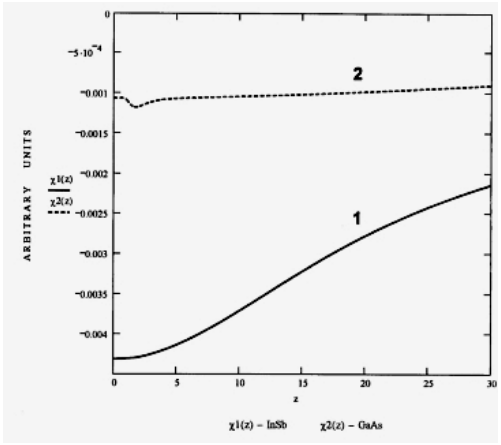

Fig 1. The dependence of magnetic susceptibility on the reduced value of the magnetic field $z=\omega_c(H)/\omega_0$ for InSb (curve 1) and GaAs (curve 2) for the nondegenerate case.

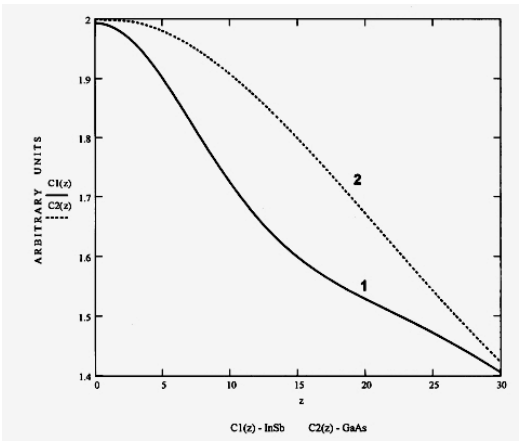

Fig2. The dependence of electron heat capacity on the reduced value of the magnetic field $z=\omega_c(H)/\omega_0$ for IbSb

THE CASE OF STRONG DEGENERATION

In the case of strong degeneracy, the magnetic susceptibility, heat capacity and thermopower change nonmonotonously having the oscillatory behavior [3,8].

In the formula given below, it is taken into account that the Fermi level is much lower than $b\cdot(L_x/2)^2$ at the considered concentrations

$$\chi = \frac{e^2}{2\pi L_x mc^2}\cdot\frac{1}{2\sqrt{1+z^2}}\cdot\sum_{N,s}\left(\eta - sg\frac{m}{2m_0}z - \left(N+\frac{1}{2}\right)\sqrt{1+z^2}\right)\cdot\left(\eta - sg\frac{m}{2m_0}\cdot\frac{2+3z}{z} - 3\left(N+\frac{1}{2}\right)\sqrt{1+z^2}\right)\cdot\hat{O}\left(\eta - sg\frac{m}{2m_0}z - \left(N+\frac{1}{2}\right)\sqrt{1+z^2}\right) \tag{24}$$

$$C_V = \frac{L_y L_z m}{\hbar^2}\cdot\sqrt{1+z^2}\,\frac{\pi}{6}\cdot k_0^2 T\cdot\sum_{N,s}\hat{O}\left(\eta - sg\frac{m}{2m_0}z - \left(N+\frac{1}{2}\right)\sqrt{1+z^2}\right) \tag{25}$$

$$\alpha(H) = -\frac{L_x L_y}{n}\cdot\frac{m\sqrt{1+z^2}}{\hbar}\cdot\frac{\pi}{6}\cdot\frac{k_0^2 T}{e}\sum_{N,s}\hat{O}\left(\eta - sg\frac{m}{2m_0}z - \left(N+\frac{1}{2}\right)\sqrt{1+z^2}\right) \tag{26}$$

where $z=\omega_c/\omega_0$, $\eta=\varepsilon_F/\hbar\omega_0$

Here, η the position of the Fermi level is determined from the expression for the concentration and depends weakly on the magnetic field:

$$n = \frac{m\omega_0}{2\pi\hbar}\sqrt{1+z^2}\cdot\sum_{N,s}\left(\eta - sg\frac{m}{2m_0}z - \left(N+\frac{1}{2}\right)\sqrt{1+z^2}\right)\hat{O}\left(\eta - sg\frac{m}{2m_0}z - \left(N+\frac{1}{2}\right)\sqrt{1+z^2}\right) \qquad (27)$$

As the magnetic field increases, the quantum levels located lower than the Fermi level intersect the Fermi level leading to the abrupt decrease in absolute value of thermopower, magnetic susceptibility and heat capacity. However, between the above abrupt decreases the density of states, the magnetic susceptibility, heat capacity and magnetothermopower increase proportionally to $\omega(H)$ and thus, the oscillatory behavior $\sigma(H)$, $C_V(H)$ and $\alpha(H)$ are observed.

The dependences $\sigma(H)$, $C_V(H)$ for InSb $n=10^{12}cm^{-2}$ (curve 1) and GaAs $n=5\times10^{11}cm^{-2}$ (curve 2) at T=4,2K are shown in fig.3 and 4, respectively. The concentrations are higher than in the nondegenerate case since our aim was to observe several oscillations.

In the case of InSb, the jumps are nonuniform due to a considerable influence of the quantum level spin splitting.

Thus, in the present paper the magnetic susceptibility, heat capacity and nondissipative transverse magnetothermopower in a quantum well have been investigated. The expressions for the density of states, magnetic susceptibility, entropy, heat capacity and thermopower of electron gas have been obtained. It is shown that in the case of degeneration, the dependence of $\sigma(H)$, $C_V(H)$, $\alpha(H)$ on the magnetic field has a nonmonotonous oscillatory behavior.

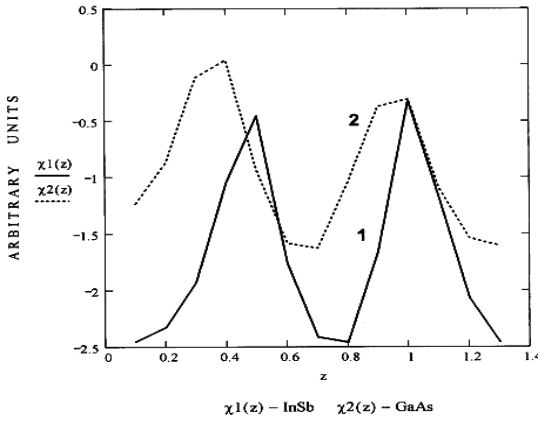

Fig 3. The dependence of magnetic susceptibility on the reduced value of the magnetic field $z=\omega_c(H)/\omega_0$ for IbSb (curve 1) and GaAs (curve 2) for the degenerate case.

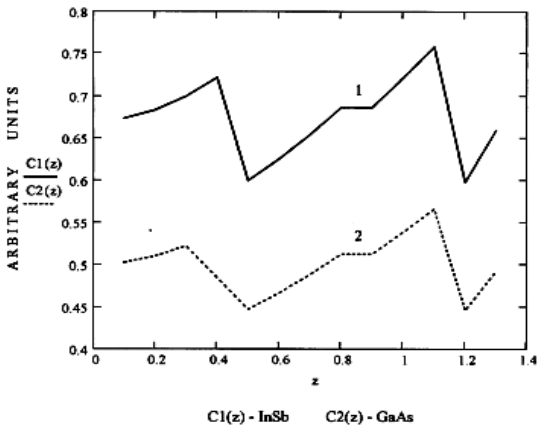

Fig.4. The dependence of electron heat capacity on the reduced value of the magnetic field $z=\omega_c(H)/\omega_0$ for IbSb (curve 1) and GaAs (curve 2) for the degenerate case.

[1] *C.W.J.Beenakker, A.A.M.Staring*. Phys.Rev. B46, 15, 9667,1992.

[2] *E.N.Bogachek, A.G.Scherbakov, Uzi Landman.* Phys. Rev. B54, 16, 11094, 1996.

[3] *J. Heremans and C.M. Thrush*. Phys.Rev. B59, 19, 12579, 1999.

[4] *B.Ludoph and J.M.van Ruitnbeek*. Phys.Rev. B59, 19, 12290, 1999.

[5] *E.N.Bogachek, A.G.Scherbakov, Uzi Landman*. Phys. Rev. B62, 15, 10467, 2000.

[6] *E.N.Bogachek, A.G.Scherbakov, Uzi Landman*. Phys. Rev. B53, 20, 13246, 1996.

[7] *W.Zawadski.* Springer Series in Solid State Sciences, Vol.87, High Magnetic Fields in Semiconductors Physics, © Springer-Verlag Berlin, Heidelberg, 1989.

[8] *J.Hammersberg and H.Weman.* Phys. Rev. B54, 7, 4835, 1996.

[9] *V.M.Galitsky, B.M.Karnakov, V.I.Kogan*. Problems on quantum mechanics. Moscow, Nauka, 1981, 684 p.

[10] *M.P.Stopa and S.D.Sarma*. Phys. Rev. B40, 14, 10048, 1989.

[11] Handbook of Mathematical Function, Ed. by *M.Abramowitz and I.A. Stegun* (Dover, New York, 1971; Nauka, Moscow, 1979.

[12] *T.Darnhofer, U.Rossler*. Phys.Rev. B47, 23, 16020 1993.

[13] *Yu. Obraztsov*. Fiz.Tverd.Tela, Vol.6, p.414, 1964, vol.7, p.573, 1965.

Received: 08.05.02

THE MATHEMATICAL MODELING OF COMPONENTS DISTRIBUTION IN SOLID SOLUTIONS InSb-InAs AT THE ZONE RECRYSTALLIZATION

G.H. AJDAROV, M.A. AKPEROV, V.V. MIR-BAGIROV, E.S. HUSEYNOVA
Institute of Physics, Azerbaijan National Academy of Sciences
H. Javid ave. 33, 370143 Baku, Azerbaijan

The mathematical modeling of components distribution in crystals of solid solutions InSb-InAs at the zone recrystallization of the material was constructed, regarding changes of component segregation coefficient with the melt content. Concentration components profiles along ingots for various values of operation parameters (compound of the melted band) were calculated. Obtained results determine the optimal mode of InSb-InAs crystals growth with the fixed homogenous and variable contents.

The significance of the study of semiconductive solid solutions of binary systems is determined by the control possibility of fundamental crystal parameters, determined optic-electron properties of the material by means of the components ration change. It is known, that the diamond-like system of solid solutions InSb-InAs refers to the rank (class) of perspective material both in scientific and applied aspects. Results of theoretical calculations of the components distribution in this system at crystals growth from the melt by Chohralskiy method were represented in paper [1]. Analogous problems were solved recently for the system Ge-Si [2-4], results of which are in agreement with experimental data. The mathematical modeling of components distribution in quasi-binary system of solid solutions InSb-InAs at the zone recrystallization of the material was constructed in the present paper, regarding the complex nature of the change of component distribution coefficient with the melt compound. The purpose of the paper is determination of optimal operation parameters for InSb-InAs crystals preparation with fixed homogenous and variable compound.

The problem was solved in the following approximation [2,5]: the evaporation and compound components resolution (decay) are absent in the melt, InSb and InAs diffusion rates are rather high in the melt and provide the compound uniformity on the overall volume, the components diffusion in the solid phases is negligibly low, the equilibrium between liquid and solid phases, determined by the state diagram of the quasi-binary system, exists in the crystallization front, the crystallization front is plane, the compound of the original polycrystalline ingot is macroscopic homogenous.

Let us introduce following notations: V_m^0 and V_m are volumes of the melted zone at initial and current moments: C_c, C_i, C_m are molecules concentrations of the second component (InAs) in the crystal, original ingot and melt, respectively, C_m^0 is concentration of the second component in the melted and at the initial moment, C is the total number of InAs in the melt, V_c is melt volume crystallized in the time unit, V_i is InSb-InAs ingot volume melted in the time unit, $K=C_0/C_m$ is equilibrium segregation coefficient InAs, L, and Z are lengths of original ingot, melted zone and recrystallized part of the ingot, respectively.

According to the problem, conditions we consider, that the rate of the melt crystallization V_c does not depend on the time and then we receive in accepted above notations:

$$C_m = \frac{C}{V_m}; \qquad \frac{\dot{C}V_m - \dot{V}_m C}{V_m^2}, \tag{1}$$

$$V_m = V_m^0 - (V_c - V_i)t \tag{2}$$

We consider, that till the final melted zone both V_c-V_i and V_c do not depend on time. In this case following relationships are right at the initial part of the ingot of the length L- :

$$V_m = V_m^0, \quad C_m^0 = C_i \text{ and } \dot{C} = V_c C_m K + V_i C_m^0 \tag{3}$$

Substituting (3) in (1) and dividing variables we receive after integration:

$$\int_{C_m^0}^{C_m} \frac{dC_m}{C_m^0 - C_m K} = \frac{V_c}{V_m^0} = \frac{Z}{l} \tag{4}$$

In limits of the latter melted

$$V_m = \mathrm{V_m^0} - \mathrm{V_c}t, \; \dot{V}_m = -V_c, \quad \dot{C} = -V_c C_m K \tag{5}$$

Substituting (5) in (1) after integration we receive:

$$\int_{C_{mf}^0}^{C_m} \frac{dC_m}{C_{mf}^0 - C_m k} = \ln \frac{V_m^0}{V_m^0 - V_c t}, \tag{6}$$

here C_{mf}^0 is the start concentration of the second component in the latter melted zone. Marking the part of the super-crystalline melt $V_c t / V_m^0$ by the symbol g, we rewrite the equation (6) in the following form:

$$g = 1 - \exp\left[- \int_{C_m}^{C_{mf}^0} \frac{dC_m}{C_m K - C_m} \right] \tag{7}$$

To calculate the integrals (4) and (7) we should know the analytic dependence of the segregation coefficient K on the melt compound C_m. For the examined system InSb-InAs versus the compound, K changes in a complex way from ~20.5 to1 and does not yield to the mathematical description. The dependence diagram of K on C_m in the overall range of component concentration was constructed in paper [1] on the base of state diagram data of this system in conjugated solid and liquid phases. Applying these data, integrals in equation (4) and (7) may be calculated by the numerical (graphic) method [2,5].

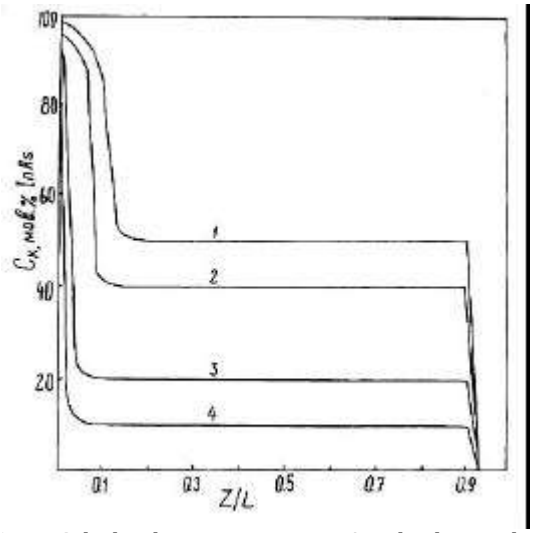

Fig.1. Calculated concentrations InAs alond crystals InSb-InAs, grown by the method of the zone melting. The length of the melted zone =*L/10*. The original compound of ingots is: 1 – C_i=*50;* 2 – *40;* 3 – *20;* 4 – *10 mole%* InAs..

The components distribution in the ingot InSb-InAS, calculated from equations (4) and (7) by the numerical method, for four various values C_i is demonstrated on fig.1. In the calculation it was accepted, that =*L/10*. As it is seen from fig. 1, at all cases the concentration InAs is maximal in the ingot origin and, then, reducing, reaches homogeneity with $C_c=C_i$, At the ingot end the second component concentration again begins to fall and reaches practically zero at $Z=L$. The length of the final part with the variable compound for all examined ingots compositions, is equal to the width of the melted zone . The extent of the original part with the variable compound depends on the initial ingot composition. It is connected with the segregation coefficient change with the melted zone compound. The rate of the compound change along the crystallization direction on the final part of the melted zone falls with C_i reduction, since the length of this zone is fixed according to the problem condition.

The control possibility of InAs concentration profile in the ingot by the change of the melted zone length is demonstrated on fig.1. As, for example, the distribution of InAs along the ingot InSb-InAs for four various values of is illustrated on fig.2. The original compound of all ingots is identical and contains 40 mole %.

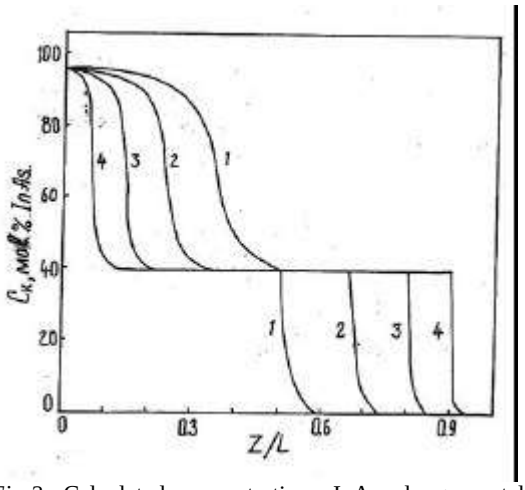

Fig.2. Calculated concentrations InAs along crystals InSb-InAs, grown by the method of the zone melting from the original compound $InSb_{0.6}InAs_{0.4}$. The length of the melted zone is: 1 – =*L/2;* 2 –*L/3;* 3 –*L/5;* 4 –*L/10*..

The influence efficiency of operation parameters on the components redistribution in the ingot InSb-InAs at the zone recrystallizat ion of the material is visually demonstrated on curves of fig.2.

As it is seen, the length of the melted zone in wide (broad) limits determines the extent of crystals parts with variable and homogenous compounds.

Family of curves of fig.1 and 2 shows the possibility of mathematical modeling for operation parameters determination and optimal technological conditions for InSb-InAs crystals growth with the fixed homogenous or variable compounds.

The following conclusion may be done on the base of aforesaid data and results.

The mathematical modeling of component distribution in solid solutions InSb-InAs, at the zone recrystallization of the material, conducted, regarding the dependence of components segregation coefficient with the melt compound, allows to value optimal technological parameters, as the original compound of the ingot and length of the melted band, with the purpose of the crystals receipt with the fixed components distribution.

[1] *G.H. Azhdarov, E.S. Huseynov, M.A. Àkperov*. Izvestiya ÀS of Azerabijan, ser.. physico-technical and math. sciences, 2000, v.20, ¹5, p.11.

[2] *G.Kh. Azhdarov, T. Kuchukomeroglu, A. Varilci, M. Altunbash, A.I. Kobya, P.G. Azhdarov*. J.Crystal Growth, 2001, v.226, p.437.

[3] *I. Yonenaga.* J. Crystal Growth, 2001, v.226, p.47.

[4] *P.G. Àjdarov, N.À. Àgayev*. Non-organic materials, 1999, v.35, p.903.

[5] *V.Ì. Glazov, V.S. Zemskov*. «Physico-chemical bases of semiconductors alloy », Moscow, «Science», p.371.

Received: 18.03.02

INFLUENCE OF ANTIOXIDANTS ON THERMAL PROPERTIES OF FIBROINS OF NATURAL POLYMER

R.S. ISMAILOVA, N.A. EYUBOVA, S.G. ALIEVA
Sector of radiation researches, NAS Azerbaijan, Baku, Azerbaijan

Thermophysical properties of fibroins of natural polymer are investigated. It is established, that at injecting of antioxidants N- (3,5-di-tret-butyl-4-hydroxyfenil) salicylaldimin into the structure of fibroins, by additional fertilizing of caterpillars by last-named, amorphous sites increase and thus the stability of silk to external influences raises, i.e. the stabilization occurs due to sewing action of antioxidant.

Correlations between crystal and amorphous phases of fibroin of natural polymer, a degree of thermostability, temperatures of fusion, vitrifying and thermal destruction, we investigated by means of derivatographical analysis.

Derivatogrammes were taken from derivatographe Q-1000 of firms ÌÎÌ. Hinge plate of samples was 50-70 mg, mg was 100, sensitivity channel DTA was 1/5, DTG was 1/10, inert substance (oxide of aluminum) was fastened at 1000°C within 10 hours.

The natural polymer silk fibroin was used as object of research, received from caterpillars, both fed up by antioxidant, and without feeding. Since the IV age tested groups were fed up by antioxidant N- (3,5-di-tret-butyl-4-hydroxyfenil) salicylaldimin, with the formula:

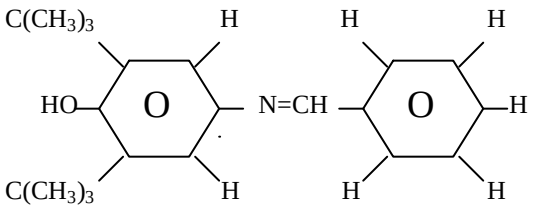

In a fig. 1 fibroin dervetogramme of control and tested samples is given. According to the figure, character of curves DTA, TG, DTG for tested and control samples are similar.

From curves of losses of weight TG we see, that in the region 70-100 $^{\circ}$C there is a loss of weight about 20-30 % (on DTG effects at 90 100°C), that is caused by secretion of adsorptive moisture [1,2].

Endothermic effect on curve DTG (insert) in the region of 150-165°C is connected with melting of a crystal part of fibroin [3]. The areas of endothermic effects on curves DTG at 330-360 $^{\circ}$C, caused by destruction of fibroin,as we see from the insert, considerably increase versus the contents of antioxidant.

At the same time, according to the insert on DTA curve reduction of the area of endothermic effect is obviously seen at 165°C, corresponding to melting of silk fibroin received with additional fertilizing of caterpillars by antioxidant. Ratios of areas of melting effect (vitrifying) of a crystal part of natural polymer between control and tested samples correspond to: Ê: Î = 4.4:3.2, i.e. the degree of crystalline of the tested sample slightly decreases (approximately on 14 %). Along with this, the growth of vitrifying temperature on 15 $^{\circ}$C is observed. Thus for the control samples T_s=150 $^{\circ}$C, and for the tested samples T_s =165 $^{\circ}$C. The presence of such changes in tested samples in comparison with control samples gives us the right to assert about increase in refractoriness of the crystal part of fibroin, received by additional fertilizing of caterpillars of silkworm by antioxidant.

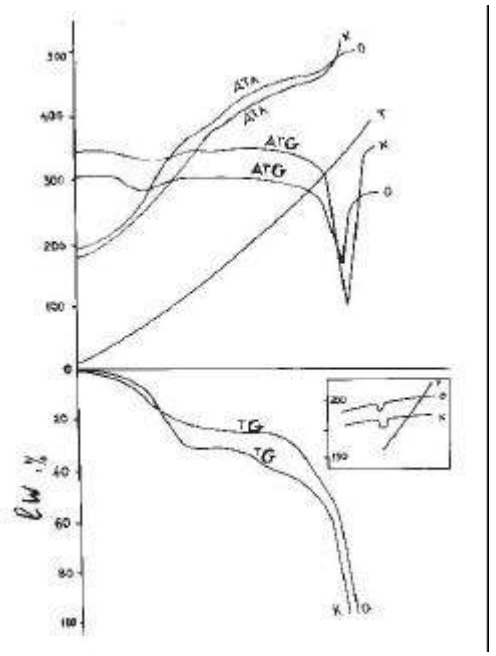

Fig.1. Derivatografical curves of fibroin: K are control, and O are tested samples

According to the fig.1, the beginning of thermal destruction of fibroin of the crystal part of natural polymer in the tested sample corresponds to 320°C, and in the control samples to 300°C. However the loss rate of weight (DTG) in the control sample is in 1,9 times more, than in the tested sample that testifies on increase of a degree of refractoriness of tested samples.

On the basis of data of derivatigraphical researches of natural polymer fibroin it is possible to conclude, that antioxidant actively includes in the molecular structure of fibroin, in consequence the degree of crystalline decreases, and this causes increase of a degree of fibroin amorphism.

The following fact also is the confirmation of given conclusions: the antioxidant [4] has property to render the antiradical action, causing the delay of formation rate of free radicals in fibroin, and thus promotes to reduction of quantity of submicrocracks in a material.

Thus, we can tell, that at injection of the antioxidant into the structure of natural polymer silk, most likely, chemical bonds, causing a branching of macromolecules of fibroin are formed in lateral chains.

[1] *S.D. Êîstuk, Ì.V. Polovnikova*. Research of thermal properties of the natural silk-silk, 1938, ¹3, p. 27-28
[2] L.G. Berg. Introduction to thermograph, Ì.Nauka 1969, p.108.
[3] Analytical chemistry of polymers, Ì. Izd. "Mir", 1965, p.471.
[4] R.S. Ismailova, S.G. Aliyeva. Stimulator for increase of mulberry efficiency growing. Kimya-biologiya elmlôri vô tôhsilinin aëtual problemlôri. Res. elmi konfrans material. (5-7 noyabr, 2001-ci il), sôh. 27-29.

Received: 14.05.02

THE ROENTGENOGRAPHIC STUDY OF LAYERED SEMICONDUCTORS OF $Ga_{0,5-x}Sn_xIn_{1,5}S_3$ TYPE

G.G. HUSEYNOV, V.A. GASIMOV, F.G. MAGERRAMOVA
Institute of Physics Azerbaijan National Academy of Sciences
H.Javid av, 33, Baku, 370143

For the first time the phase-formation in the system $Ga_{0,5-x}Sn_xIn_{1,5}S_3$ was investigated in details by the method of the thermal, roentgenographic, microstructural analysis. Their monocrystals are obtained by the method of the direct crystallization. It was established, that they belong to the initial stage of the ordered polytype series of the structure of the layered type on the vourcite base.

Introduction

The significance of the physical-chemical and structural study of substance with semiconductive properties is obvious. The synthesis, the monocrystals growth, the study of their physical-chemical and structural peculiarities, phase-formation regularities and the mechanism of structural phase transition have a great scientific-practical mean. In this aspect Ga_2S_3-In_2S_3 system compounds are perspective objects for the solution of questions of the structurization, polymorphy, polytype, methods of the phase stabilization and the clarification of characteristics physical-chemical properties.

The phase equilibrium in Ga_2S_3-In_2S_3 quasi-binary cut of the triple system Ga-In-S were for the first time studied by authors [1,2], where the formation of just one triple phase GaInS, melting uncongradually, was established. It should be noted, that in these papers there is a visible discrepancy in the state diagram and values of hexagonal cell parameters. Neither was determined the crystal structure of the compound.

Judging from experimental facts on the presence of some polymorphy modifications in sesqui chalcogenide of A_2S_3 (A-Al, Ga, In) type, authors [3,9] investigated in details the phase-formation in the given system.

Applying the method of chemical transport reaction (CTR), the presence of polymorphy phases line, polytype forms and three independent compounds (table 1) was established as result of roentgenostructural study of monocrystals, obtained from before synthesized contents $Ga_{0,5}In_{1,5}S_3$ and $GaInS_3$ in various temperature gradients.

To reveal the influence of multivalent tetrahedral atoms on the stabilization of polymorphy modifications $(GaIn)_2S_3$, partially substituting tetrahedral placed atoms Ga and In by atoms Cu and Mn (conserving the total balance of the valency) by the method of direct synthesis, authors [10,11] realized 2H and 3R polytypes, having the layered structure of polytype line a= 3,82 Å, c 15Å· n (n = 2,3) and a = 3,82Å, c 18 Å· n (n = 2).

Experimental part

The objective of the present work is to receive the monocrystals on the base of $Ga_{0,5}In_{1,5}S_3$ with the partial substitution of tetrahedral coordinate atoms In(Ga) by atoms Sn and the study of their structure and phases stabilization .

The synthesis was conducted in pumped-out quartz ampoules (10^{-2} Pa) in the one-temperature furnace at 1223-1273 K (the heat rate is 100 grade/hour). After half an hour keeping at this mode the ampoule was slowly cooled up to the temperature 673-693 K and was held at the given temperature during 72 hours, As a result samples from yellow ($Gà_{0,17}Sn_{0,5}In_{1,5}S_3$) to red ($Gà_{0,33}Sn_{0,25}In_{1,5}S_3$) colors, lightly cracked on the fine plate-layered crystals, were obtained.

Table 1

Crystallographic data of polymorphic phases and polytype forms of compounds of $(GaIn)_2S_3$ content.

The content of the phase	Sp.gr.	à, Å	â, Å	Ñ, Å	Z
$GaInS_3$	Ð3ml	3,81		18,19	2
$GaInS_3$	P3ml	3,81		54,61	6
$GaInS_3$	$P6_1$	6,65		17,92	6
$GaInS_3$	$P6_3mc$	3,81		30,62	10/3
$GaInS_3$	P3m	3,81		45,89	5
$GaInS_3$	$Bb2_1m$	19,06	6,19	3,81	4
$Ga_{0,5}In_{1,5}S_3$	P3ml	3,84		12,33	1
$Ga_{0,5}In_{1,5}S_3$	R3m	3,81		100,04	11
$Ga_{0,67}In_{1,33}S_3$	2H	7,64		74,00	8
$GaInS_3$	R3m	3,82		63,41	6
$Ga_{0,25}In_{1,75}S_3$	C2/m	6,55	3,72	12,62 â=100°	4
$GaInS_3$	Shpinell str. Type	10,79			8

It should be noted, that temperature conditions at the initial stage of the synthesis were chosen by the experimental way with the involvement of the literature data analysis on the receipt of binary compounds In_2S_3, $Gà_2S_3$, SnS and the thermographic record of synthesis process of each content. By this it was supposed, that the fusing temperature grows almost in a linear fashion with the content change. Though the obtained material has the crystal-mosaic nature, the method is reliable and may be successfully applied to obtain many sulphides, having the layered structure.

The roentgenographic study showed, that all synthesized samples are homogeneous and applicable for the detailed roentgenographic analysis. The diffractograms were obtained on the device DRCI (the roentgen diffractogram of common use) (the radiation Cu-K_α). The analysis of calculated inteplane distances (d) showed, that investigated contents are isostructural and formed on the base of the ordered phase $GaInS_3$, realized in the temperature gradient 873-973 K with the part of crystal J_α (CTR). The indexing of interplane distances allowed to reveal, that both contents are isostructural and crystallized, unlike the ordered modification $GaInS_3$, in the

rhombohedral lattice with parameters: a=6,500 Å; c= 18,685 Å, V=684,13Å^3, Z=6, sp.gr. $P6_2$, V_s= 38,45 Å^3 and a=6,485 Å; c= 18,653 Å^3, V=679,81Å^3, Z=6, V_s= 37,77 Å^3; for $Gà_{0,17}Sn_{0,5}In_{1,5}S_3$ and $Gà_{0,33}Sn_{0,25}In_{1,5}S_3$ respectively. Roengenographic data of the samples under investigation are presented in table 2.

Synthesized compounds with regard to various solvents are mainly stable (concentrational mineral acids dilute them with the hydrogen sulphide emission), and keep the primary characteristics fore a long time.

Microhardenesses were determined on polished semicrystalline samples. The research showed, that the microhardeness of samples under investigation depends on the orientation of fine-crystalline faces of the surface for $Gà_{0,33}Sn_{0,25}In_{1,5}S_3$ and $Gà_{0,17}Sn_{0,5}In_{1,5}S_3$ respectively.

Table 2

Roentgenographic data of phases $Gà_{0,17}Sn_{0,5}In_{1,5}S_3$ and $Gà_{0,33}Sn_{0,25}In_{1,5}S_3$

$Gà_{0,17}Sn_{0,5}In_{1,5}S_3$			$Gà_{0,33}Sn_{0,25}In_{1,5}S_3$		
d_{exp}	I/I_0	HKL	d_{exp}	I/I_0	HKL
6,2282	55	003	6,2195	45	003
3,2503	100	110	3,2433	100	110
3,1146	15	006	3,1104	10	006
2,8810	20	113	2,9159	10	113
2,8053	15	200	2,8070	10	200
2,7352	15	106	2,7565	10	106
2,6984	80	202	2,6952	70	202
2,2936	10	116	2,2325	12	116
2,0767	60	009	2,0731	50	009
1,9489	12	109	1,9411	10	109
1,9058	90	118	1,9018	80	118
1,8413	10	302	1,8289	10	302
1,6260	10	220	1,6218	8	220
1,5856	10	223	1,5713	8	223
1,5564	12	0012	1,5531	10	0012

Discussion

Results of the experimental study on the synthesis and roentgenographic analysis of polytype forms of compounds of $Gà_{0,5-X}Sn_XIn_{1,5}S_3$ type were described above. It was established, that they are individual compounds and isostructural with the ordered structure on the base of vourcite, and are photosensitive in visible region of the spectrum. Certainly, the presence of experimental data on the transmission, absorption, voltamperic characteristics is necessary for the discussion of optic and electrooptic properties of materials under investigation. These works are still underway and it is planed to report on results in the nearest future. We should note only the fact, that the width of the forbidden band of investigated samples is visibly reduced in comparison with the ordered phase $GaInS_3$, for which F_g makes 2.84 eV.

In the present paper we found that it is necessary to discuss experimental facts of the phase-formation and the influence of various cations on the stabilization of polymorphic modifications. $Gà_2Sn_3 – In_2S_3$ system phases, realized to the present time, are assembled in table 1. Their structural data are described in papers [3-9,12]. It should be noted, that three stable polymorphy varieties of $(GaIn)_2S_3$ type-monoclinic, rhombohedral, cubic and five polytype lines, the line beginning from structural variant ã – In_2S_3, i.e. c 9 Å· n, the line with period c 12 Å· n; c 15 Å· n ; c 18Å· n, with the constant value a 3,8 Å and the ordered line with the constant a 6,5 Å, c 18 Å are distinguished among revealed phases.

The preliminary crystal-chemical analysis of indicated structural facts allows to reveal, that unlike the influence of copper atoms, where the polytype line

c 15 Å· n and Mn-Ohm polytype line with c 12 Å· n are mainly stabilized, at the tin part, as a stabilizing atom, the ordered phase, realized in limits of the spatial group of $P6_2$ symmetry and non $P6_1$ for the ordered phases $GaInS_2$, is formed. Such situation allows to conclude, that, except the valency of “elements-stabilizers”, ion radii and Jn and Ga atoms ratio have the essential part for the phase stabilization.

Conclusion

Therefore, crystallographic and physical-chemical properties of crystals $Gà_{0,17}Sn_{0,5}In_{1,5}S_3$ and $Gà_{0,33}Sn_{0,25}In_{1,5}S_3$ are for the first time synthesized and investigated. It was established, that these crystals are wide band semiconductors and form the ordered structure of the layered nature.

[1] *M.I. Zargarova, R.S. Gamidov*. Izv. ÀN USSR. Non-organic materials, 1969, v.5, ¹5, p.371.

[2] *V.P. Ambros, I.Y. Andronik, V.P. Mushinskii and etc*. Some questions of chemistry and physics of complex structure semiconductors. Ujgorod, USU Issue, 1984, p.238.

[3] *I.R. Amiraslanov, R.B. Valiyev, G.G. Huseynov, Y.G. Asadov*. Reports of Azerbaijan SSR AS, 1990, v. 44, Issue 1, p.33-36.

[4] *G.G. Huseynov, M.G. Kazimov, A.S. Guliyev and etc*. Reports of Azerbaijan SSR AS, 1988, v. 44, ¹ 7, p.26-29

[5] *I.R. Amiraslanov, G.G. Huseynov, H.S. Mamedov, A.S. Guliyev*. Crystallography, 1988, v.33, ¹ 3, p.767-768

[6] *G.G. Huseynov, I.R. Amiraslanov, A.S. Guliyev, H.S. Mamedov*. Izv. AS SSSR, “ Non-organic materials”, 1987, v.23, ¹5, p.854-856.

[7] *G.G. Huseynov, I.R. Amiraslanov, A.S. Guliyev, H.S. Mamedov*. Crystallography, 1987, v.32, ¹1, p.243-244.

[8] *I.R. Amiraslanov, Y.G. Asadov, P.A. Maximov, V.N. Molchanov. and etc*. Crystallography, 1981, v.36, ¹2, p.332.

[9] *M.G. Kazimov, G.G. Huseynov, A.B. Magerramov, I.G. Aliyev*. Fizika, 1999, v.5, ¹1, p.18-19.

[10] *M.G. Kazimov, G.G. Huseynov, I.G. Aliyev, A.B. Magerramov*. The Influence of atoms of copper and manganese on the structure of polymorphy modifications $Gà_{0,5}In_{1,5}S_3$ at the partial structure of

gallium atoms.- Report thesis of the First International Scientific-Technical Conference on mat6erial history and diamond-like semiconductors - 1994 , v.1, p.188

[11] *M.G. Kazimov, J.G. Aliyev, O.M. Aliyev, G.G. Huseynov*. Satellite Conf. of the XXX Annual meeting of the European 1 pres. Res. Group. Physics of Multicomponent Semiconductors. Baku, 1992, p.54

[12] *I.R. Amiraslanov, G.G. Huseynov, A.S. Guliyev, T.H. Azizov, H.S. Mamedov*. Monocrystals growth, the structure and crystallochemistry of polymorphy modifications $GaInS_3$- Preprint ¹183, Azerbaijan I9PAS, Baku, 1986, p.39.

Received: 10.05.02

TENSOMETRIC PROPERTIES OF VOLUMETRIC CRYSTALS OF GERMANIUM-SILICON SOLID SOLUTIONS

SH.M. ABBASOV
Radiation Research Department of Azerbaijan National Academy of Sciences
H.Javid ave. 31[a], Baku 370143

In the present work the tensometric properties of monocrystal of Ge-Si solid solution of p-type with Si content 5-10 at.% have been studied. From the studied crystals the strain gauge sensors have been made. To do this, the section was cut out from a sample perpendicular or parallel to the crystal (111) axis, and then crystal was cut on plate of 200 mcm thickness. The samples after polishing had a thickness 30-40 mcm and a length 2 mm.

The semiconducting materials hold a special place among the substances, possessing the tensor effect. The investigations [1-3] established that the resistance semiconducting tensometers have a variety of advantages in comparison with the wire ones.

The most widely used semiconducting materials in strain gauge sensors and transformers are germanium and silicon offering the significant tensor effect [4-6]. The successful use of tensoresistors in different fields of science and engineering specifies the necessity for the further study of the tensometric properties not only of germanium and silicon but also of the germanium-silicon solid solutions. As to the solid solutions of the germanium-silicon system, their tensometric properties have been studied [2-3]. Here the monocrystals Ge – Si have been studied. From the works [2-3] it follows that the systematical investigation of Ge – Si solid solutions has not been carried out. Evidently, for elucidation of all the advantages of Ge – Si solid solutions the further research in this direction is necessary.

In the present work the tensometric properties of monocrystal of Ge – Si solid solution of p – type with Si content 5-10 at.% have been studied.

From the studied crystals the strain – gauge sensors have been made. To do this, the section was cut out from a sample perpendicular or parallel to the crystal (111) axis, and then crystal was cut on plate of 2 mcm thickness. The samples after polishing had thickness 30-40 mcm and length 2 mm.

Since the semiconducting crystals limiting deformation increases with decrease of their diameter [3-5] as well as the surface areas are slightly damaged in cutting, the samples are etching in hydrofluoric acid. As a contact material there has been used the golden microwire prekept in antimony vapours. The contact quality was checked by their volt-ampere characteristics.

The unit described in [3] was used in investigation. For determination of the tensosensitivity coefficient the tensoresistor was fastened to an elastic cell which was given the known value of deformation. In this case the dependence between deformation and deflection was used. This dependence for the clean bend is determined by formula:

$$\varepsilon = \frac{Mh}{2EJ} = \frac{h}{2r} = \frac{4hy}{l^2 + 4y^2}$$

where l is a distance between supports, y is a value of deflection, M is a bending moment, h is a thickness of elastic cell (beam), E is a module of elasticity, J is a inertia moment, ñ is a radius of curvature

Dependence of resistance change on deformation (ε) is presented on the Fig.1.

The samples are different in base that has led to the lack of coincidence of their graduation characteristic though they have been cut out from the same Ge – Si solid solution. In the case, when the axis of Ge – Si solid solution tensoresistor is parallel to the plane (111), the tensosensitivity coefficient is equal to 0 unlike the tensoresistors orientated in the direction (111) when tensosensitivity coefficient is large and the graduation curves are characterized by the linear dependence.

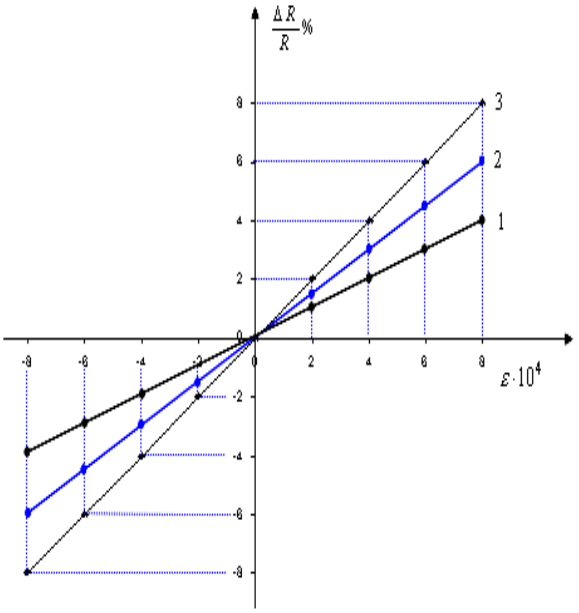

.

Fig.1. Dependence of $Ge_{1-x}Si_x$ crystals resistance change ($\frac{\Delta R}{R}$) on deformation at x values: 1-0; 2-0.05; 3-0.10

For the investigation of the mechanical properties of the studied Ge – Si solid solutions tensoresistors the method of tensile strain was used.

The deformation and tension of the elastic region was calculated by formula:

$$\varepsilon = \frac{d}{l^2 / 3r} \quad \sigma = \frac{F}{\pi r^3 / 2l}$$

where å is a relative strain, ó is a tension, r is a radius, l is a length of a sample, ä is an arrow of flight.

Thus, the tensometers made from Ge – Si solid solution have the high tensosensitivity coefficient, the

dependence of the resistance change on strain change in the strain region under investigation is linear one, hysteresis is absent, the influence of different physical factors on the tensometers operation is minimum; therefore the marked samples may be recommended as tensoresistors.

The nature of strength change depending upon Si content in Ge. The presented plots show that in these dependences two representative regions are observed: strong softening and little change of the mechanical parameters. With Si content up to 10 at. % the mechanical strength of $Ge_{1-x}Si_x$ crystals increases as compared with higher Si content and this agrees well with the results of works [1]. It is seen that with the most sharp changes and going into the saturation of microdefect values at different doses the foregoing statement is well confirmed, i.e. at $10^{15} \div 10^{16}$ el/ñm^2 doses the annihilation of defects plays a leading part and at 10^{17} el/cm^2 the annihilation process and microdefect are saturated. It should be taken into account that in $Ge_{1-x}Si_x$ crystals under study the local heterogeneities with linear sizes ~2 and ~12mcm connected with dislocations [7] are available. It is established that $Ge_{1-x}Si_x$ crystals strength increases with increase of irradiation dose up to 10^{16} el/ñm^2 and at the large (~10^{17} el/ñm^2) doses it decreases. As it is shown above the nature of $Ge_{1-x}Si_x$ crystals strength change, is well explained by interaction of point defects created by the irradiation with the structural defects and dislocations.

Obtained in experiments the whole complex of data on the study of the accelerated electrons flow action on mechanical properties on $Ge_{1-x}Si_x$ base is possible to be explained assuming that under the accelerated electron flow action the simplest disturbances of the crystal lattice, arising at irradiation and being the defects of "vacancy" type lattice take place.

From these considerations for the explanation of the radiation effects in $Ge_{1-x}Si_x$ crystals there has been proposed a model based on the ideas of the structural heterogeneities of the solid solutions consisting of the regions enriched either by silicon or germanium. The interface between these regions serves as the efficient drain for interpoint atoms forming as a result of irradiation. Their intense absorption and enrichment of volume with free vacancies determine the features of the radiation processes in $Ge_{1-x}Si_x$ crystals and in devices on their basis.

[1] Sandulova A.V., Bogayavlensky P.S., Dronyuk M.M. Doklady AN SSSR, 1963, v.153, ¹ 2, p.380.
[2] Semiconducting strain gauges. Edited by M.Dick. Moscow, "Energiya", 1965
[3] Koltakov B.K., Vandishev B.A., Savitskii. Proceedings of metrologic Institutes of USSR, Moscow, 1974, 156, 216 p.
[4] Abbasov Sh.M., Abbasov Sh.I., Klimovskaya A.I., Baitsar RI., Ostrovsky P.I., Krasnozhonov E.P. NAN Azerb. Respub. Baku, Publishing house "Elm", 2000, v.2a, ¹ 2, p.117-121.
[5] Akhromenko Yu.G., Baitsar R.I., Krasnozhonov E.P. Phys. Electronika. – Lvov. 1985. V.20. p.31.
[6] Kerimov M.K., Abbasov Sh.M., Abbasov Sh.I. Fizika. Baku «Elm», 2002, v.8. ¹1. p.3-5.
[7] Ukhin N.A., Bakirov M., Abiyev A.K., Abbasov Sh.M., Gasumov G.M. FTP, 1983, v.18, ¹ 6, p.981-985.

Received: 05.06.02

ON THE APPLICATION OF VARIOUS SWITCHING ELEMENTS FOR INFORMATION TRANSMISSION AND DISTRIBUTION

G.A. ABBASOV, M.N. IBRAGIMOV, M.J. RADGABOV
Azerbaijan Architectural-Building University,
h.5, A. Sultanova str., Baku, Azerbaijan.

Peculiarities of the switching elements use in switching systems are being observed. Electromagnetic and electron elements may be used as switching elements in switching points. Two separated electric circuits are used for the fulfillment of the switching system function at application of electromagnetic relay as the switching element. If electron elements are used in the switching system, then they may be divided into 2 groups on the operating principle: elements with and without memory property.

Electron elements, having the memory property in the state of the stable balance, don't consume the energy. Diodes on the base of compound semiconductors, which don't consume the energy from the source in the balance state, may be used as non-contact switching elements with 2 stable states. Schemes of logic elements, whose work is based on the signals coincidence on the entry, may be used in switching systems in switching points. Then the controlling circuit and the informational circuit are joined in a single element in each switching point.

In switching systems, providing information transmission and distribution, switching elements are used for closing and opening of electric circuits. Various switching elements may be used versus the application region and claims, raised to switching systems, respectively. Electromagnetic and electron elements are usually used in switching systems for the closing and opening of electric circuits [1,2].

Neutral electromagnetic relays of the direct current, named usually as electromagnetic relays with opened and sealed contacts, are most widely used in the technology of the automatic switching as electromagnetic elements.

In switching systems respective switching elements are set in the open state for the closing of electric circuits. If electromagnetic relay is used as the switching element, then the respective relay responses for the closing of the necessary electric circuit.

The response of the respective relay is realized by the special control signal. Respective contacts, forming the transmission section for information signals, are closed at the relay response. Thus, at the application of the electromagnetic relay as the switching element in switching systems two separated electric circuits are used for the fulfillment of the switching system function. One of these circuits is controlling, the other is informational. The relay is switched on and off by means of the controlling circuit, and information transmission is realized by means of the informational circuit, i.e functions, fulfilled by these electric circuits, are different. It is necessary to take into account this peculiarity at the switching nodes formation with the interconnection mechanism of the controlling device with the switching system.

Such interconnection device must provide the output of respective control signals for the response of electromagnetic switching elements. As the control circuit and the information circuit are separated at the use of the electromagnetic relay as the switching element in the switching system, then all controllable relays are joined in one matrix for the control of switching elements.

The selection and the switching of respective switching elements are realized by means of control signals, i.e. the control signal is used only for the controlling circuit of the switching system, but this signal isn't connected with the informational circuit.

It allows to use the signal of the necessary shape and force for the control of electromagnetic elements. Various non-contact elements, having two stable states, are used as electron elements in switching systems. Non-linear dependence between physical values, giving the opportunity of jump-shaped transition of the element from one state into another, is used at the work of these elements.

On the operating principle, electron elements may be with and without memory. In any case the element changes its state under the influence of the external controlling signal, but in one case the element conserves this state up to next appearance of the controlling signal, and in another case it is only temporary, until the controlling signal exists. Electron switching elements, with the memory property, acquire the especial importance, because these elements don't consume the energy from the feed source in the state of the stable balance.

Diodes on the base of compound semiconductors, specifically diodes on the base of copper selenide (Cu_2Se) may be used as non-contact switching elements with 2 stable states [3,4,5].

The scheme of the memory element with the diode on the base of compound semiconductors, worked out by researches of Institute of Physics of Azerbaijan AS, is shown on fig.1.

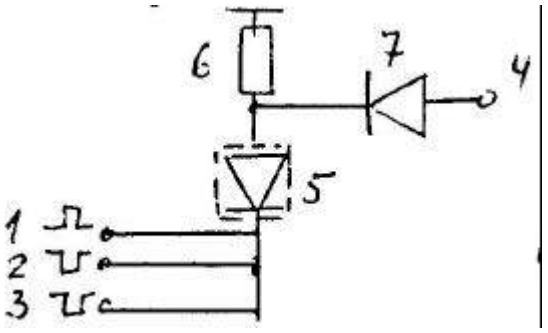

Fig.1. The scheme of the memory element on the base of Cu_2Se.

Element contains the controlling entry (1), informational entry (2), limiting resistor (3), exit (4) and the diode on the base of compound semiconductors (5). The information transmission from the entry 2 to the exit 4 is provided at the receipt of the controlling signal to the entry 1. The switching peculiarity at the use of diodes on the base of compound

semiconductors in switching systems is concluded in the fact, that controlling signals and informational signals are separated in the time and space. Such peculiarity of diodes on the base of compound semiconductors allows to construct switching systems of high reliability.

Schemes of logic elements, for example, the scheme of the logic element "I", whose work is based on the signals coincidence on the entry, are used at the contemporary stage of electron technology development in switching systems. Then both the control circuit and the informational circuit are joined in a single element in each switching point. The controlling signal and informational signal fulfill identical functions. The signal on the exit of the scheme of the logic element is respective output signal of the switching system.

The indicated peculiarity of logic elements allows to construct switching schemes on the matrix principle.

It should be noted, that the use of the same or another elements as the switching element depends on the region of the switching system application and on claims, raised to them.

[1] *O.N. Ivanova.* "Automatic switching", "Radio and communication", Moscow, 1988.

[2] *K.P.Kulikovskiy,V.Y. Kupe.r*"Methods and means of measurements", Moscow, electroatom issue, 1986.

[3] *G.B. Abdullayev, Z.A. Aliyarov, G.A. Abbasov.* "Analytic calculation and the construction of equivalent schemes with the use of d iodes on the base of compound semiconductors", For technical progress, ¹9, Baku, 1974.

[4] *G.B. Abdullayev, Z.A. Aliyarova, G.A. Abbasov and etc.* " Author certificate ¹ 82581, Priority from the 28th of January, 1972.

[5] *G.B Abdullayev, E.N. Zamanova, G.A Abbasov, Z.A. Aliyarova*. "The semiconductive switch", Author certificate ¹ 664419, priority from the 7th of December, 1979.

Received: 07.06.02

THE PRODUCTION OF HIGGS BOSONS IN NON-ELASTIC NEUTRINO-QUARK SCATTERING

V.Z. MUSTAFAYEV
Baku State University
Z. Khalilov st., 23, Baku, 370148, Azerbaijan

The neutral Higgs boson production has been discussed in the $nq \to nlH^o$ inelastic scattering. The cross section of the process has been obtained in the $m_q << m_w$ region and for the ratio of this section to the one for $nq \to lq$ reaction it has been shown that linear growth is possible (~Gs).

As is well known, the Standard Model (SM) of Electroweak Interaction assumes existence of neutral massive scalar Higgs bosons [1]. However, in spite of the fact that many predictions of the model were proved by experiments, and particularly, heavy $W^{\pm}$ and Z^0 bosons were discovered /2/, the Higgs sector of the model has not been yet studied. The search for Hiqqs particles were extended to the energy area of 200 GeV in cms and intensively continued, since the mass of these particles is a free parameter of the theory and can be found in a relatively wide range: *7GeV£mH£1TeV* [3]. Therefore, the current requirement is the theoretical investigation of all possible reactions with participation of Higgs bosons.

The present paper discusses the production of Higgs particles in non-elastic neutrino-quark scattering:

$$\nu(k_1) + q(p_1) \to l(k_2) + q(p_2) + H^0(k) , \quad (1)$$

where 4 momenta of particles are indicated in brackets.

The coupling constant of Higgs boson and other particles is proportional to the mass of particles. Taking into account that quark's mass is $m_q << m_w$ (this is true for *u,d,s,c,b*-quarks but untrue for *t*-quark with mass of m_t *~170 GeV*), it is possible to assume that a diagram with radiation of Higgs boson by intermediate *W* bosons will be the main contribution into the process (1).

The corresponding amplitude can be written as follows:

$$M = -\frac{Gm_w^2}{\sqrt{2}} g_H j D_1 D_2 l_m \left(\delta_{mn} + \frac{q_{2m} q_{2n}}{m_w^2}\right) J_n , \quad (2)$$

where l_m and J_ν are lepton and quark weak currents,

$D_{1,2} = (q_{1,2}^2 + m_w^2 - i\tilde{A}_w m_w)^{-1}$, $q_{1,2}$ - 4-impulses of virtual *W*-boson prior and after remission of Higgs boson,

$g_H = (\sqrt{2}G)^{\frac{1}{2}} m_w^2$ is the couplings constant of Higgs and *W*-bosons.

Assuming reasonably the left longitudinal polarization of the final lepton and summing up by quark polarization, we obtain for the square matrix element the following:

$$|M|^2 = 64G^2 m_w^4 g_H^2 d_1 d_2 (k_1 p_1)(k_2 p_2) , \quad (3)$$

where $d_{1,2} = \left[(q_{1,2}^2 + m_w^2)^2 + \tilde{A}_w^2 m_w^2\right]^{-1}$. Here, we took into account that quarks, masses are $m_{1,2} << m_W$.
In accordance with the general rules, the differential effective cross section of the process (1) can be written as

$$d\sigma = (2\pi)^4 N_c \frac{|M|^2}{4\varepsilon_1 m_1} \delta^4(k_1 + p_1 - k_2 - p_2 - k) \frac{d^3k_2}{(2\pi)^4 2\varepsilon_2} \frac{d^3p_2}{(2\pi)^4 2E_2} \frac{d^3k}{(2\pi)^4 2\omega} , \quad (4)$$

where ε_1, ε_2, ω are energies of the initial and final quarks and Higgs boson, respectively, N_c=3 is the color factor.

Since out of three final particles only lepton is actually detected, then the section that has been integrated by momenta of quark and Higgs boson is of real interest , i.e. dependent only on the lepton parameters. The integration is convenient to perform by using invariant method. Introducing the integration by intermediate 4-momentum q_1, the section can be presented as follows:

$$d\sigma = \frac{2G^2 m_w^4 g_H^2}{(2\pi)^5} \frac{d^3k_2}{\varepsilon_2} \int d^4q_1 \delta^4(k_1 - k_2 - q_1) d_1(k_2 Q) , \quad (5)$$

where

$$Q_m = \int \frac{P_{2m}}{\omega E_2} d_2 \delta^4(q_1 + p_1 - p_2 - k) d^3p_2 d^3k , \quad (6)$$

It is evident that 4-vector Q_m depends solely on p_1 and q_1 and can be written in the following way:

$$Q_m = Ap_{1m} + Bq_{1m} \quad (7)$$

Let us introduce the standard kinematic invariants of the reaction:

$$s \equiv -(k_1 + p_1)^2 = 2m_1\varepsilon_1 + m_1^2 > 0, \qquad t \equiv q_1^2 = 4\varepsilon_1\varepsilon_2 \sin^2\frac{\theta}{2} > 0$$
$$\nu \equiv -p_1 q_1 = m_1(\varepsilon_1 - \varepsilon_2) > 0, \qquad u = 2\nu - t + m_1^2 > 0, \tag{8}$$

where energies ε_1, ε_2 and the exit angle of lepton θ are given in L.S. *A* and *B* coefficients are expressed through kinematic invariants with the help of two functions f_1 °p_1Q, f_2 °q_1Q:

$$A = -\frac{f_1 t + f_2\nu}{\nu^2 + m_1^2 t}, \quad B = \frac{f_2 m_1^2 - f_1\nu}{\nu^2 + m_1^2 t} \tag{9}$$

It is convenient to calculate f_1 and f_2 functions in the frame, where $\vec{q}_1 + \vec{p}_1 = \vec{p}_2 + \vec{k} = 0$. Being expressed through invariants, they are equal (everywhere, where possible, it has been assumed that $m_1, m_2 \ll m_W$ and $m_1, m_2 \ll E_1E_2$) to:

$$f_1 = \frac{\pi}{2\sqrt{\nu^2 + m_1^2 t}}(J_0 - \ln y), \qquad f_2 = -\frac{\pi}{2\sqrt{\nu^2 + m_1^2 t}}\left[(a+1)J_0 - \ln y\right] \tag{10}$$

$$J_0 = \frac{1}{x}\left(arctg\frac{y}{x} - arctg\frac{1}{x}\right), \quad y = 1 + a\frac{u + t + m_1^2}{u}, \quad a = \frac{u + m_2^2 - m_H^2}{m_W^2}, \quad x = \frac{\tilde{A}_W}{m_W}.$$

In such a manner, the process section (1) in *L*-system takes the form:

$$\frac{d^2\sigma}{d\varepsilon_2 \sin\theta d\theta} = \frac{2G^2 g_H^2}{(2\pi)^4}\frac{\varepsilon_2}{\left(\frac{q_1^2}{m_W^2} + 1\right)^2 + \frac{\tilde{A}_W^2}{m_W^2}}\left(Am_1\varepsilon_2 + B\frac{q_1^2}{2}\right) \tag{11}$$

Taking into account the relationship $\varepsilon_2 d\varepsilon_2 \sin\theta d\theta = \frac{dtd\nu}{s - m_1^2}$ and at the same time disregarding the small value $\tilde{A}_W^2 / m_W^2$ in the denominator, we finally write down the cross section in the completely invariant form:

$$\frac{d^2\sigma}{dtd\nu} = \frac{G^2 g_H^2}{(2\pi)^4}\frac{A\left(1 - \frac{2\nu}{s - m_1^2}\right) + B\frac{t}{s - m_1^2}}{\left(1 + \frac{t}{m_W^2}\right)^2} \tag{12}$$

Let us compare this expression with the same one for inelastic scattering $\nu q \to lq$ without Higgs production:

$$\frac{d\sigma_0}{dt} = \frac{G^2}{\pi}\frac{s - m_2^2}{s - m_1^2}\frac{1}{\left(1 + \frac{t}{m_W^2}\right)^2} \tag{13}$$

For high energies of the neutrino $(s >> m_1^2, m_2^2)$ comparison of cross sections will give the ratio:

$$R = \frac{d\sigma / dt}{d\sigma_0 / dt} = \frac{\sqrt{2}Gm_W^4}{16\pi^3}F, \tag{14}$$

where

$$F = \int_{\nu_{min}}^{\nu_{max}}\left[\left(1 - \frac{2\nu}{s}\right)A + \frac{t}{s}B\right]d\nu,$$
$$\nu_{min} \approx \frac{m_H^2}{2}, \quad \nu_{max} \approx \frac{s}{2} \tag{15}$$

It is difficult to estimate the integral, but assuming a weak ν-dependence of the integrand, we may consider that the integral value is proportional to the range of integration: $F \sim s / m_W^4$ (the mass in the denominator is required by the for the right of dimensionality reasons). In this case we obtain $R \sim Gs$, i.e. it shows a linear growth.

[1] *S.L.Glashow*. Nucl.Phys. 1961,v.22, p.579; *S. Weinberg*. Phys. Rev. Lett. ,1967, v.19, p.1264; *A. Salam.* Elementary Particle Theory. Ed.*N.Svartholm.* Almquist and Wiksell,1968, p.367.

[2] *G. Armison et al*. (UA1-Collaboration), Phys.Lett., 1983, v.122B, p.103; *M. Banner et al*. (UA2-Collaboration), Phys.Lett. 1983, v.122B, p.476; *G. Armison et al*. (UA1-Collaboration), Phys.Lett., 1983, v. 126B, p.398;

[3] *P. Bagnaia et al*. (UA2, Collaboration), Phys.Lett., 1983, v. 129B, p.310; *L.B.Okun, Leptons and Quarks.* M.: Nauka, 1990.

Received: 06.06.02

FREE CARRIERS LIGHT ABSORPTION IN SEMICONDUCTIVE QUANTUM WIRES AT THE ELECTRON SCATTERING ON THE ALLOYED DISORDER

G.B. IBRAGIMOV
The Institute of Physics, National Azerbaijan Academy of Sciences,
H.Javid ave. 33, Baku

The theory of free-carriers light absorption is developed in quasi-one dimensional triple semiconductive structures at the carriers scattering on the alloyed disorder and the direction of the photons polarization along the wire length. Obtained expressions for the absorption coefficient show the oscillatory dependence on the photons frequency and on the area of the wire cross-section. The absorption coefficient grows with the reduction of semiconductive wires cross sizes. Obtained results are compared with those of the quasi-two-dimensional case. The examined absorption is compatible with that, caused by the electron-photon interaction.

Last years semiconductive heterostructures are successfully used in optic and microelectronics. The modern technology allows to create semiconductive heterostructures with quantum wells and quantum points. The quantum wires research is of great interest, so far as it's possible to observe in these systems optical and kinetic properties, untypical for massive crystals.

In ultrathin semiconductive wires, called usually wires with the quantum well, carriers are quantized in two cross directions, move only along the wire length and behave as quasi-one- dimensional electron gas. Optical electron transitions are widely investigated for a long time in various quantum nanostructures. Particularly, free carriers light absorption (FCA) in quantum wells is investigated in details in papers [1-11].

FCA in the quantum wires is mainly examined at the scattering on photons [12-13]. However, if the material of the quantum well is the solid solution, then it's necessary to take into account the electron scattering on the alloyed disorder side by side with the simple scattering mechanism. This additional scattering process comes because of the disordering atoms locations in the alloy lattice nodes. The electron scattering in triple structures [14-17] and quantum wells on the base of triple semiconductors are investigated in many papers [18-24].

The purpose of the present paper is to examine the light absorption by the quasi-one-dimensional (Q1D) electron gas at the electrons scattering on the alloyed disorder.

We consider the quantum wire from the alloy, marked by a symbol $A_{1-x}B_xC$. We put down the well-known expression for the energy spectrum and wave function of the electron in the rectangular wire

$$\mathrm{E}_{knl} = \mathrm{E}_k + \mathrm{E}_n + \mathrm{E}_l = \frac{\hbar^2 k^2}{2m^*} + n^2 \mathrm{E}_a^0 + l^2 \mathrm{E}_b^0,$$

$$E_a^0 = \frac{p^2 \hbar^2}{2m^* a^2} \quad , \qquad E_b^0 = \frac{p^2 \hbar^2}{2m^* b^2} \qquad n, l = 1,2,3,\ldots , \tag{1}$$

$$Y_{knl} = \left[2/(abL)^{1/2}\right] \sin(pnx/a) \sin(ply/b) \exp(ikz),$$

Where a and b are cross sizes, L is the wire length. In quasi -one –dimensional systems the second order of the perturbation theory is used at the FCA coefficient calculation. The matrix transition element from the state knl into the state $k'n'l'$ is determined by the following formula:

$$< k'n'l'|M|knl >= \sum_{k''n''l''} \left[\frac{< k'n'l'|H_R|k''n''l'' >< k''n''l''|H_{dis}|knl >}{E_{knl} - E_{k''n''l''}} + \frac{< k'n'l'|H_R|k''n''l'' >< k''n''l''|H_{dis}|knl >}{E_{knl} - E_{k''n''l''} + \hbar\Omega} \right] \tag{2}$$

Where indices $nlk, n''l''k''$ and $n'T'k'$ denote the initial, intermediate and final electron states, Ω is the photon frequency, H_R is the electron-photon interaction operator, H_{dis} is the scattering potential on the alloyed disorder. The matrix element of electrons interaction with photons is equal to

$$\left\langle k'n'l' \left| H_R \right| knl \right\rangle = -\frac{e\hbar}{m^*} \left(\frac{2p\hbar n_0}{V\Omega\epsilon} \right)^{1/2} (e\hat{e}) \delta_{\hat{e}\hat{e}'} \delta_{nn'} \delta_{ll'}, \tag{3}$$

Where ϵ is the high-frequency dielectric constant, n_0 is the photons number in the radiation field, ε is the polarization vector, V is the crystal volume. Here electromagnetic waves are polarized along the wire length (in the x direction)

When the quantum well consists of triple semiconductors (like $Ga_{1-x}In_xAs$). Then in the approximation of the virtual crystal the electron scattering potential on the alloyed disorder has the form [18,25-26]:

$$H_{dis} = dV\left\{(1-x)\sum_{r_{In}} Y_{\Omega_0}(r-r_{In}) - x\sum_{r_{Ga}} Y_{\Omega_0}(r-r_{Ga})\right\}, \quad (4)$$

Where $Y_{\Omega_0}(r_a - r_b) = 1/\ \Omega_0$, when r_a *and* r_b are inside of the same unity cell and vanish elsewhere, and summations run over all unit cell, Ω_0 is the volume of the unit cell. At such potential form, the matrix transition element from the state *knl* into the state $k'n'l'$ has the form;

$$\left\langle k'n'l'\right|\mathrm{H}_{dis}\left|knl\right\rangle = dV\left[\frac{\Omega_0}{V}x(1-x)\left(1+\frac{1}{2}d_{nn'}\right)\left(1+\frac{1}{2}d_{ll'}\right)\right]^{1/2} \quad (5)$$

We receive for the transition rate at the transition from the initial state into the final state

$$W_{knl,k'n'l'} = \frac{4p^2\mathring{a}^2 n_0 (dV)^2 \Omega_0 x(1-x)}{m^{*2}\,\Omega^3 \in V^2}\sum_{n'l'}\left(1+\frac{1}{2}d_{n\,n'}\right)\left(1+\frac{1}{2}d_{ll'}\right)\left|k'-k\right|^2 \cdot d\left(E_{k'n'l'} - E_{knl} - \hbar\Omega\right) \quad (6)$$

The absorption coefficient is calculated by summation of all occupied initial and unoccupied final states. We receive for the FCA coefficient at the electron scattering on the alloy disorder:

$$a = \frac{2p\mathring{a}^2 (dV)^2 W_0 x(1-x)}{\hbar^4 W^3 \in^{1/2} (ab)^2 c}\times$$
$$\times\sum_{nl}\sum_{n'l'}\left(1+\frac{1}{2}d_{nn'}\right)\left(1+\frac{1}{2}d_{ll'}\right)\iint\frac{(E_{k'}+E_k)}{\sqrt{E_{k'}}\sqrt{E_k}}(f_{knl}-f_{knl})d(E_{k'n'l'} - E_{knl} - \hbar W)dE_{k'}dE_k \quad , \quad (7)$$

where f_{knl} is the electron distribution function. In the case of the nondegenerate electron gas:

$$f_{knl} = \frac{(2p)^{1/2}\hbar n_e ab}{gd\left(m^* K_B T\right)^{1/2}} exp\left[\frac{n^2 E_n^0 + l^2 E_n^0}{K_B T}\right] exp\left(-\frac{\hbar^2 k^2}{2m^* K_B T}\right) \quad (8)$$

where: $g = \sum_n \exp\left(-\frac{n^2 E_n^0}{K_B T}\right)$,

$d = \sum_l \exp\left(-\frac{l^2 E_l^0}{K_B T}\right)$

here n_e is the electron concentration.

Substituting (8) in (7), we receive the formula for the FCA coefficient

$$a = \frac{2^{5/2} p^{3/2}\mathring{a}^2 (dV)^2 W_0 x(1-x) n_{\mathring{a}} (K_B T)^{1/2}}{c\hbar^3 W^3 \in^{1/2} abm^{*3/2} gd}\left(1-exp\left(-\frac{\hbar W}{K_B T}\right)\right)\sum_{nl}\sum_{n'l'}\left(1+\frac{1}{2}d_{nn'}\right)\left(1+\frac{1}{2}d_{ll'}\right)\times$$
$$\times exp\left[-\frac{n^2 E_n^0 + l^2 E_l^0}{K_B T}\right] Z\,exp(Z)K_1(Z) \quad (9)$$

where:

$$Z = \frac{\hbar\Omega - E^0{}_n\left(n'^2 - n^2\right) - E^0{}_l\left(l'^2 - l^2\right)}{2K_B T}$$

Here $K_1(Z)$ is the modificated Bessel function. As it follows from (9), the FCA coefficient is the oscillatory function of the photons frequency and the cross size of the quantum wire.

Let's further analyse the simplest case of low temperatures, when electron occupies just the first subzone bottom. This situation is realized, when. $E_a/K_BT>>1$, $E_l/K_BT>>1$. If the quantum energy isn't enough for the electron transference in second and high subzones, then summands give the main contribution to (9) at $n=n¢=l=l¢=1$. In this case we receive for the FCA coefficient:

$$\alpha = \frac{9\pi^{3/2}\hbar^2(\Delta\Xi)^2\Omega x(1-x)}{\sqrt{2}\varepsilon^{1/2}ab(m^*K_BT)^{1/2}c\hbar^2\Omega^2}\exp\left(\frac{\hbar\Omega}{2K_BT}\right)\left(1-\exp\left(-\frac{\hbar\Omega}{2K_BT}\right)\right)K_1\left(\frac{\hbar\Omega}{2K_BT}\right) \quad (10)$$

It's known, that the absorption coefficient reduces as ω^2 in long waves limits and has the semiclassic form [27]. This expression, which will be received below; is considered as semiclassical, because the electron movement is quantum – mechanical, and the classic Drude theory takes into account the light interaction with electrons.

The semiclassical expression is obtained in approximation $K_BT>>\hbar\Omega$ for the nondegenerat electron gas. At the asymptotic application of the modified Bessel function for small argument values ($\frac{\hbar\omega}{2K_BT}$ <<1) the FCA coefficient has the form:

$$\alpha^{sc} = \frac{9\pi^{3/2}e^2(\Delta V)^2\omega_0 x(1-x)n_e}{\sqrt{2\varepsilon ab(m^*K_BT)^{1/2}c\hbar^2\omega^2}} \quad (11)$$

Using the formula [24], for the electron gas at the scattering on the alloy

$$m = \frac{4\sqrt{2}eab\hbar^2}{9\sqrt{\pi}m^{*3/2}(\Delta V)^2\omega_0 x(1-x)} \quad (12)$$

We receive

$$\alpha^{sc} = \frac{4\pi e^3 n_e}{\varepsilon^{1/2}m^{*2}c\omega^2 m} \quad (13)$$

For the comparison we present the absorption coefficient of the Q1D electron gas at the scattering on the acoustic phonon [13]:

$$\alpha_{ac} = \frac{2^{7/2}\sqrt{\pi}n_e e^2 E_d^2 (K_bT)^{3/2}}{\varepsilon^{1/2}c\rho u_s^2 m^{*1/2}abgd}\frac{\left[1-exp\left(-\frac{\hbar\omega}{K_BT}\right)\right]}{(\hbar\omega)^3}\times$$
$$\times\sum_{nl}\sum_{n'l'}\left(1+\frac{1}{2}\delta_{nn'}\right)\left(1+\frac{1}{2}\delta_{ll'}\right)exp\left[-\frac{n^2E_n^0+l^2E_l^0}{K_BT}\right]Z\exp(Z)K_1(Z) \quad (14)$$

From (10) and (14) we determine for $\alpha_{alloy}/\alpha_{ac}$

$$\frac{\alpha_{alloy}}{\alpha_{ac}} = \frac{\pi(\Delta V)^2\omega_0 x(1-x)\rho u_s^2}{2E_d^2K_BT} \quad (15)$$

Where ρ is the crystal density, υ_s is the sound velocity, E_d is the deformational potential. This ratio value estimation for $Ga_{0.47}In_{0.53}As$ –516/T, i.e. the scattering on the alloyed disorder gives the greater contribution to the common FCA coefficient, than on acoustic photons.

For comparison we present the FCA coefficient of the Q1D electron gas at the scattering on the alloyed disorder [11]

$$\alpha_{alloy}^{2d} = \frac{9\pi^2e^2\Omega_0(\Delta V)^2n_e x(1-x)K_BT}{8\varepsilon^{1/2}\hbar^4cd\Omega^3}\left[1-\exp\left(-\frac{\hbar\Omega}{K_BT}\right)\right]\left(1+\frac{\hbar\Omega}{2K_BT}\right) \quad (16)$$

Where *d* is the quantum well thickness. As it follows from (15) and (10), $\frac{\alpha_{alloy}^{1d}}{\alpha_{alloy}^{2d}}$ has the form:

$$\frac{\alpha_{alloy}^{1d}}{\alpha_{alloy}^{2d}} = \frac{4\sqrt{2}e^{\frac{\hbar\Omega}{K_BT}}\left(1-e^{-\frac{\hbar\Omega}{2K_bT}}\right)K\left(\frac{\hbar\Omega}{2K_BT}\right)\hbar^2\Omega d}{\sqrt{\pi}abm^{*1/2}(K_BT)^{3/2}\left(1-e^{\frac{\hbar\Omega}{K_BT}}\right)\left(1+\frac{\hbar\Omega}{2K_BT}\right)} \quad (17)$$

Using asymptote of the modified Bessel function $K_1(Z)$ for greater argument values, we receive from (16)

$$\frac{\alpha_{alloy}^{1d}}{\alpha_{alloy}^{2d}} = \frac{2\sqrt{2}\hbar^{3/2}\pi^{1/2}d}{abm^{*1/2}\left(1+\frac{\hbar\Omega}{2K_BT}\right)K_BT} \qquad (18)$$

Graphs constructed by means of (9), are shown on fig.1-2. Schemes types correspond to the mentioned above analytical results on the FCA coefficient behaviour. Calculations were conducted for the absorption coefficient $Ga_{0.47}In_{0.53}As$. Peaks, which correspond to intersubzone transitions, are observed in frequency Ω (fig.1).

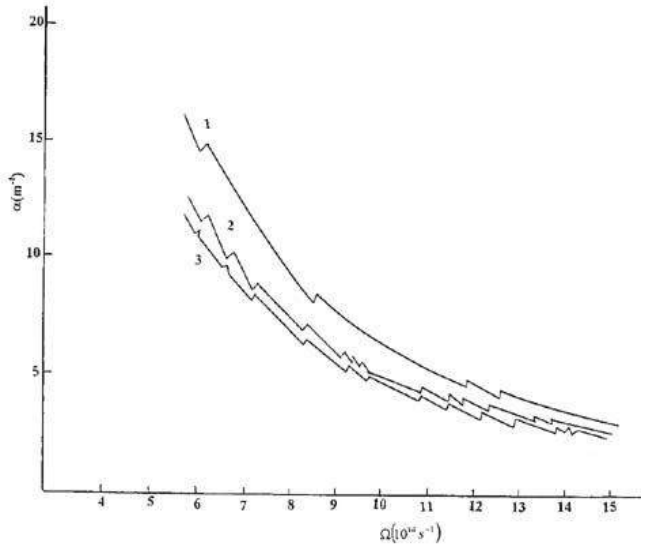

Fig 1. The free –carrier light absorption in a quantum wire is shown as a function of the photon frequency for the case of alloy-disorder scattering for various transverse sizes of the wire. We have chosen1.$a=b=10^{-6}$ñì; 2.$a=2\times10^{-6}$ñì; $b=10^{-6}$ñì; 3. $a=b=2\times10^{-6}$ñì.

In the dependence $\alpha(\Omega)$ peaks shift to the part of the high photons frequency at the reduction of cross sizes. It's connected with the fact, that the distance between subzones increase with the reduction of wire cross sizes. It was determined in [24], that the electron scattering on the alloyed disorder in Q1D structures grows with the reduction of wire cross sizes. Such rise is explained by the FCA coefficient growth with the reduction of semiconductive wire cross sizes. When the photon energy is higher, than the distance between various subzones, then the electron, simultaneously absorbing a photon, scatters and makes transitions in the same or other subzones. With the wire cross sizes reduction, the distance between neighbour subzones increases and then transitions occur by means of the alloyed scattering only in the same subzone. In this case, the absorption process depends on the rate of the electron on the alloyed disorder.

The dependence of the absorption coefficient α on the cross section is given on fig.2 for various values of waves lengths. It's seen from figure, that the absorption coefficient dependence on the area of the quantum wire cross section has the oscillatory form. Schemes, constructed by means of (18), are shown on fig.3.

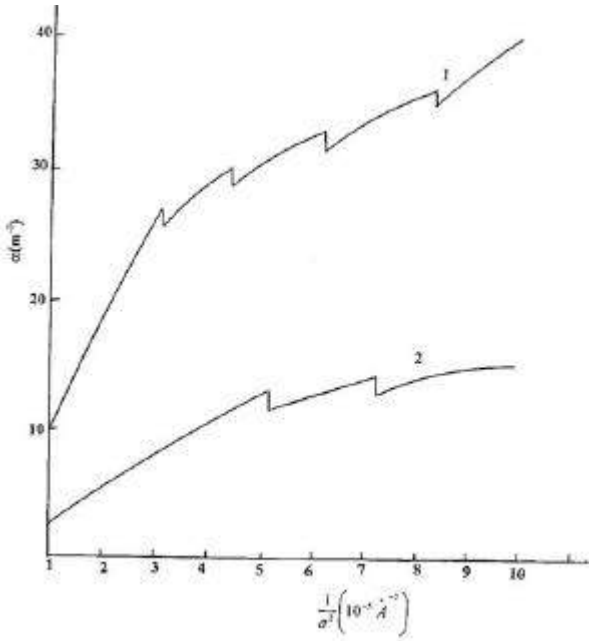

Fig. 2. The free-carrier absorption coefficient is shown as a function of the reciprocal of the cross section of the quantum well wire, $1/a^2$, at 300K. Curve 1is for the wavelength λ=5 μm and curve2 is for l=3μm

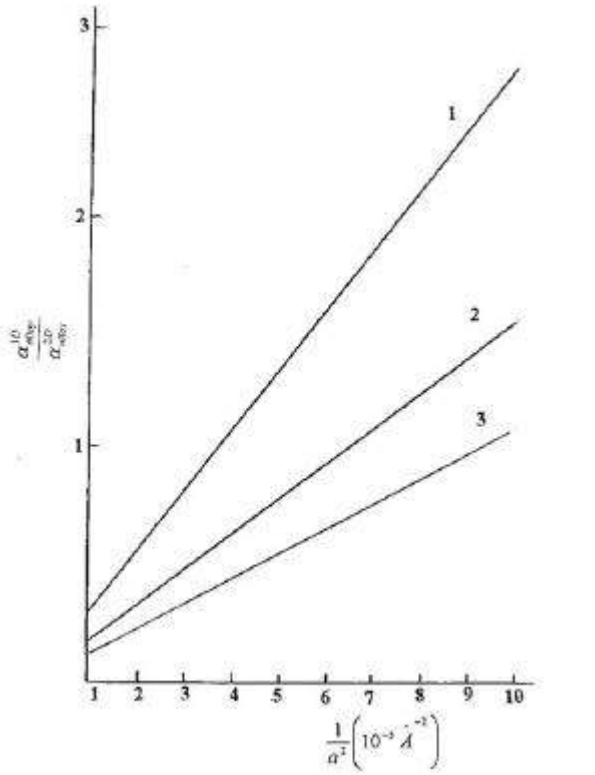

Fig. 3. The ratio of the free-carrier absorption in a quantum wire to its value in the quantum well is shown as a function of the reciprocal cross section of the quantum well wire $1/a^2$. Curve 1 is for the wavelength l=10μm, curve 2 is for the wavelength l=5μm, curve 3 for the wavelength l=3μm.

The author would like to thank M.I. Aliev and F.M.Gashimzade for helpful discussions.

[1] H.N.Spector. Phys.Rev B28, 1983, 971.
[2] H.Adamska and H.N.Spector. J.Appl. Phys. 56 (4), 1984, 11239.
[3] C.Trallero Ciner and M.Anton. Phys. Stat. Sol (b), 1986, 133, 563.
[4] V.L.Gurevich, D.A.Parshin and K.E.Stengel. Fiz.Tverd. Tela 30, 1988, 1468.
[5] C.C.Wu and C.J.Lin. J.Appl. Phys. 1996, 79, 781.
[6] J.S.Bhat, S.S.Kubakaddi and B.G.Mulimani. J.Appl. Phys. 1992, 72, 40, 4966.
[7] C.C.Wu and C.J.Lin. J. Phys; Condens matter 1994, 6, 10147.
[8] F.M.Gashimzade and E.V.Tahirov. Phys. Stat. Sol (b)1990, 160, 17.
[9] I.Vurgaftman and J.R.Meyer. Phys.Rev B60, 1999, 14294.
[10] G.G. Zegrya, V.E.Perlin Fiz.Tekh. Poluprovodn. 1998, 32, 466.
[11] G.B. Ibragimov, Phys.Stat.Sol.(b), 2002, 231, 589.
[12] H.Adamska and N.Spector, J.Appl. Phys.1986, 59(2), 619.
[13] S.S. Kubakaddi and B.G. Mulimani J.Phys.C: State Phys.18, 6647, 1985.
[14] J.W.Harrison and J.R.Hauser. Phys.Rev B. 1976, 13, 5351.
[15] M.A.Littlejohn, J.R.Hauser and T.H.Clisson. Appl. Phys. Lett. 1977, 30, 242.
[16] K.Sieranski and J.Szatkowski. Phys. stat. Sol (b), 1981, 104, 57.
[17] M.I.Aliev, Kh.A.Khalilov, G.B.Ibragimov. Phys. stat. Sol (b), 1987, 140, K83.
[18] G.Bastard. J.Appl. Phys. Lett. 1983, 43(6), 591.
[19] D.Chattopadhyay. Phys.Rev. B.31, 1985, 1145.
[20] P.K.Basu and D.Raychaundhury. J.Appl. Phys. 1990, 68(7), 3443.
[21] U.Bockelmann, G.Abstreiter, G.Weimann and W.Schlapp. Phys.RevB41, 1990, 7864.
[22] P.Ray and P.K.Basu. Phys.Rev B46, 1992, 9169.
[23] G.B.Ibragimov. Int.Conf.Opt.Semicond. OS 2000, (Ulyanovski) 25, Fizika 5(2), 1999, 49.
[24] G.B.Ibragimov Fizika 7(4), 2001, 17.
[25] T.Ando, J.Phys.Soc.Jap.51, 1982, 3900.
[26] S.Jaziri, and R.Ferreira, J.Appl.Phys. 1998, 84, 893.
[27] B.Jensen. Appl.Phys.(N.Y.), 1975, 95,229.

Received: 01.06.02

THE NEW SUBTYPE FOR THE SPECTRAL CLASSIFICATION OF SOME WOLF-RAYET TYPE STARS

J.N. RUSTAMOV
Shamakha Astrophysical Observatory of Azerbaijan Academy of Sciences, F.Agaev 9, Baku, Azerbaijan

The modern schemes for the spectral classification of WR type stars are analyzed. The new subtype WO5 for the spectral classification of some WO stars is proposed. The importance of introduction of the subtype WO5 is substantiated. It is proposed that according to point of view of evolution, the WO5 stars are intermediate between WC and WO stars.

1. Statement of the problem

Stars are separated on defined groups with the aid of reasonable spectral classification. In the ideal case the spectral classification depends only on effective temperature and luminosity. In the classification system for the absorption spectra of 'normal' stars the effective temperature and luminosity are closely related. This is result of the fact that in the case of 'normal' stars, the absorption line spectrum and continuum spectrum forms approximately in the same region of the star.

In the case of Wolf-Rayet (WR) stars, having expanding envelope, however, the emission lines are formed in the 'stellar wind' or in the envelope of the star, which removed from the level, emitting the continuum radiation. Therefore, for the WR stars, the spectral types do not connect with the effective temperature and luminosity. The spectral subtypes of the WR stars indicate the temperature of the wind, at least qualitatively.

It has often been suggested that the ionization state of a WR spectrum is related to the ionization temperature in the wind and possibly even to an effective temperature, but this connection has not yet been established physically. It is possible that the ionization state of the wind is mainly determined by the density, and may have little or nothing relation to the effective or an ionization temperature.

2. Spectral classification of WN and WC stars.

According to the scheme proposed by Beals and Plaskett [1], the WR stars have been divided into two spectral types: the WN and WC types. WN stars which exhibit emission lines of predominantly He and N ions with little evidence for C, have been considered as C-poor objects, while WC stars, showing predominantly He and C lines and virtually no evidence for N, have been considered as N-poor. In both subtypes the visible spectra show little or no evidence for hydrogen. In 1968 Smith improved classification scheme [2] for the spectral classification of galactic Pop.I WR (WN and WC) stars. Further, essential changes of line strengths among these ions have been observed from star to star. Therefore for the spectral classification of WN stars WN4-9 (Table I) subtypes and for the spectral classification of WC stars WC4-9 (Table II) subtypes were proposed [1, 2]. These subtypes certainly represent different ionization conditions in the stellar wind of the WR stars. WN and WC stars have different chemical composition, but not all astronomers agree with this assumption [3].

Classification strongly depends on lines ratios, mainly of NIII, NIV, and NV ions for the WN subtypes, and the CIII and CIV ions (along OV) for the WC subtypes respectively. In the case of WC stars, emission lines widths are also additional criterion. Among the late WN stars, the appearance of the helium spectrum is also an criterion (Table I, Table II).

We would like to note that the spectral criteria for determination of WN subtypes depend mainly on the lines in the blue part of the spectrum, namely λλ4000-4700 ÅÅ; and for determination of WC subtypes, mainly in the yellow part of the spectrum, namely λλ5500-5900 ÅÅ.

It was established that the WN3, WN4 and WN5 stars could be easily separated by means of ratios of the NIII, NIV and NV ions. Early WN subtypes correlate well with the Smith subtypes. This is, mainly, because of the gradual weakening and then disappearance of, first NIII, and then NIV with transition from WN5 to WN3. The great overlap was found for the WN6, WN7 and WN8 stars. In other words there are some WN6 stars which have nitrogen line ratios similar to those of some WN7 stars, and some WN7 stars with ratios similar to WN8 stars, and conversely. WN7 and WN8 stars are similar, but they can be separated clearly on the basis of the strength and displays of the HeI spectrum.

WN subtypes are usually separated to two subgroups WNL (WN7-9) and WNE (WN2-6) versus presence of little H or absence of H in their spectra.

However in the case of WC stars there is the good agreement with the Smith subtypes.

It is known that WN stars contain CIVλλ5801, 5812 in the optical region and CIVλ1550 in the UV region.

The WC subtypes contain little or no nitrogen. The only evidence for nitrogen ions in the optical region is possible weak blends of NIII ions side by side with very strong carbon features (which might even be due to other carbon ions) according to [4, 5]. In UV region NIV, and NV lines may be weakly present but blends make the identification a little uncertain [6].

The theoretical investigations suggest that the apparent composition anomalies in WN and WC subtypes are related to stellar evolution [7]. According to modern statements, WN subtypes are result of stars evolution in which CNO equilibrium products are observed on the stellar surface (in the wind). These include enhanced helium and nitrogen, and diminished carbon and oxygen (in comparision with 'normal'). WC subtypes result from the appearance of products of helium burning in which carbon and oxygen are enhanced at the expense of helium and nitrogen.

3. Spectral classification of WO stars.

In 1982 Barlow and Hummer [8] introduce the new type WO for the spectral classification of some WR stars. Table III presents spectral criteria for the definition of the WO subtypes. As we see from Table III the WO subtypes are

defined by the relative strengths of OIV, OV and OVI. In [8] authors propose that the spectra of WO stars reflect an actual enhancement of the abundance of oxygen, relatively to the WC stars. Such enhancement of oxygen can be interpreted as due to α particle capture by carbon nuclei during the late stages of core helium burning in initially massive stars. The enriched material is eventually exposed on the surface by mass loss stripping. In this scenario the WO stars represent the next evolution stage after the WC phase, either at the end of core helium burning or already in the core carbon burning stage. The small number of WO stars in comparison with WC stars, is in agreement with this hypothesis.

Table 1. Spectral classification of WN stars according to [1,2].

WN subtypes	**N ions**	**Other criteria**
WN9	NIII present, NIV weak or absent	HeI, lower Balmer series P Cyg
WN8	NIII >> NIV	HeI strong P Cyg, NIIIλ4640 ≈HeIIλ4686
WN7	NIII > NIV	
WN6	NIII ≈ NIV, NV present but weak	
WN5	NIII ≈ NIV ≈ NV	
WN4.5	NIV > NV, NIII weak or absent	
WN4	NIV ≈ NV, NIII weak or absent	
WN3	NIV << NV, NIII weak or absent	
WN2	NV weak or absent	Strong HeII

Table 2. Spectral classification of WC stars according to [1,2].

W**C subtypes**	**CIII l5696/CIV l5805**	**CIII l5696/OV l5592**	**Other criteria**
WC9	CIII > CIV	OV weak or absent	CII present
WC8.5	CIII > CIV	OV weak or absent	CII not present
WC8	CIII ≈ CIV	OV weak or absent	
WC7	CIII < CIV	CIII >> OV	
WC6	CIII << CIV	CIII > OV	
WC5	CIII << CIV	CIII < OV	
WC4	CIV strong, CIII weak or absent	OV moderate	

Table 3. Spectral classification of WO stars according to [8] and our investigations.

WO subtypes	**The criteria for the classification**
WO5	CIVλ5810, OIVλ3400, OVIλλ3811, 3834 is strong, CIIIλ5696/OVλ5590 1, The intensity of OVIλλ3811, 3834 is smaller than the intensity of OIVλ3400 (OVI< OIV)
WO4	The lines of CIV are strong, the CIII lines are absent, OIVλ3400, OVIλλ3811, 3834 are strong; the intensities of the lines OVI λλ3811, 3834 and OIVλ3400 are approximately equal (OVI≈OIV)
WO3	The intensity of the lines OVIλλ3811, 3834 is greater than for the line OIV λ3400 (OVI>OIV)
WO2	The OIV lines are absent; the intensity of the line OVλ5590 is smaller than for the line CIVλ5810 (OV<CIV)
WO1	The intensity of the line OVλ5590 is greater than or is equal to Intensity of the line CIVλ5810 (OV≥CIV)

In order of excitation increase the WO subtypes runs: WO4, WO3, WO2, WO1.

The difference between WN, WC and WO subtypes can be understood purely in terms of ionization, excitation and structural differences among them. Different subtypes represent different composition. It is suggested that they

result from the stellar evolution. The separation of WR stars to WN, WC, and WO types is connected with the different chemical composition and related to stellar evolution. According to modern evolutionary status, the WN and WC stars represent the early and late stages of core helium-burning phase, respectively, during the evolution of massive stars [7, 9]. On the other hand, according to [8], the WO stars represent the next evolution stage after the WC phase. Therefore, we obtain such an evolution scheme for the WR types:

$$WN \rightarrow WC \rightarrow WO$$

4.The reason for the proposition of new subtype WO5.

The new subtype WO5 is proposed because of uncertainties in the spectral classification of some WR-OVI stars. Below we discuss some of them.

HD 16523. According to [10] the spectral subtype of the WR-OVI star HD 16523 is WC5, and according to [2] the spectral subtype of this star is WC6.

Table IV presents the classification criteria for the WC5, WC6, WC8 stars according to [10] and our results for the WR-OVI stars HD 16523, HD 17638, HD 192103.

From Table IV we see that the spectral subtype of the WR-OVI star HD 16523 is uncertain as estimated from the different criteria: the ratio CIIIλ5696/CIVλ5810 and width at the half intensity for the CIII, CIVλ4650 corresponds to the subtype WC5, but the ratio CIIIλ5696/OVλ5590 corresponds to the subtype WC6.

HD 17638. According to [10], the spectral subtype of the WR-OVI star HD 17638 is WC6. From Table IV we may infer that the spectral subtype of this star is uncertain as estimated from different criteria: the intensity ratio of the line CIIIλ5696 and

OVλ5590 (CIIIλ5696 /OVλ5590), the intensity ratio of the emission lines CIIIλ5696 and CIVλ5810 corresponds to the subtype WC6, but widths of the CIII, CIVλ4650 correspond to the subtype WC5.

HD 192103. According to [10] in the spectra of the HD 192103 the emission doublet OVIλλ3811, 3834 of middle intensity presents. Our results for this star correspond to the subtype WC8, which is given in [10].

We may infer that in two cases (HD 16523 and HD 17638) the spectral subtype of the WR-OVI stars, as estimated from different criteria, is uncertain. The spectra of the WR-OVI stars, HD 16523 and HD 17638 differ from the spectra of usual WC5 and WC6 stars because the emission doublet OVIλλ3811, 3834 with the different intensity present in spectra of these stars. The Sanduleak stars [11] were also considered earlier as WC4 and WC5 stars [10]. However, Barlow and Hummer [8] argued that the Sanduleak stars [11]may be considered as WO stars and for the spectral classification of these stars they proposed spectral subtypes WO1-4 (Table III). The argument for this conclusion is the presence of the strong emission doublet OVIλλ3811, 3834 in spectra of these stars. In the spectra of the WO stars, the carbon lines are very weak or not observable. The stars HD 16523 and HD 17638 differ from the usual WC5 and WC6 stars because in these stars the emission doublet OVIλλ3811, 3834 presents. The stars HD 16523 and HD 17638 differ from usual WO (WO1-4) stars, because carbon lines have a considerable intensity in the spectra of these stars. We see that the WR-OVI stars HD 16523 and HD 17638 have a spectral characteristic intermediate between WO (WO1-4) and WC4-6 stars. In the spectra of the WR-OVI stars HD 16523 and HD 17638, the intensity of the emission doublet OVIλλ3811, 3834 is smaller than that of the emission line OIVλ3400 (OVI<OIV). From Table III we see that in the spectra of WO4 stars the intensities of the emission doublet OVIλλ3811, 3834 and OIVλ3400 are approximately equal (OVI ≈ OIV), and in the spectra of the WO3 stars already OVI>OIV. Therefore, according to the ratio of the intensities of the emission doublet OVIλλ3811, 3834 and of the emission line OIVλ3400, the stars HD 16523 and HD 17638 continue WO4 stars at lower ionization potentials. According to this result we argue that for the define spectral classification of the WR-OVI stars, whose optical spectra are intermediate between WO4 and WC4-6 stars, the new spectral subtype WO5 may be proposed. Table IV lists the classification criteria for the determination of the WO5 subtype.

Table 4. The spectral classification of the WR-OVI stars.

Subtype	CIIIλ5696/OVλ5590	CIIIλ5696/CIVλ5810	The widths of the CIII, CIV λ4650(Å)
WC5	< 1	<< 1	85
WC6	> 1	<<1	45
WC8	OV weak or absent	~ 1	20
Our results			
HD 16523	1.20	<< 1	88
HD 17638	2.74	<< 1	76
HD 192103	13.25	1.13	18

[1] *C.S. Beals, and H.H. Plaskett.* Trans. IAU. 1935. ¹ 5. p.184.

[2] *L.F. Smith.* Monthly Notices Roy. Astron. Soc. 1968. ¹ 138. p.109.

[3] *A.B. Underhill. In: M.K.V. Bappu and J. Sahade (eds.)* Wolf-Rayet and High Temperature Stars. IAU Symp. ¹49. 1973. p.237.

[4] *A.B. Underhill.* Pub. Dom. Astrophys. Obs. Victoria. 1959. ¹ 11. P. 209.

[5] *M.K.V. Bappu In: M.K.V. Bappu and J. Sahade (eds.)* Wolf-Rayet and High Temperature Stars. IAU Symp. ¹ 49. 1973. p. 59

[6] *A.J. Willis.* In Proc. 2nd European IUE Conference, ESA SP-157. 1980. p.11.

[7] *B. Paczynski In: M.K.V. Bappu and Sahade (eds.)* Wolf-Rayet and High Temperature Stars. IAU Symp. ¹49, 1973, p. 143

[8] *M.J. Barlow and D.G. Hummer. In: C.W.H. de Loore and A.J.Willis (eds)*. Wolf-Rayet Stars: Observations, Physics, Evolution. IAU Symp. ¹ 99, 1982, p. 295.

[9] *A.J. Willis and R. Wilson.* Monthly Notices Roy. Astron. Soc. 1978. ¹ 182, p. 559.

[10] *K.A. van der Hucht, P.S. Conti, I. Lundstrom, B. Stenholm.* Space Science Reviews. 1981. ¹ 28. p. 227.

[11] *N. Sanduleak.* Astrophys.J. 1971. ¹ 164, p. L71.

[12] *D.N. Rustamov, A.M. Cherepashchuk.* Pisma v Astron. J. 1986, ¹ 10, p. 370.

Received: 14.05.02

THE EFFECT OF THERMAL TREATMENT AND THE DOPINGS CONTAINING OXYGEN ON THE ESR SPECTRA OF CHLOROPRENE RUBBER (II)

S.I.MEHTIYEVA, R.L.BAYRAMOVA, S.A.ABASOV
Institute of Physics National Academy of Sciences of Azerbaijan
370143, H.Javid Av. 33 a, Baku, Azerbaijan

Y.LENGER ÖZCANLI, SH.V.MAMEDOV
Yýldýz Technical University, Department of Physics
Davutpasa Campus, 34210, Topkapi, Istanbul, Turkey

The previous study [1] is developed to prove the concept, that is, contribution of oxygen and impurities effect the free-radical (FR) processes participating in the reactions of the side groups of macromolecules in rubbers. For this purpose, instead of the impurities which are distinguishable and which contain chloroprene rubber having a multi-component ESR (Electron Spin Resonance) spectrum and oxygen, we used the doping of diepoxysilane. It is proven that the effect of oxygen is superior to the others in reactions in which FR's take part, provided that the amount of oxygen in the polymer system is sufficient. The dopings selected help the concentration of the FR's in rubber decrease and the structure of the material be more homogeneous. It is found that there is an adverse correlation between the decrease in the concentration of the FR's and the amelioration of the strength characteristics of rubber.

INTRODUCTION

In reference [1] it was suggested that the FR's processes which take parting the reaction of side groups of the macromolecules, in general are affected by whereas in this study the conclusions of the effects of a more special doping on the FR processes (that is, in isoprene and chloroprene rubbers) are made. For instance, the isoprene rubber is interesting by its few characteristics. First, through the microstructure point of view, it is the most similar one to the natural polyisoprene rubber. Spectroscopically and according to the chemical structure analysis we can write for the best of polyisoprene rubber which has a stereo ordering the ordered cis-1, 4 structure.

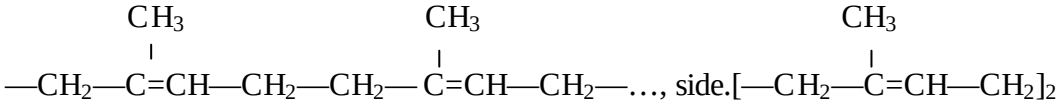

According to chemical activity the structure of cis-1, 4 of the synthetic polyisoprenes looks like that of natural rubber, so that all the results obtained for the isoprene rubber can be used for the natural rubber as well. Secondly, the isoprene rubber is a semicrystalline polymer belonging to the class of rubbers whose crystalline phase is minimum (from 15 % up to 50 %). Due to the presence of the structures 1, 2 and 3, 4 crystallization is difficult in this rubber and in general the rubber is composed of an amorphous phase. Therefore, the processes of oxydation and degradation that signify the use parameters of the materials manufactured on the basis of this rubber occur, in general, in amorphous parts. Consequently, the investigations in the chloroprene rubber can unveil the effect of the external agents on all kinds of rubber and in oxydation and degradation processes in more detail. On the other hand, the chloroprene is different than the isoprene rubber due to the presence of the chlorine (Cl) atom having an unpaired nuclear spin and a high electronegativity and which takes place instead of the side group of CH_3. Thus, since the electron freed in the polymer chain is more strongly localized on the Cl atom the results obtained for this rubber should be different than the results of ESR for other rubbers cited in reference [1] where the examinations on the chloroprene rubber with the addition of Se and Te were reported. These results are different than those of the other rubbers. Therefore, we developed these studies with a doping having a greater molecular mass and oxygen containing groups.

In the above mentioned processes it is obvious from the references that the FR's play an important part in the polymer structure due to some reasons. On the other hand, the processes of polymerization depend on the type (character) of active centre and these centres may be FR's, ions or coordination complexes [2-7]. Hence, there are two principal types of polimerization: radicals and ions. In the processes of radical polymerization, as the p - bond between two carbon atoms breaks under the effect of the active centre, the electron pairs separate (homolotical breaking) and as a result of the joining of monomer molecule with the active centre a FR regenerates. In the ionic processes, the p - bond breaks in such a way that each of the electrons in a pair passes on to a carbon atom and the other carbon atom is charged positively (heterotical breaking). Hence, as a result of the interaction of the active centre and the monomer molecule, an ion forms that has a charge of the same sign as that in the active centre. Therefore, the active groups of the enlarging polymer chain either become FR's or ions. Recently a greater emphasis is given to the radical polymerization of the rubbers. Because the FR's affect both the polymerization process of rubber and its molecular and supra molecular structure (SMS) by interacting with themselves and with active centers, that is, the physico-chemical characteristics and use parameters of the materials made taking this rubber as a basis happen to vary. Indeed, the physico-mechanical characteristics of polymers depend on the degree of crystallization, the ratio of

the amorphous to crystalline regions, molecular mass and so on [2-5, 8-17].

We explain the important role that the FR's play in the physico-mechanical and use characteristics of rubbers. Due to the above mentioned reasons, it is scientifically interesting to investigate the processes of FR's in rubbers for different dopings and side atoms. The results given in the study are the results that the authors obtained recently, but no extensive studies have been published except the abstract of some conferences [15-18]. Then, after new ideas have appeared through both references and the authors, preliminary mechanisms have been developed. Therefore, although a bit late, we decided to present these conclusions in an extensive and detailed publication.

METHODS AND PREPARATION OF THE SAMPLES

The chloroprene rubber is used as the material of investigation and silicon organic compound-diepoxysilane (α, ω- di(γ-glycyl-oxypropylmethylfenylsilane)) –

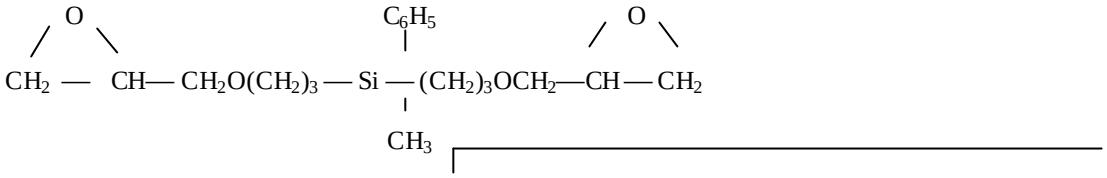

is used as the doping. The ratio of the doping is 0-10 weight %. The dopings are mixed in rolling machine with some ingredients as powder and at (323±5) K during 35-38 minutes. The temperature and period of vulcanization are respectively 423 K and 5, 10, 20, 40 and 60 minutes and the pressure is 1.2 MPa. The reason to choose doping material is to use in polymer systems, this doping together with its analogs and inorganic silicon compounds as plastifier and as filling material. The methods of measurement for ESR and IR spectra are given in [1]. In all cases the results are calculated statistically according to the Student criteria and the probability of validity is $\beta = 0.95$. In order to compare the validity of the results of our spectroscopic researches, in most of the cases, the physico-mechanical characteristics of the mixtures of resins specially prepared chloroprene rubber are measured and explored.

RESULT AND DISCUSSION

In all the samples a multi-component spectrum is observed. In pure chloroprene rubber a 7-component and practically isotropic Hyper Fine Structure (HFS) is observed [1], whereas in the doped case, in addition to this (additional spectrum) also a wide asymmetric peak ($g \approx 2$) is observed. A typical spectrum of this kind is shown in Figure 1a. Let us now examine the characteristics of all the observed spectra:

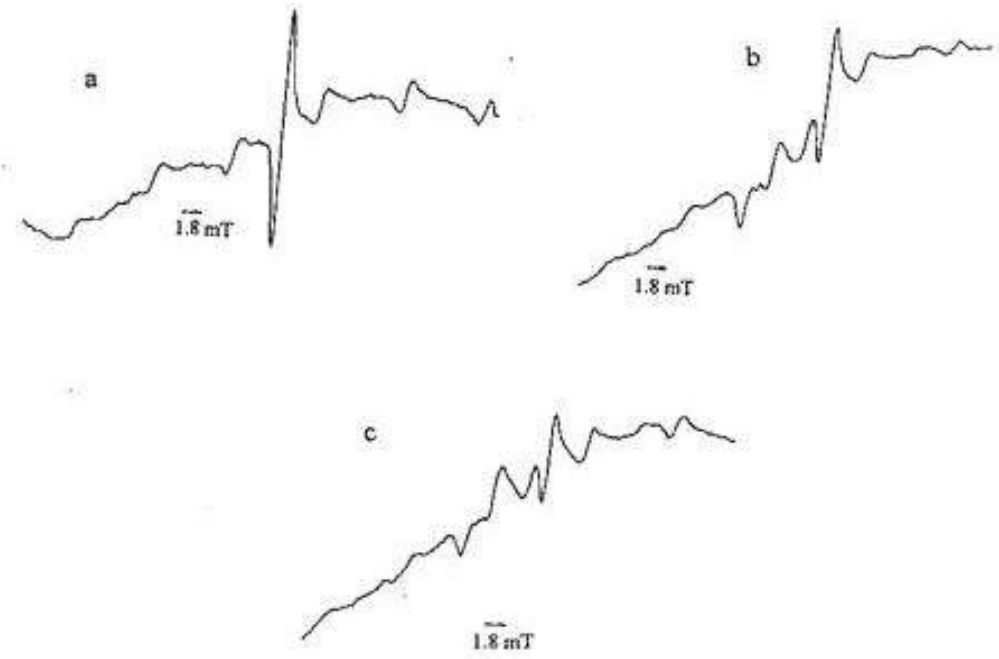

Fig.1. The ESR spectra in the rubber chloroprene with the amount of diepoxysilane a) after the vulcanization, b) after rolling, c) the variation of the ESR spectrum components in the rubber chloroprene with the amount of diepoxysilane after rolling.

It could have been thought that the multi-component ESR spectrum observed in the chloroprene rubber belonged to the Mn^{+2} ion, but the number of components, intensity (I) and the HFS constant vary greatly depending on the treatment temperature (T_{treat}), the conditions of manufacturing the sample and the vulcanization of the rubber (see the ESR spectra given in the article). Sometimes a well distinguished spectrum of 9-10 components is observed. Here, a singlet whose intensity is higher than those of the other components is observed at the centre. On the other hand, all this multi-

component spectrum sits on a very wide peak. The fine structure of the Mn^{+2} ion should be composed of 6 components of equal intensity, while the HFS should be a 36-peak spectrum. However, the HFS constant is 6.8 -7.7 mT, whereas for the spectrum that we obtained this value goes up to 9.0 – 9.5 mT as mentioned. All these data are against the idea that the multi-component spectrum that we observed in chloroprene rubber belongs to the Mn^{+2} ion, as conforming to the transition elements.

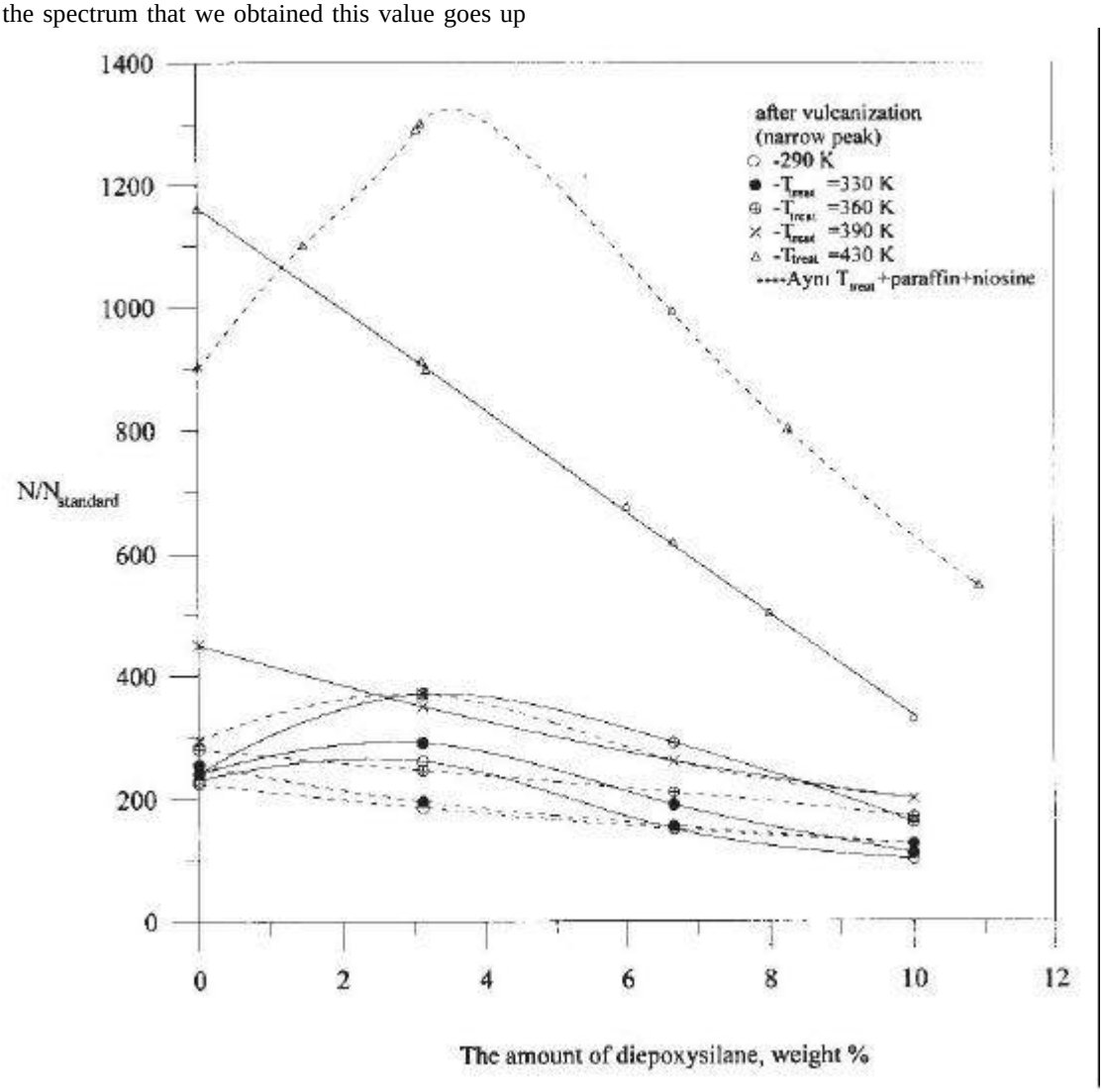

Fig.2. The dependence of the concentration of paramagnetic centers on the amount of diepoxysilane, in the rubber chloroprene and for the narrow peak, after vulcanization

The narrow central peak has g=2.003±0.0005 and the width DH_m=0.9±0.05 mT. These parameters do not depend on other things except T_{treat} and 10 weight % percentage. In only one 10 weight % DH_m increases up to 1.1 – 1.4 mT. The width is the same for all the components of the 'isotropic' spectrum and DH_m is (1.2 – 1.4 mT) and the HFS parameter is both the same and around 8.5 – 9.0 mT. The width of the wider peak varies greatly depending on both T_{treat} and the ratio of the dopings. Its value changes around 30 – 60 mT and increases as the amount doping gets higher, but diminishes as T_{treat} increases. This conclusion can be thought as the effect of the vulcanization. When we drop the temperature down to 77 K it decreases practically to half.

"The additional spectrum" can only be observed in the samples collected from the rolling machine and can be explained in two ways, that is, the HFS of the isotropic spectrum is practically observed at around 8 – 9 mT and the number of components depends on the conditions of manufacturing the sample. Furthermore, an asymmetric peak which is in the interval 7 – 7.5 mT is seen from the central peak (Figure 1b). The positions and the intensities of these peaks vary in an uncontrolled way and strongly (they slide from the central peak in either direction) (Figure 1b, 1c) but the HFS constant remains fixed. The distance between the central peak and the first distinguished component is 1.8 – 2.5 mT towards the low magnetic field side, while around 8 – 9 mT towards the strong magnetic field side. This shift is sometimes so strong that these peaks slide towards the central narrow peak and unite with it (overlap) and as a result, a hardly distinguished doublet is observed (Figure 1c). The width of the above mentioned components increases depending on the percentage of the doping, from 1.2 up to 2.0 mT. The more important variations are in the intensities of the narrow and wide peaks and also proportional to the intensities of the components of both 'isotropic' and 'additional spectra'.

Narrow peak: a- In the absence of ingredients after the vulcanization, for 3 weight % diepoxysilane, paramagnetic centres (PC) get their greatest concentration (N). But it drops at 10 weight % and in this case N becomes less than even that

of the pure (undoped) samples (Figure 2). As T_{treat} increases N becomes higher at each value of the ratio, but the general shape of the curves does not change. Only at T_{treat} = 433 K a drop is observed, that is, at 3 weight % a striking maximum is seen (when there are paraffin and niosine ingredients). At T_{treat} = 433 K, N is almost four times greater than what it is at other values of T_{treat} for all values of the doping. b- after rolling at all values of T_{treat} a minimum is observed at 3 weight %. However, as paraffin and niosine are added the rubber becomes stabilized, that is, as the doping gets higher N drops slowly. But at T_{treat} = 433 K and for 3 weight % a minimum is observed. As T_{treat} increases the general trend stays the same, that is, N increases as well (Figure 3).

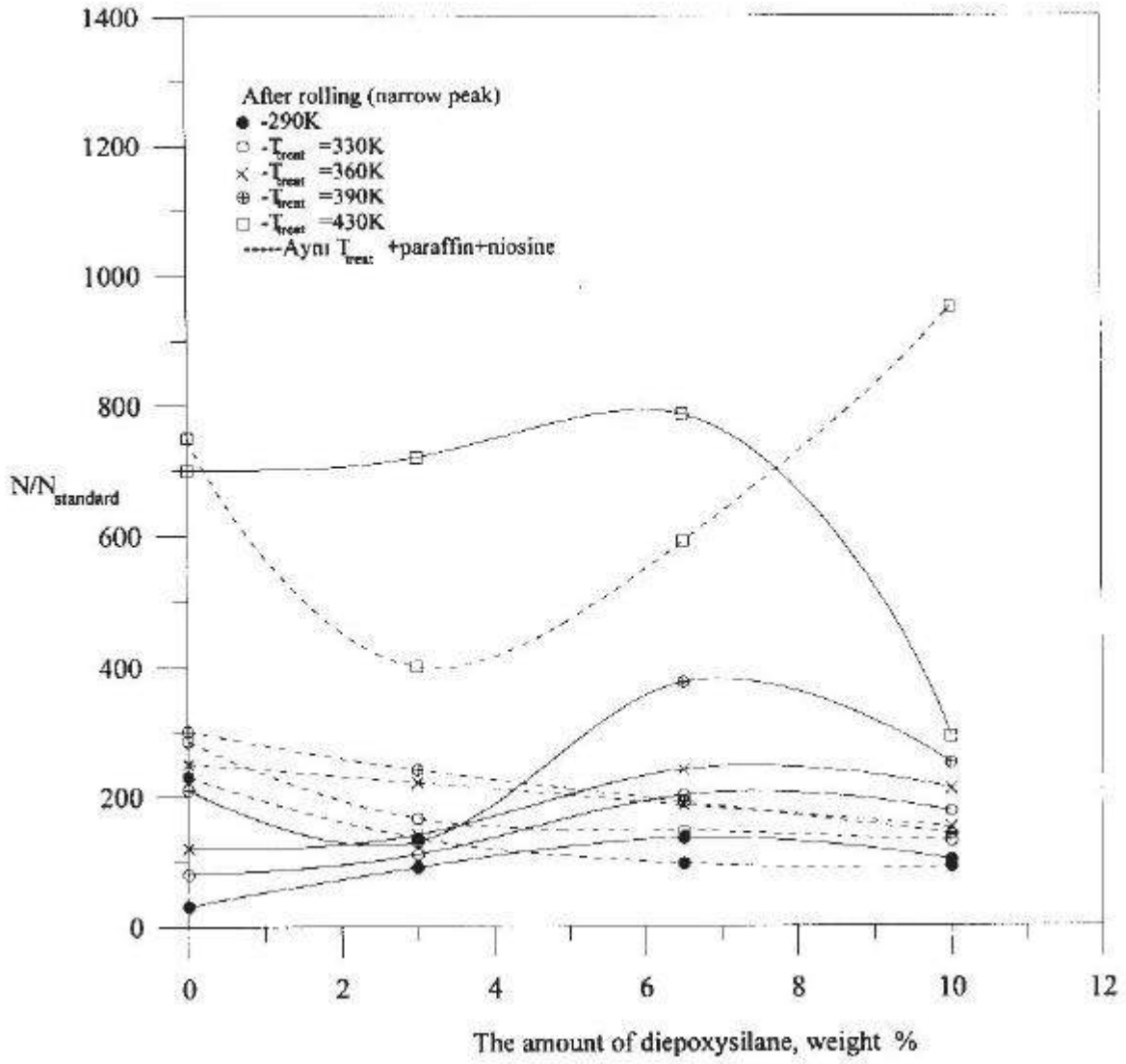

Fig.3. The dependence of the concentration of paramagnetic centers on the amount of diepoxysilane, in the rubber chloroprene and for the narrow peak, after rolling.

Wide peak: a- after the vulcanization, it is generally observed that it obeys the stability rule. 3 weight % and 6.5 weight % (at low and high values of T_{treat}, respectiveliy) but for higher than 6.5 weight % N increases absolutely (7 – 8 fold). When paraffin and niosine are added the shapes of the curves do not change, but N increases a bit all the time (Figure 4). This trend is observed to be weaker for narrow peak. As T_{treat} gets bigger so does N, but at 433 K a sudden drop is seen (N becomes less than even that of the pure sample). All these phenomena are observed in more detail when the ingredients are added. b- Following the process at the rolling machine as the amount of diepoxysilane gets greater, so does the value of N for the PC. However, at 293 K at 3 weight % a minimum is observed. For all the ratios of doping, as T_{treat} increases so does N and when the ingredients are added N becomes even greater (2 – 3 fold) (Figure 5). But at 10 weight % it is different. At T_{treat} = 433 K the PC's appropriate for the peak are not practically observed, but at 10 weight % another narrow peak is seen.

That the HFS is not observed in the rubber divinylnitrile [1] shows that the unpaired electrons (UE) arise from the breaking of the chemical bonds as a result of the mechanical processes, are strongly localized on the C atoms and do not interact with the side protons. The observation of the 7-component spectrum in pure rubber of chloroprene shows that these UE's are drawn from the C atom toward the Cl atom (due to the high electronegativity of the Cl atom) and in mutual interaction with the nucleus of the Cl atom (spin of

the nucleus I = 3 / 2). It is known that the number of peaks in the HFS must be (2nI + 1) (where n is the number of nuclei that are in mutual interaction). Consequently, the 7-component spectrum in the rubber of chloroprene can be explained by the interaction with the nuclei of the two Cl atoms (n = 2). The isotropy of HFS proves the equivalence of these two chlorine nuclei. The above explanation is supported by the rule that gives the ratio of the intensities for the interaction of the HFS components with the two equivalent nuclei [19], that is, 1: 2: 3: 4: 3: 2: 1. There may sometimes be small deviations from these ratios that originate from the weak interaction between the Cl atom and side protons, because the UE has moved to the side atom. These variations are more pronounced when silicon organic compounds are added. That is, dopings play a filling role rather than a cross role. Indeed, the concentration of the FR's increases as a result of the breaking bonds on the one hand (narrow peak, in Figure 6a) and the N value of the PC's that are appropriate for the wide peak increases on the other (Figure 6b, 6c). It may be thought that the wide peak originates from the formation of the peroxide radicals, the mutual reinforcement of the UE's with the UE's of the oxygen molecule and the formation of the anion radicals as a result of the joining of the oxygen containing groups of diepoxysilane. This thought is supported by the fact that the narrow central component of the spectrum widens (as a result of the spin-orbital interaction) and the exchange is cancelled. The narrowing of the peak as the measurement temperature of the wide peak drops supports also the explanation we have given for the formation of this peak.

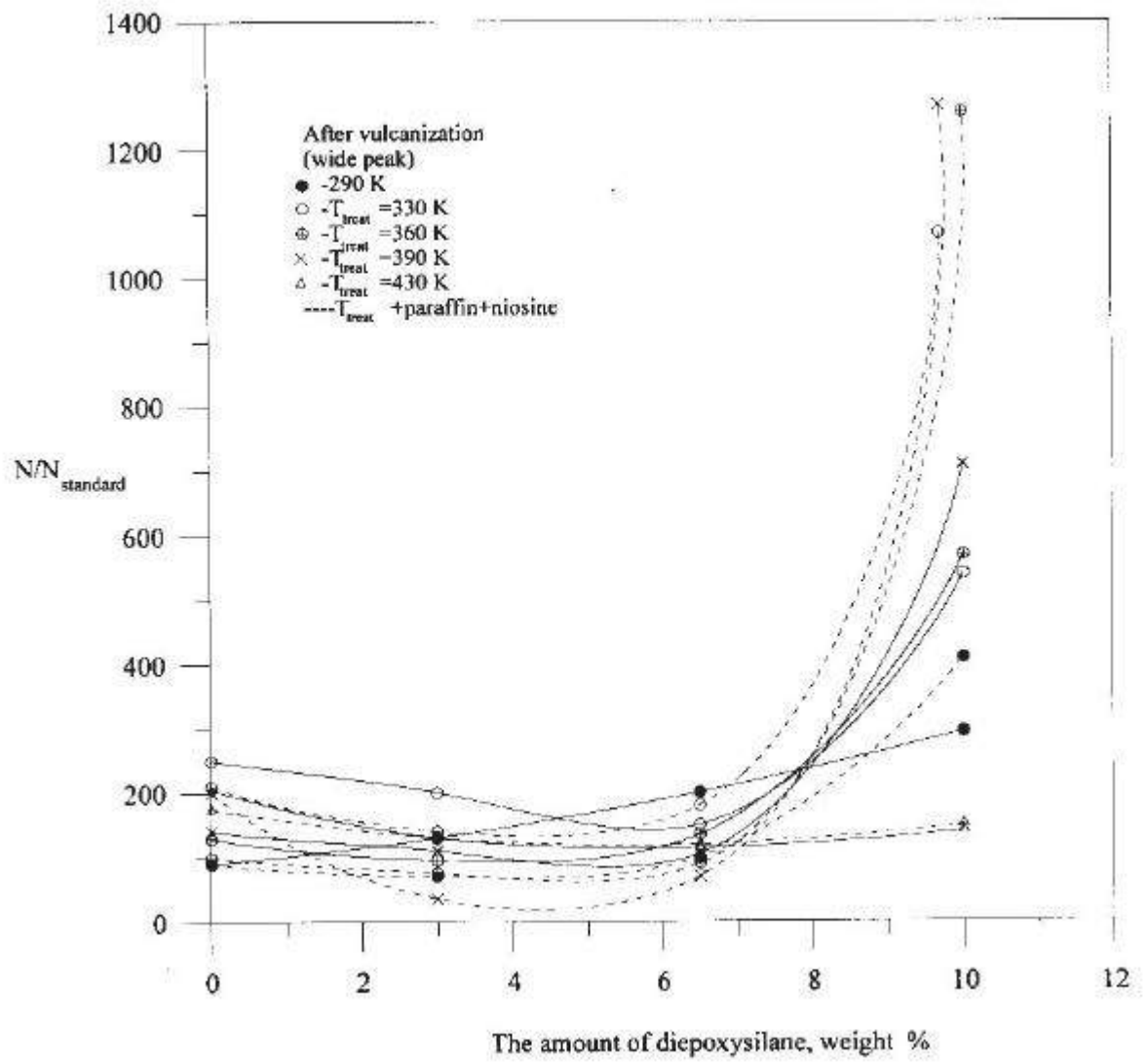

Fig.4. The dependence of the concentration of paramagnetic centers on the amount of diepoxysilane, in the rubber chloroprene and for the wide peak, after vulcanization

If we take into account the formation of FR's above the narrow central peak that has a HFS, the formation mechanism of the wide peak and the dependence of N / N_{st} (where $N_{st} = 5.4 \times 10^{15}$ is the amount of spin in a spin-standard sample) on various factors (Figures 6a-c) then we can explain the obtained results as follows. The silicon organic compound causes a great deal of bond breakings by playing a filling role. Indeed, the increase in the value of N for the PC's belonging to the narrow peak as the dopings and T_{treat} get higher, supports this idea. This phenomenon becomes more emphasized by the presence of the diepoxysilane bigger molecular volume. Consequently, the supra molecular structure (SMS) of the rubber equalizes according to its dimensions, that is, the rubber becomes more homogeneous structurally. Therefore, the successive steps of polimerization and vulcanization become easier.

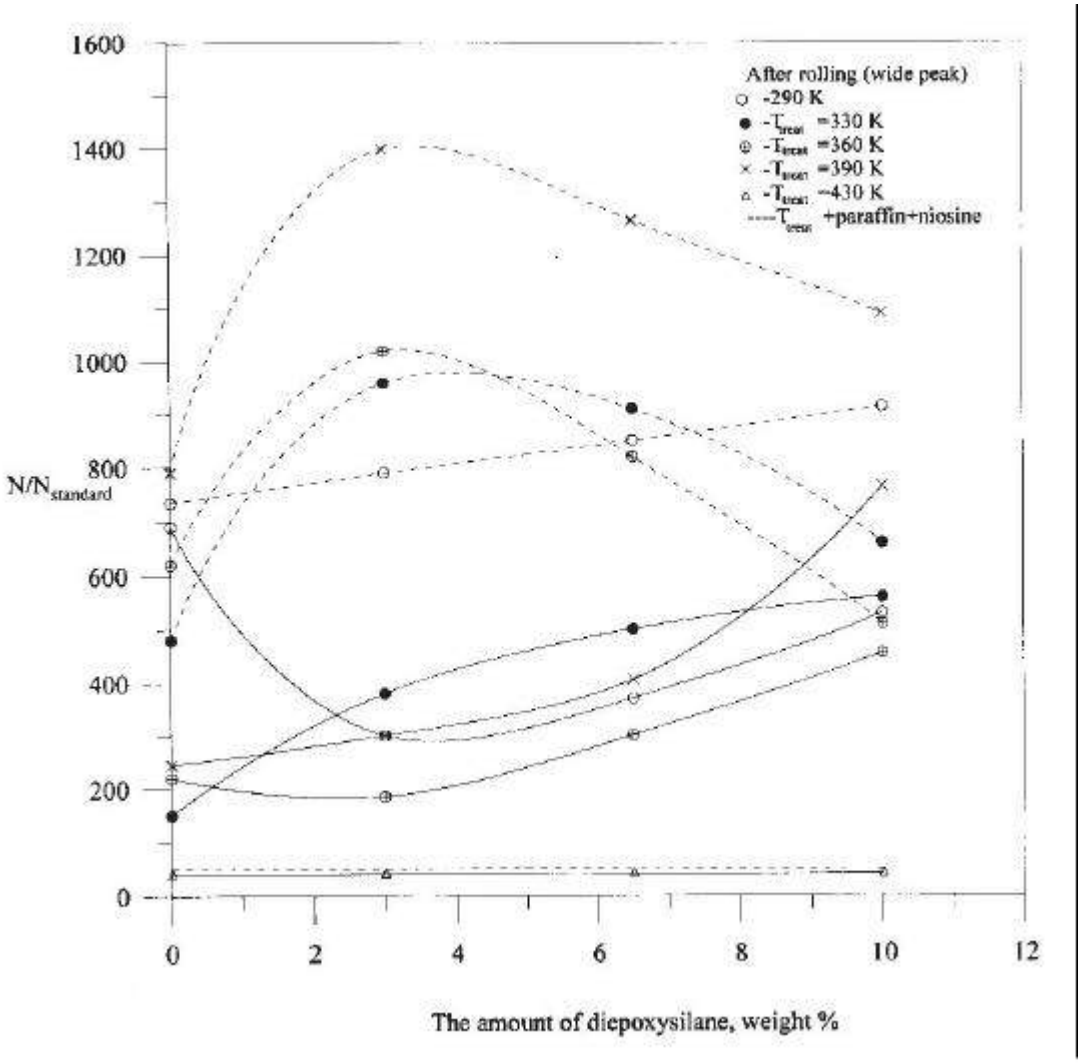

Fig.5. The dependence of the concentration of paramagnetic centers on the amount of diepoxysilane, in the rubber chloroprene and for the wide peak, after vulcanization

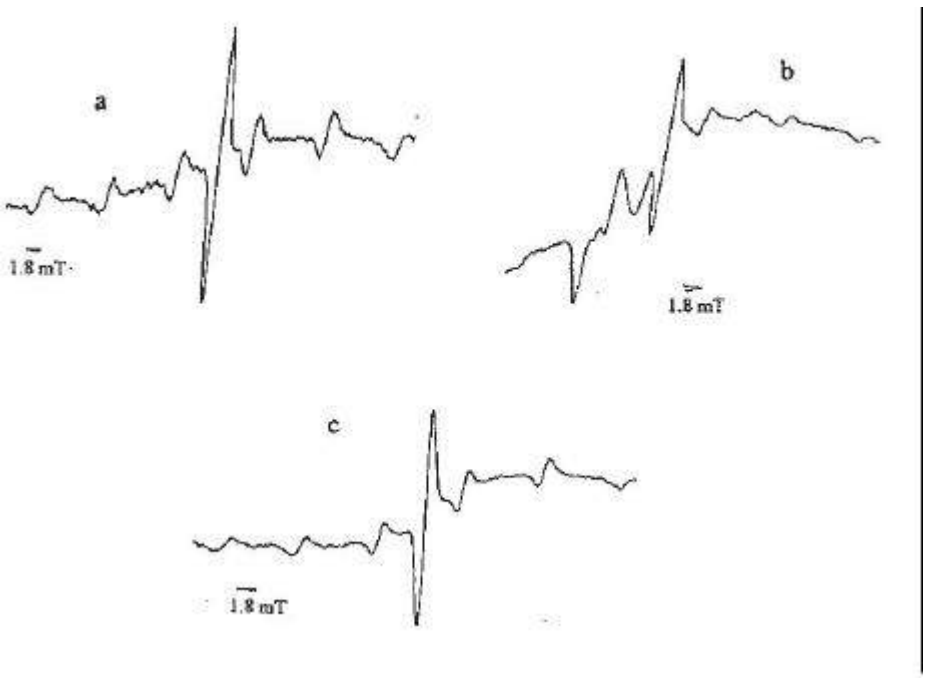

Fig.6. a) ESR spectrum with the narrow peak, in the rubber chloroprene with the amount of diepoxysilane after the vulcanization; b) the ESR spectrum with the wide peak, in the rubber chloroprene with the amount of diepoxysilane after the vulcanization; c) the isotropic ESR spectrum in the rubber chloroprene after vulcanization.

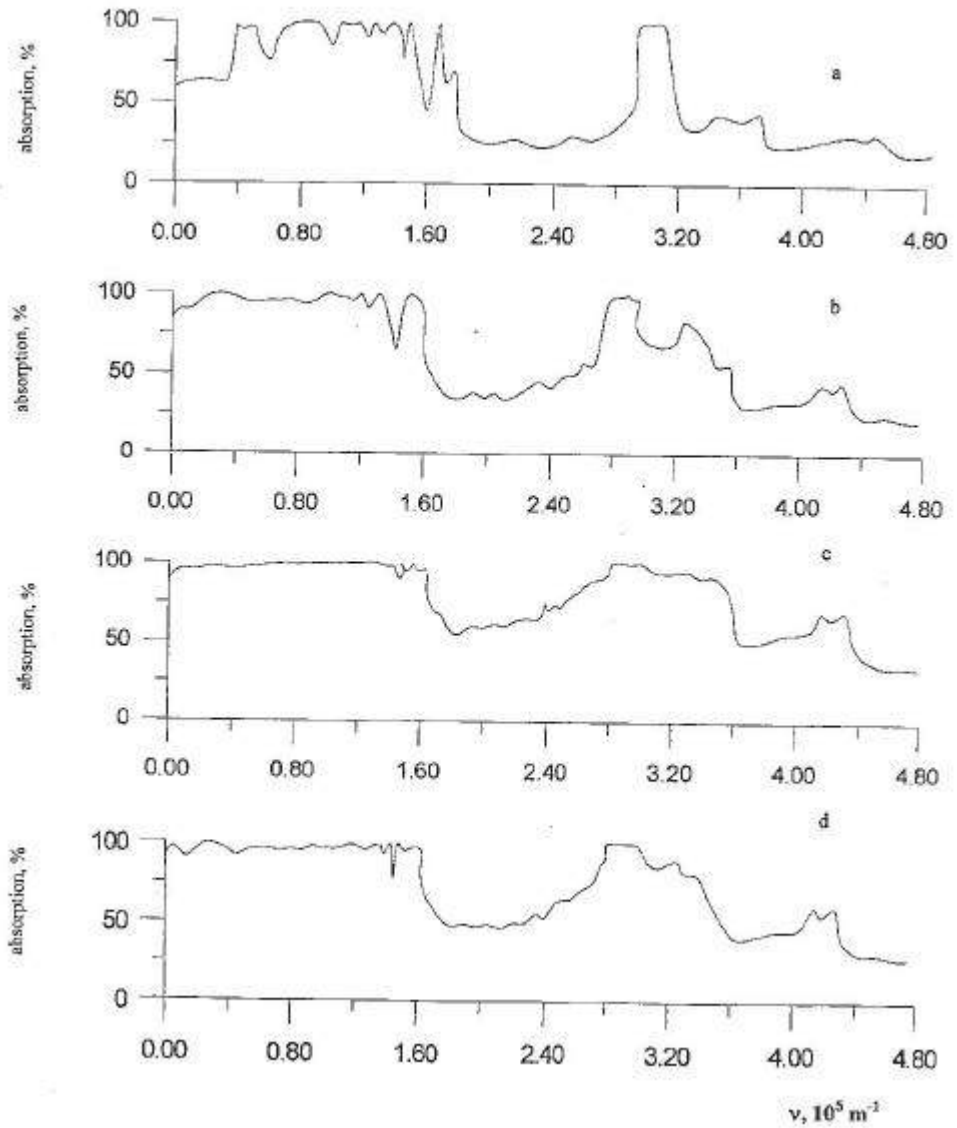

Fig.7. The characteristic IR absorption spectrua in the rubber chloroprene with the amount of diepoxysilane: a) pure rubber; b) 3 weight %, c) 6.5 weight %, d) 10 weight%.

Since an ordered vulcanization network results during vulcanization the nuclei of Cl become completely equivalent and thus an absolutely isotropic spectrum occurs (Figure 1a, 6a, 6c). If the samples undergo only the process of rolling the above mentioned homogeneity is not observed, the isotropy of the spectrum is deteriorated (Figure 1b, 1c, 6b) and also both the intensities of the HFS components and the distances between them change considerably. On the other hand, an additional spectrum with the HFS, which is a bit different than the HFS constants of the isotropic spectrum is observed and this spectrum is placed with the peaks of the isotropic spectrum in pairs. The intensity, number and the placement of the 'additional spectrum' vary according to the prehistory of the sample. All the above said can be explained by the results of the mechano-chemical processes of the rubber. In fact, the multi chemical bonds that are uncontrolled during rolling break and these breakings are random. Simultaneously with it form various associates which are quite different from each other. Therefore, the UE's interact with the nonequivalent nuclei of Cl and protons. Furthermore, the UE's that are localized in different structural units form different ESR spectra [19, 20], that is, the shape, parameters and the gathering kinetics of the PC's vary strongly, since they depend on the local environment of these centres. The possibility of observing the additional spectrum in the ESR spectrum shows that the SMS's in the rubber are not homogeneous.

The contribution of the silicon organic compounds causes with the addition of oxygen containing groups (that exist in the structure of diepoxysilane), the chemical complexes and unifications. Consequently, due to the above said, as a result of the addition of diepoxysilane to the structure of rubber chloroprene, a binary situation arises. The structure of rubber is homogeneous according to the SMS's on the one hand and the FR processes vary greatly on the other. If we consider the stimulating role of the FR's in the radical polymerization processes of the elastomers, then they take part in two "competing" processes [2], that is, radical polymerization and oxidation reaction. In the later stages of the vulcanization of the rubber whose prehistory was given above (the one that has SMS and PC's with FR's) some part of the FR's continue the oxidation chain and worsen the characteristics of the rubber (that is, material) and some other part make the characteristics better by starting the radical polimerization

(that is, stimulating). The resulting effect, whether positive or negative, depends on the superposition of these factors. The disappearance of the FR's that occurred by the addition of oxygen after the vulcanization proves that they pass on to the oxidized form. The greater the concentration of FR's of this type, the more oxidized becomes the rubber. Its properties worsen and this is observed better at higher values of the ratio of the doping and on the contrary, the observation of the multi-component isotropic spectrum shows that the UE's become stable in the homogeneous structure of the rubber. In other words, the better the network of vulcanization, the better will be the degree of isotropy of HFS. This is observed better at 3 weight % of diepoxysilane. Under these circumstances, it can be said that ordered SMS's that have optimum dimensions form beforehand and help the process of vulcanization. Therefore, the final structure of the rubber based resins is more homogeneous and the physico-mechanical and use characteristics of this resin should be ameliorated.

As can be seen, the ESR results of the rubber chloroprene that was produced by the contribution of the diepoxysilane plays a vital role in both manufacturing and using processes of the FR's that we suggested in reference [1]. The ideas that we gave above are also supported by the results of the IR absorption spectra in the same type of rubber samples that we used for ESR. A typical example of these spectra is given in Figure 7. When we added the contribution two types of phenomena are observed: the optical densities of the peaks that belong to the C=C and C=O bonds vary and a scattering occurs at the limit of SMS of the IR rays. Furthermore, the optical densities of the peaks become respectively minimum and maximum for the C=O and C=C bonds at 3 weight % of the silicon organic compounds. Also at certain values of l the l-dependent scattering is observed to have a maximum value. If we take into account the mechanisms that we suggested in this study and in reference [1] and explain the formation of the background by the dispersion of the IR rays at the limits of the SMS's, then at the 3 weight % of the contribution, the SMS's occur spontaneously, dispersion diminishes and thus, the vulcanization network that has formed as a result of the vulcanization becomes more ordered. Therefore, the load that affects the rubber externally is distributed homogeneously in its volume and consequently increases the strength of the rubber against degradation and breaking. The interpretation for the ESR and IR spectra of the rubber chloroprene given above supports both the results of the dynamic-mechanical and electrical measurements of the diepoxysilane used in these rubbers and also the results of the use parameters of the appropriate mixtures of resin. Indeed, as the amount of the diepoxysilane increases, so does, the breaking tension-s and at 10 weight % it becomes maximum (the strength gets 35 % greater). The electrical strength varies in the same manner. The glass transition temperature drops gradually and becomes saturated, relative deformation increases first, at 6.5 weight % it becomes maximum, then decreases a little. The resin materials made of such mixtures have good technological and use parameters.

CONCLUSIONS

We can summarize the results for the characteristics of the ESR in linear rubbers that we presented as follows. Although in references the ESR is observed in these rubbers, all of these PC's arise under various strong external factors. But, in spite of some thoughts in favour of the addition of the FR's in the degradation and breaking processes of these rubbers, no PC is observed in them after the processes. Our results prove that such centres play an important role in the oxidation and breaking processes with FR's and this determines the degradation and breaking properties of the materials made of these rubbers in later stages. Consequently, FR's result after breaking the chemical bonds, in the processes of synthesis of the rubbers. Since the FR's have a great chemical activity, they develop the oxidation reactions similar to the chain following degradation. The chemical bonds with the neighbouring macromolecules in the region where FR's settle become excited and brittle, also the breaking activation energy diminishes. The breaking in chains can continue through the thermal fluctuations. These radicals which have a long lifetime are secondary type of FR materials and are generally localized in amorphous regions and where the structure is defective. As one passes from the rubber devinylnitrile to rubber chloroprene, the ESR spectrum becomes more like the component form instead of singlet. We can explain this, in case that there are atoms or groups of atoms in the side chains, whose electronegativity is greater, by its stronger interaction with these groups. As can be seen from the observed ESR spectra, as the amount of oxygen increases in the rubber system, the concentration of FR's becomes higher. When different structures are added to the structure of the rubber, both the concentration of FR's, the SMS and the molecular structure of the rubber change. The structure of the rubber becomes more homogeneous, that is, the following network of vulcanization becomes better. On the other hand, a correlation is observed between both the concentration of the FR's and structural variations and also the physico-mechanical and electrical strengths of the rubbers and other use parameters. For all that we said we can conclude the following. The rubber materials have a certain structural information, the so called 'prehistory' before they are manufactured and this factor determines later the degradation and breaking phenomena of these materials.

The concentration of FR's shows an extremal variation in both the amount of the oxygen containing groups and the physico-mechanical and electrical strength of the rubbers, depending on the ratio of T_{treat} and the dopings. This extremal situation which depends on the molecular and SMS of the rubbers can be explained with the mechanism that we presented in our previous paper [1], that is, the presence of the supra molecular compounds which are special for each of the rubbers. As we thought, the overall effect of the dopings goes up to the point that the dopings cover the surface of the above said structure with a mono atomic or mono molecular layer [21, 22, 23]. For the optimum amounts of dopings and T_{treat}, some optimum ratio of the amorphous and crystalline phases occurs and this brings about the best physico-mechanical and technological properties of the materials. Therefore, the results of these two papers allow to arrange the use parameters of the rubbers and resins we investigated and to choose the composites and mixtures of resins that have the best parameters.

[1] *S.I.Mehdiyeva, R.L Bayramova*. Fizika, 2000, V.VI, No:3, p.23.
[2] *B.A.Dogadkin, A.A.Dontsov,V.A.Shershnev.* Khimiya Elastomerov, M:Khimiya, 1981 (in Russian), 374 p.
[3] *N.M.Emanuel, A.I.Buchahenko.* Khimicheskaya Fizika Stareniyai Stabilizatsii Polymerov, M.: Nauka, 1982, 359 p (in Russian).
[4] Noviye Cauchuci; Svoystva i primeneniye, IIL, M, 1958, 272 p, (in Russian).
[5] *Sh.V.Mamedov*. Abstract of Doctor Dissertation (in Russian), 1986, 43p.
[6] *V.Hofman*. Vulkanizatsiya i vulkaniziruyushiye agenti (Translation from Germany into Russian). Editor I.Y. Poddubni.L.,Khimiya, 1968, 464p.
[7] *A.A.Dontsov*. Prosessi strukturiravaniya elastomerov.M.: Khimiya, 1978, 287p (in Russian).
[8] *L.H.Sperling*. Introduction to Physical Polymer Science. John Wiley and Sons, Inc., New York and other publ., Second Edition, 1992, 594p.
[9] *Malcolm P.Stevens.* Polymer Chemistry, An Introduction, Second Edition, New York, Oxford, 1990, 633p.
[10] *B.C.Anderson, Y.Ýmanishi* (Eds.).Progress in Pacific Polymer Science; Proceedings of the First Pasific Polymer Conference, Springer-Verlag (Berlin, Heidelberg, New York and other Publ.), 1991, 430p.
[11] *A.Akelah and A.Moet*. Functionalized Polymers and Their Applications, Chapman and Hall, London-New York and other Publ., 1990, 354p.
[12] IANM. Compbell.Introduction to Synthetic Polymers, Oxford, New York, Tokyo, 1997, 213p.
[13] *N.G.McCrum, C.P.Buckley, C.B.Bucknall*. Principles of Polymer Engineering, Second Edition, Oxford, New York, Tokyo, 1997, 447p.
[14] Vishu Shah.Handbook of Plastics Testing Technology, Second Edition, John Wiley and Sons, Inc., New York and other Publ., 1998, 527p.
[15] *Sh.V.Mamedov, S.A.Abasov, H.H.Ahmedov, R.B.Aslanov*. Thesis of rapors of All Union Science. Thechnical Conf. On the Dielectric's Physics, Baku, 1-3 December, 1982.
[16] A.S. ¹ 790738 (USSR). *H.B.Abdullayev, H.H.Ahmedov, S.A.Abasov, R.H.Babayev, Sh.F.Sadigov, Sh.V.Mamedov*. Authors Certificate, from 21 August 1980.
[17] *Sh.V.Mamedov, S.A.Abasov, H.H.Ahmedov,R.B.Aslanov*. Thesis of rapors of All Union Scienc. Thechnical Conf on the Dielectric's Physics, Baku, 1982, pp.12-14.
[18] *Sh.V.Mamedov, R.L.Bayramova, Y.Lenger, D.Ören*.Thesises of 3rd General Conference of the Balkan Physical Union, 2-5 September, 1997, Cluj-Napoca, Romania, p.99.
[19] *John E. Wertz, James R.Bolton*. Electron Spin Resonance. Elementary Theory and Practical Applications, New York, 1972, 499p.
[20] *V.K.Milinchuk, E.R.Klinshpont,S.Y.Pshejetsky.*Macroradikali, M.:Khimiya, 1980, 263p (in Russian).
[21] *G.B.Abdullayev, Sh.V.Mamedov, Z.M.Abutalibova, N.I.Ibragimov, Y.Y.Volchenkov*. Izv.An Azerb.SSR,Ser.FTMN, 1971, ¹ 4, pp.100-113.
[22] *G.B.Abdullayev, Sh.V.Mamedov, Z.M.Abutalibova, Y.Y.Volchenkov*. Izv.AN Azerb. SSR, Ser.FTMN, 1977, ¹ 1, pp.67-75.
[23] *Sh.V.Mamedov, V.A.Alekberov, Y.Lenger, D.Ören, S.A.Abasov, M.Subasý and R.L.Bayramova*. Polymer Composites, 1999, v.20, ¹ 2, p.216.

Received: 13.06.02

ELECTROPHYSICAL PROPERTIES OF $TlIn_{1-x}Sm_xSe_2$ (0£õ£0,08) CRYSTALS

E.M. GOJAYEV, K.D. GULMAMEDOV, D.A. HUSEYNOV
Azerbaijan Technical University, Baku, 370143, H. Cavid ave. 27

In the present paper we outline the research results of the temperature dependence of the specific electroconductivity, the Hall coefficient and thermo e.m.f. in the temperatures ranges 300÷1100 K of $TlIn_{1-x}Sm_xSe_2$ ($0\le õ\le 0,08$) alloys. The width of the forbidden band of indicated alloys system is determined. It was revealed, that the width of the forbidden band reduces according to the additivity law at the partial substitution of indium atoms by samarium ones in $TlSmSe_2$. By investigating the influence of the directed deformation on electron properties of $TlIn_{1-x}Sm_xSe_2$ alloys we found their dependence on temperature and deformation. These crystals have high coefficient of the strain sensitivity.

The information about the existence of $TlIn_{1-x}Sm_xSe_2$ type alloys was given in papers [1-6].

In present paper we outline research results of electrophysical properties of $TlIn_{1-x}Sm_xSe_2$ crystals. The alloys synthesis was carried out according to the methods described in [1]. As initial substances Tl-99,99 mass%; In-99,99 mass%; Se- specially pure, Sm, containing as impurities (mass%): sizes-0,05, Cu-0,01, Fe-0,01 were used. Monocrystals of $TlIn_{1-x}Sm_xSe_2$ alloys system with content up to 5mole % of $TlSmSe_2$ were obtained by the method of the zone growth from before synthesized samples. Monocrystal samples with average sizes 2õ4õ6 mm^3 were cut out from the average part of ingots. Alloys, containing (6÷8) mole % of $TlSmSe_2$ were semicrystal. Curves of the concentration dependence of the microhardness (h), electroconductivity (σ) and thermo e.m.f. (α) were plotted to reveal boundaries of the solid solutions existence.

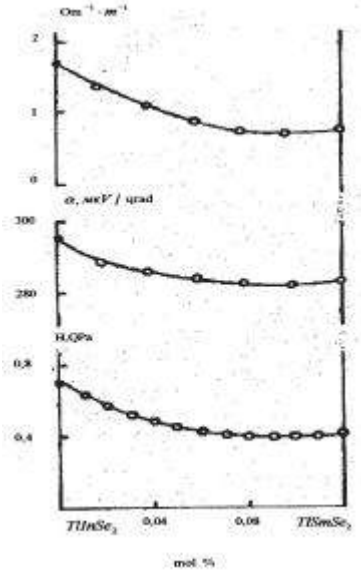

Fig. 1. Concentration dependences of microhardness (H), electroconductivity (*s*) and thermo-e.m.f. (*a*) of system alloys $TlInSe_2$-$TlSmSe_2$ alloys system.

The microhardness was measured on the PMT-3 device. Loads of ~10H were used. Numerical values of the crystal microhardness for each alloy were obtained by the statistical treatment of 10 measurements results. The measurements results of the system $TlIn_{1-x}Sm_xSe_2$ are presented on fig 1. At the partial substitution of indium atoms by samarium ones H reduces and beginning from 8 % of $TlSmSe_2$ it remains constant. The H reduction corresponds to the homogeneity region. Such supposition is in agreement with measurements results of α and σ, in the range 0÷8 mole % of $TlSmSe_2$ thermoelectric parameters change, α and σ do not practically change across limits of the indicated concentration region. In whole, concentration dependence of H, σ and α are well correlated and allow to reveal boundaries of the solid solution homogeneity of the indicated system.

Electric properties of crystals were measured by the compensational method in the constant magnetic field at the constant current in the temperature range 300÷1100 K on four samples with identical concentration of electrons and $TlSmSe_2$ content, whose electric heterogeneity does not exceed 5 %.

Temperature dependences of the electroconductivity (*s*), Hall coefficient (*R*) and thermo e.m.f.

(*a*) were investigated. The errors of measurement of *a*, *s* and *r* were 4,8 and 5 %, respectively. The forbidden band width of solid solutions of the indicated system was determined from high-temperature dependences of $lg\,s=f(10^3/T)$ and $lgRT^{3/2}=f(10^3/T)$. As it follows from fig.2a, the alloys electroconductivity of the $TlInSe_2$- $TlSmSe_2$ system at low temperature reduces mainly with the temperature growth, but, further, it grows with the own carriers appearance. The thermal dependence of the Hall coefficient for the indicated system alloys corresponds to the thermal dependence of the electroconductivity (fig. 2b), i.e. the free carriers concentration remains constant at low temperatures, but the Hall mobility is limited mainly by the scattering on longitudinal acoustic oscillations. Therefore, the mobility as well as the electroconductivity of these alloys fall with the temperature growth (fig. 2a).

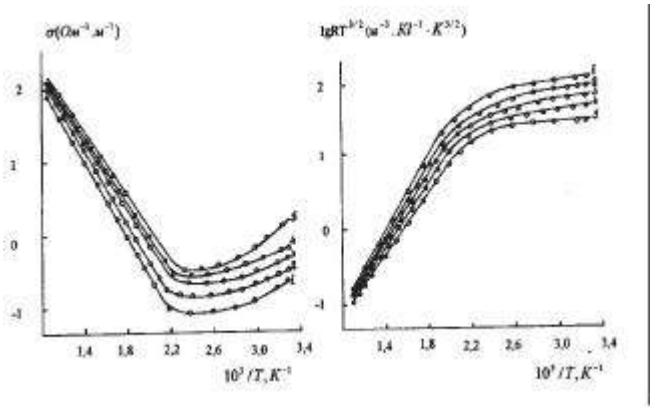

Fig.2. Temperature dependences of electroconductivity (a) and Hall coefficient (b) of $TlIn_{1-x}Sm_xSe_2$ alloys system, where *1-õ=0; 2-õ=0,02; 3-õ=0; 4-x=0,06; 5-x=0,08*.

The dependence of thermo-e.m.f. on the temperature for alloys $TlInSe_2$-$TlSmSe_2$ is presented on fig. 3. In the impurity region the thermo-e.m.f. increases with the temperature growth, reaching maximum in the biased region and it reduces with the own conductivity receipt, what is typical for all investigated phases.

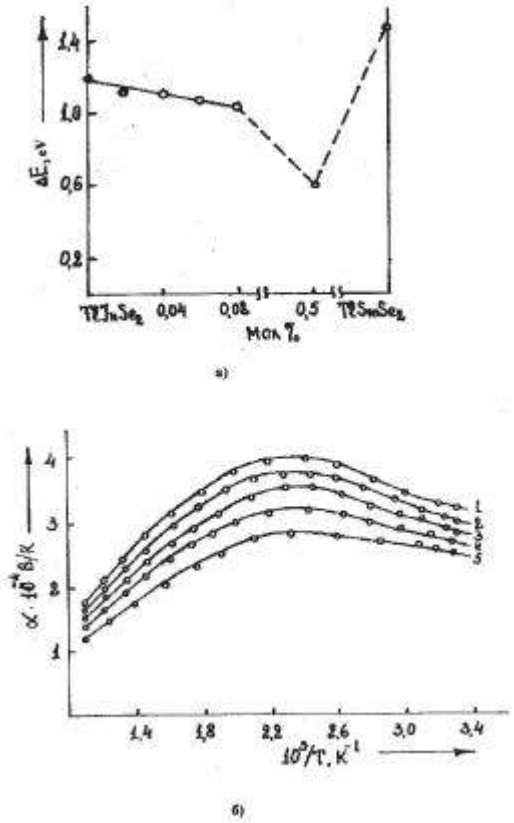

Fig.3. Concentration dependence of the forbidden band width (a) and the temperature dependence of thermo-e.m.f. (b) of $TlIn_{1-x}Sm_xSe_2$ alloys system

The concentration dependence of the forbidden band width, determined by high-temperature slope of curves lg $\sigma \sim 10^3/T$ and lg $RT^{3/2} \sim 10^3/T$ of $TlIn_{1-x}Sm_xSe_2$ alloys is presented on fig. 4. These data show, that the width of the forbidden band reduces according to the additivity law at the partial substitution of indium atoms by samarium ones in the $TlInSe_2$ lattice. Obviously, it is connected with the fact, that in $TlInSe_2$ the valent band is mainly formed by fissionable 4r-levels of selenium ions and partial by 5r5s-levels of indium ions, but the conductivity band is formed by 5r5s levels of indium ions and 6r-levels of tallium ions. D-states of samarium atoms, which are energetically placed upper, are hit in the conductivity band at the partial substitution of indium atoms by samarium ones. In the $TlInSe_2$-$TlSmSe_2$ system at the samarium concentration growth their valent electrons transfer into the itinerant state, which causes the strong electron interaction and the lattice "distension". In this regard in the $TlInSe_2$-$TlSmSe_2$ system at the transition from the $TlInSe_2$ to the solid solutions on its base the width of the forbidden band reduces.

As it is well known [7] $TlInSe_2$ is crystallized by the tetragonal syngony. The growth of the samarium concentration in $TlInSe_2$ does not lead to the compound structure breakdown. It means, that in the case given the samarium atoms reveal the trivalence, approved by semiconductive properties. However, it is possible to form the trivalence state with spare, mobile electrons, weakly connected with f-orbit and providing in solid solutions the growth of velocity of electrons, weakly connected with f-orbit, what, in its turn, leads to the change of the forbidden band width.

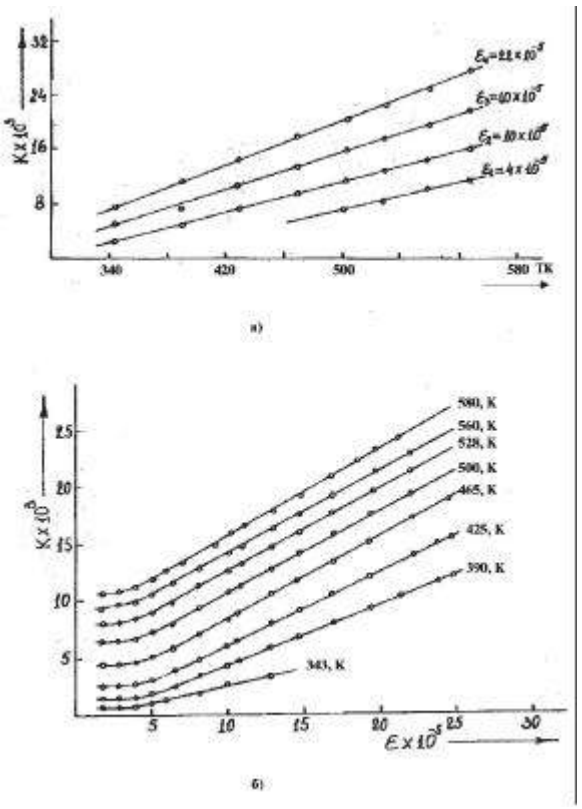

Fig. 4. The dependence of strain sensitivity on the temperature at various deformations (a), and the dependence of the strain sensitivity on the deformation at various temperatures (b) of alloys $TlIn_{1-x}Sm_xSe_2$ where *1-õ=0*; *2-õ=0,03*.

The influence of the directed deformation on the electron process in $TlIn_{1-x}Sm_xSe_2$ crystals was investigated. Ohmic contacts were formed by the indium melting in the gas flow with the following soldering of copper wires (*d*=0.01 mm) on obtained needle crystal billets with mirror faces without additional treatment.

Plates from 45 steel with the thickness of 0,5 mm and the length 50 mm were tared beams for pasted sensors. The substrate surface according to the treatment range corresponded to the 7 class. Before the sublayer application substrates were treated by the ethyl spirit. On the cleaned substrates the sublayer of the epoxy-cresol varnish (EP-96), presented as the solution of the epoxide resin (E-40 is the modification of same acids with the addition of butanomodified pesol (PB) and the resin K-421-02) was applied.

The sublayer thickness was 10 mk. The uniform (with respect to the thickness) covering was provided in the process of the sublayer application.

After an hour heating (keeping) at the room temperature the substrate was carried in the drying cabinet for the high-temperature polymerization.

The slow temperature increase up to 480 K and the heating during 1 hour at this temperature provide the full

polymerization and exclude the air bubbles appearance. The second layer of the varnish, a bit exceeding the strain resistor sizes, was applied on the prepared substrate.

$TlIn_{1-x}Sm_xSe_2$ crystals with soldered tapings were placed on the varnish layer and slightly pressed, the crystal surface was fully covered by the varnish. The crystal was simultaneously set in the necessary position in the substrate plane. The sensor drying was being carried out at 318÷323 K during an hour with the following annealing, at 490 K during 2 hours. The indicated drying mode showed to be the most optimal one and the devices showed the maximal sensitivity.

The strain sensitivity coefficient, being the main characteristic of the strain resistor, was determined by the formula $K = \frac{\Delta R}{R_o \varepsilon}$ where $\varepsilon = \frac{\Delta l}{l}$ is the relative change of the samples length or the relative deformation, $\Delta R/R_o$ is a relative change of the resistance, $\Delta R = R - R_o$ is the resistance change, where R_o is the sample resistance before deformation, and R is the sample resistance after deformation, l is the samples length, Δl is its change.

The temperature dependence of $TlIn_{1-x}Sm_xSe_2$ crystals strain sensitivity (K) was carried out in the temperature range 300-560 K.

As a particular case, K dependences on the temperature at the constant deformation are presented on fig. 5, but K dependences on the deformation at various temperatures are presented on fig. 6 for $TlInSe_2$.

From conducted research it follows, that for $TlInSe_2$ the dependence of the strain sensitivity coefficient on the deformation is linear at various temperatures, beginning from room up to 580 K.

CONCLUSIONS

By our research of electrophysical properties of $TlIn_{1-x}Sm_xSe_2$ alloys system depending the content and temperature it was established that the width of the forbidden band reduces in the solubility region ($0 \le x \le 0,08$) at the partial substitution of indium atoms by samarium ones in $TlInSe_2$. It was found, that $TlIn_{1-x}Sm_xSe_2$ ($0 £ õ £ 0,03$) crystals have high coefficient of the strain sensitivity.

[1] *E.M. Gojayev, M.M. Zarbaliyev, K.M. Rzayev* - Electric properties of compound alloys of $TlIn_xLn_{1-x}C_2^{VI}$, where 0≤õ≤1, C=Se,Te; Ln-La, Ñe, Pr, Nd, Sm, Eu. Reports of All-Union Conference on physics and chemistry. Saint Petersburg, 1976, p.62.

[2] *E.M. Gojayev, V.A. Mamedov*. The system $TlInSe_2$-$TlCeSe_2$. "Non-organic chemistry" journal, 1976, p.160-163.

[3] *E.M. Gojayev, K.D. Orudgev, V.A. Mamedov*. The system research $TlInSe_2$-$TlNdSe_2$ and $TlInTe_2$-$TlNdTe_2$, Izv. AS SSSR-" Non-organic materials", 1981, v.17, ¹ 16, p. 1388-1391.

[4] *E.M. Gojayev, V.A. Mamedov, Sh.M. Huseynov* - The state diagram and research of electrophysical properties of system alloys $TlInTe_2$-$TlSmTe_2$. Izv. AS SSSR, "Non-organic materials", 1983, v. 19, ¹ 11, p. 1813-1815.

[5] *E.M. Gojayev, V.A. Mamedov, P.G. Rustamov*. Roentgenographic research and electric properties of solid solutions of $TlInTe_2$- $TlLnTe_2$ (Ln- La, Ce, Pr) system- Izv. AS SSSR, " Non-organic materials", 1986, ¹ 6, p. 1039-1041, v.22.

[6] *E.M. Gojayev, A.M. Nazarov*. Solid solutions $TlInS_2$-$TlPrS_2$ system- Izv. RAS. "Non-organic materials", 1998, v.34, ¹ 10, p.1-5.

[7] *G.D. Guseinov, E.M. Kerimova, R.S. Gamidov, I.V. Alekseev, M.Z. Ismailov*. On some properties of $TlInS_2$ (Se_2, $Tå_2$) single crustals. Phys. Stat. Solids, 1969, v.34, ¹ 1, p.34-38.

Received: 14.06.02

SOLUTIONS OF THE PRINCIPAL CHIRAL FIELD PROBLEM FOR THE HIGH-RANK SIMPLE ALGEBRAS

M.A. MUKHTAROV
Institute of Mathematics and Mechanics
370602, Baku, F.Agaev str. 9, Azerbaijan

New solutions of the principal chiral field problem are constructed by means of discrete symmetry transformations for the algebra SL(3,C). The generalization to the case of arbitrary semisimple algebra of the rank higher than two is discussed.

1. The problem of constructing of the solutions of self-dual Yang-Mills (SDYM) model and its dimensional reductions, the principal chiral field problem in our case, in the explicit form for semisimple Lie algebra, rank of which is greater than two, remains important for the present time. The interest arises from the fact that almost all integrable models in one, two and (1+2)-dimensions are symmetry reductions of SDYM or they can be obtained from it by imposing the constraints on Yang-Mills potentials [1-10].

This work is a direct continuation of [13], where the exact solutions of the principal chiral field problem have been derived for the case of algebra SL(2,C). The discrete symmetry transformation method [12] applied here allows to generate new solutions from the old ones in much more easier way than applying methods from [11], and the case of SL(3,C) algebra gives us a key to construct solutions for an arbitrary semisimple algebra.

2. Equations of the principal chiral field problem are the systems of equations for the element f, taking values in the semisimple algebra,

$$(\mu_i - \mu_j)\frac{\partial^2 f}{\partial x_i \partial x_j} = \left[\frac{\partial f}{\partial x_i}, \frac{\partial f}{\partial x_j}\right] \qquad (1)$$

In the case of two-dimensional space: μ_1=1, μ_2=-1, $x_1 = x$, $x_2 = t$.

Following [12], for the case of a semisimple Lie algebra and for an element f being a solution of (1), the following statement takes place:

There exists such an element S taking values in a gauge group that

$$S^{-1}\frac{\partial S}{\partial x_i} = \frac{1}{\tilde{f}_-}\left[\frac{\partial \tilde{f}}{\partial x_i}, X_M^+\right] - \mu_i \frac{\partial}{\partial x_i}\frac{1}{\tilde{f}_-} X_M^+ \qquad (2)$$

Here X_M^+ is the element of the algebra corresponding to its maximal root divided by its norm, i.e.,

$$\left[X_M^+, X_M^-\right] = H, \left[H, X_M^\pm\right] = \pm 2 X_M^\pm \quad ,$$

$-\tilde{f}_-$ - is the coefficient function in the decomposition of $\tilde{f}$ of the element corresponding to the minimal root of the algebra, $\tilde{f} = \sigma f \sigma^{-1}$ and where σ is an automorfism of the algebra, changing the positive and negative roots.

In the case of algebra SL(3,C) we'll consider the case of three dimensional representation of algebra and the following form of $\sigma = \begin{pmatrix} 0 & 0 & 1 \\ 0 & 1 & 0 \\ -1 & 0 & 0 \end{pmatrix}$.

The discrete symmetry transformation, producing new solutions from the known ones, is as follows:

$$\frac{\partial F}{\partial x_i} = S\frac{\partial \tilde{f}}{\partial x_i}S^{-1} + \mu_i \frac{\partial S}{\partial x_i}S^{-1} \qquad (3)$$

3. Let's represent the explicit formulae for transformation in the case of SL(3,C) algebra

$$f = \alpha_1 X_1^+ + \alpha_2 X_2^+ + \alpha_{1,2} X_{1,2}^+ + \tau_1 h_1 + \tau_2 h_2 + a_1 X_1^- + a_2 X_2^- + a_{1,2} X_{1,2}^- \quad , \qquad (4)$$

In connection with the general scheme, first of all, it is necessary to find the solution of the equations (2) for the SL(3,C) valued function S for given f, solution of equations (1).

From (2) it is clear that S is upper triangular matrix and can be represented in the following form:

$$S = \exp \beta_1 X_1^+ \exp \beta_{1,2} X_{1,2}^+ \exp \beta_2 X_2^+ \exp \beta_0 H \quad , \qquad (5)$$

where $H=h_1+h_2$.

After substitution of the last representation of S into (2) and taking into account (4), we have at every step of the recurrent procedure the following relations

$$\beta_0 = \ln \alpha_{1,2}\ ,\ \beta_1 = \alpha_2\ ,\ \beta_2 = \alpha_1$$
$$(\beta_{1,2})_{x_i} = (\alpha_{1,2})_{x_i} - (\delta_1 + \delta_2)_{x_i}\alpha_{1,2} - (\alpha_1)_{x_i}\alpha_2 \qquad (6)$$

As the initial solution we'll take the explicit solution f belonging to the algebra of upper triangular matrixes:

$$f = \alpha_1 X_1^+ + \alpha_2 X_2^+ + \alpha_{1,2} X_{1,2}^+ + \tau_1 h_1 + \tau_2 h_2 \qquad (7)$$

The component form of self-duality equations for this case is following

$$\frac{\partial^2 \tau_n}{\partial x_i \partial x_j} = 0\ ,$$
$$\frac{\partial^2 \alpha_n}{\partial x_i \partial x_j} = \{\delta_n, \alpha_n\}_{x_i, x_j} \quad , \quad i=1,2, \qquad (8)$$

$$\frac{\partial^2 a_{1,2}}{\partial x_i \partial x_j} = \{ \boldsymbol{d}_1 + \boldsymbol{d}_2, \boldsymbol{a}_{1,2} \}_{x_i, x_j} \quad ,$$

where $d_1 = 2t_1 - t_2, d_2 = 2t_2 - t_1$ and figure brackets of two functions g_1 and g_2 denotes:

$$\{ g_1, g_2 \}_{x_i, x_j} = \frac{\partial g_1}{\partial x_i}\frac{\partial g_2}{\partial x_j} - \frac{\partial g_2}{\partial x_j}\frac{\partial g_1}{\partial x_i} .$$

The general solution of system (8) takes the form

$$\boldsymbol{t}_i = \sum_{s=1} \boldsymbol{t}_i^s (x_s) , \ \boldsymbol{a}_i = \oint_c \boldsymbol{a}_i (\boldsymbol{l}) \exp(-\bar{\boldsymbol{d}}_i (\boldsymbol{l})) d\boldsymbol{l},$$

$$\bar{\boldsymbol{d}}_i (\boldsymbol{l}) = \sum_{s=1} \frac{\boldsymbol{t}_i^s (x_s)}{\boldsymbol{l} + \boldsymbol{q}_s},$$

$$a_{1,2} = \oint_c a_{1,2}(l) \exp(-\bar{d}_1(l) - \bar{d}_2(l)) dl +$$

$$+ \oint_c a_1(l) \exp(-\bar{d}_1(l)) dl \oint_c \frac{dl' a_2(l') \exp(-\bar{d}_2(l'))}{l - l'} \quad (9)$$

Here the circle integration goes over the complex parameter $\boldsymbol{l}$.

By the direct check one can be convinced that (9) are the solutions of equations (8). The formulae (9) can also be obtained as a solution of homogeneous Riemann problem in the case of the solvable algebra [11].

Let's represent two types of Backlund transformation by means of which one can construct new types of solutions of equations (8) from the known solution (9). For solutions of first two equations of (8) this two Backlund transformations are the same:

$$\boldsymbol{q}_s (\boldsymbol{a}_i^k)_{x_s} - (\boldsymbol{d}_i)_{x_s} \boldsymbol{a}_i^k = (\boldsymbol{a}_i^{k+1})_{x_s} , i = 1,2 \quad (10)$$

For solutions of the third equation of the system (8) they are different:

$$\boldsymbol{q}_s (\boldsymbol{a}_{1,2}^{0,k})_{x_s} - (\boldsymbol{d}_1 + \boldsymbol{d}_2)_{x_s} \boldsymbol{a}_{1,2}^{0,k} - (\boldsymbol{a}_1^k)_{x_s} \boldsymbol{a}_2^k = (\boldsymbol{a}_{1,2}^{0,k+1})_{x_s} \quad (11)$$

and

$$\boldsymbol{q}_s (\boldsymbol{a}_{1,2}^{k,0})_{x_s} - (\boldsymbol{d}_1 + \boldsymbol{d}_2)_{x_s} \boldsymbol{a}_{1,2}^{k,0} - \boldsymbol{a}_1^k (\boldsymbol{a}_2^k)_{x_s} = (\boldsymbol{a}_{1,2}^{k+1,0})_{x_s} \quad (12)$$

Note that starting, zero step of upper transformations procedure coincides with initial solutions (9).

Let's return to the solution of the equation (7) at the first step of the recurrent procedure.

Comparing (6) and (12) we came to the conclusion that $\boldsymbol{b}_{1,2} = \boldsymbol{a}_{1,2}^{0,1}$.

Finally, knowing all components of matrix $\boldsymbol{S}$ and using (3) we can express the solution

$$F = F_1^+ X_1^+ + F_2^+ X_2^+ + F_{1,2}^+ X_{1,2}^+ + F_1^0 h_1 + F_2^0 h_2 + F_1^- X_1^- + F_2^- X_2^- + F_{1,2}^- X_{1,2}^-$$

of self-duality equations at the first step of the recurrent procedure in terms of chains (10)-(12):

$$F_1^0 = \boldsymbol{t}_1 + \frac{\boldsymbol{a}_{1,2}^{1,0}}{\boldsymbol{a}_{1,2}^{0,0}}, F_2^0 = \boldsymbol{t}_2 + \frac{\boldsymbol{a}_{1,2}^{0,1}}{\boldsymbol{a}_{1,2}^{0,0}}$$

$$F_{1,2}^- = \frac{1}{\boldsymbol{a}_{1,2}^{0,0}}, F_1^- = \frac{\boldsymbol{a}_2^0}{\boldsymbol{a}_{1,2}^{0,0}}, F_2^- = -\frac{\boldsymbol{a}_1^0}{\boldsymbol{a}_{1,2}^{0,0}}$$

$$F_1^+ = -\frac{1}{\boldsymbol{a}_{1,2}^{0,0}} \begin{vmatrix} \boldsymbol{a}_1^0 & \boldsymbol{a}_1^1 \\ \boldsymbol{a}_{1,2}^{0,0} & \boldsymbol{a}_{1,2}^{1,0} \end{vmatrix}, F_2^+ = -\frac{1}{\boldsymbol{a}_{1,2}^{0,0}} \begin{vmatrix} \boldsymbol{a}_2^0 & \boldsymbol{a}_2^1 \\ \boldsymbol{a}_{1,2}^{0,0} & \boldsymbol{a}_{1,2}^{0,1} \end{vmatrix}$$

$$F_{1,2}^+ = \frac{1}{\boldsymbol{a}_{1,2}^{0,0}} \begin{vmatrix} \boldsymbol{a}_{1,2}^{0,0} & \boldsymbol{a}_{1,2}^{0,1} \\ \boldsymbol{a}_{1,2}^{1,0} & \boldsymbol{a}_{1,2}^{1,1} \end{vmatrix}$$

The general formulae of the recurrent procedure as well as the expression for the group element will be considered in further publication.

As it is seen from formulas (11-12) for algebras of the rank higher than two, the number of corresponding Backlund transformations of the initial problem solutions will be equal to the rank of the algebra. Thus, it is necessary only to overcome the routine calculations using, for example, Mathematica 4-0 software.

[1] *R.S. Ward, Phil. Trans.* R. Soc. Lond.A315, 451 (1985); Lect. Notes Phys., 1987, 280, 106; Lond. Math. Soc. Lect. Notes Ser., 1990, 156, 246.

[2] *L.J. Mason and G.A. J.Sparling.* Phys. Lett., 1989, A137, 29; J. Geom. and Phys., 1992, 8, 243.

[3] *S. Chakravarty, M.J. Ablowitz and P.A. Clarkson*. Phys. Rev. Lett., 1990, 1085.
[4] *I. Bakas and D.A. Depireux*. Mod. Phys. Lett., 1991, A6, 399.
[5] *M.J. Ablowitz, S. Chakravarty and L.A. Takhtajan*. Comm. Math. Phys., 1993, 158, 1289.
[6] *T.A. Ivanova and A.D. Popov*. Phys. Lett., 1992, A170, 293.
[7] *L.J. Mason and N.M.J. Woodhouse*. Nonlinearity 1, 1988, 73; 1993, 6, 569.
[8] *M. Kovalyov, M. Legare and L. Gagnon*. J. Math. Phys., 1993, 34, 3425.
[9] *M. Legare and A.D. Popov*. Pis'ma Zh. Eksp. Teor. Fiz., 1994, 59, 845.
[10] *A.A. Belavin and V.E. Zakharov*. Phys. Lett., 1978, B73, 53.
[11] *A.N. Leznov and M.A. Mukhtarov*. J. Math. Phys., 1987, 28 (11), 2574; Prepr. IHEP, 1987, 87-90. Prepr. ICTP 163, Trieste, Italy, 1990; J. Sov. Lazer Research, 13 (4), 284, 1992.
[12] *A.N. Leznov*. IHEP preprint-92/87, 1990.
[13] *A.N. Leznov, M.A.Mukhtarov and W.J.Zakrzewski*. Tr. J. of Physics 1995, 19, 416.

Received: 23.05.02